HOUSTON LDAR II NETWORK: DESIGN, OPERATION, AND PERFORMANCE ANALYSIS

A Dissertation

by

BRANDON LEE ELY

Submitted to the Office of Graduate Studies of
Texas A&M University
in partial fulfillment of the requirements for the degree of

DOCTOR OF PHILOSOPHY

August 2008

Major Subject: Atmospheric Sciences

HOUSTON LDAR II NETWORK: DESIGN, OPERATION, AND PERFORMANCE ANALYSIS

A Dissertation

by

BRANDON LEE ELY

Submitted to the Office of Graduate Studies of
Texas A&M University
in partial fulfillment of the requirements for the degree of

DOCTOR OF PHILOSOPHY

Approved by:

Chair of Committee,	Richard E. Orville
Committee Members,	Lawrence D. Carey
	Courtney Schumacher
	George Kattawar
Head of Department,	Kenneth Bowman

August 2008

Major Subject: Atmospheric Sciences

ABSTRACT

Houston LDAR II Network: Design, Operation, and

Performance Analysis. (August 2008)

Brandon Lee Ely, B.S., State University of New York at Oswego;

M.S., Texas A&M University

Chair of Advisory Committee: Dr. Richard E. Orville

The Houston LDAR II network is an array of twelve VHF time-of-arrival (TOA) sensors operated by Texas A&M University. The goals of the network are to conduct in-depth studies of thunderstorm electrification and provide timely lightning threats to the Houston area. Before analyses are conducted using data from the Houston LDAR network, it is necessary to understand the LDAR network's performance and limitations, such as the LDAR source detection efficiency, network range, and location accuracy.

Initial results from the 31 October 2005 Mesoscale Convective System (MCS) timing error analysis revealed an RMS timing error for the Houston LDAR network of 90 ns for 6 sensor solutions. This gives a three-dimensional location accuracy of 1 km at a distance of 150 km and 100 m over the center of the network. Reanalysis with updated sensor positions decreased the RMS timing error to 75 ns. This decrease in RMS timing error increased the median three-dimensional location accuracy by ~100 m at a 100 km range.

The network has been operated at both 70 MHz and 40 MHz. Model results of detection efficiency suggest that the change to 40 MHz yields an increase of 9 – 10 dB in network sensitivity. Analysis of VHF source power distributions shows a similar shift from that expected from the model. These results show that the 40 MHz LDAR network detects ~3.3 times more VHF sources than the 70 MHz network.

The analysis of the usable network range for research purposes is currently set by rough guidelines of location accuracy and detection efficiency. For location accuracy, a 1 km limit allows storm analysis out to a range of more than 150 km. For the detection efficiency analysis, results based on source power distributions suggest a gradual fall off with range. Examining the change in VHF source density by range reveals different results. VHF source density remained fairly constant out to a range of 100 km at which point a significant fall off was observed. Based on these results the usable network range for the Houston network is 100 km.

DEDICATION

To my grandfather, Robert J. Ely,

who helped inspire my interest in weather and especially lightning.

ACKNOWLEDGEMENTS

I would like to give a large thank you to my committee chair, Dr. Orville, and committee members, Dr. Larry Carey, Dr. Courtney Schumacher, and Dr. George Kattawar. Without their advice and direction, this work would not have been possible.

To my peers, I offer my sincere appreciation for their help in classes and research. I would like to individually acknowledge my officemates Shane Motley, Chas Hodapp, Scott Steiger, Jamie Smith, and Joe Jurecka for their in-depth lightning discussions, the hard work they contributed to installing the Houston LDAR II network, and all the fun times we had.

I owe my deepest debt of gratitude to my parents. Without their support and encouragement over the years, it would not have been possible to get this far academically. I would also like to thank Dan Zhang for her support and encouragement that got me through the most difficult times of my academic career. Last, but certainly not least, I would like to thank my son, Justin Ely, for all his laughs and smiles. They all helped me get through the last few, tough months of writing this dissertation.

TABLE OF CONTENTS

Page

Page

LIST OF FIGURES

FIGURE Page

FIGURE Page

FIGURE Page

LIST OF TABLES

1. INTRODUCTION

The Houston Lightning Detection and Ranging (LDAR) network, a VHF total lightning detection system, began operation in mid-August 2005. The Houston LDAR network is an array of twelve VHF time-of-arrival (TOA) sensors built by Vaisala Inc. and operated by Texas A&M University. The main goals of the network are to conduct in-depth studies of the effects a major metropolitan city has on thunderstorm electrification [Orville et al., 2001; Steiger et al., 2002] and provide timely lightning threats via the Houston National Weather Service office. Unlike the National Lightning Detection Network (NLDN), which only detects cloud-to-ground (CG) lightning, the Houston LDAR lightning network is capable of detecting VHF impulses (referred from here on as VHF sources) related to the electrical breakdown and propagation of lightning in three dimensions. This gives scientists the ability to examine the total lightning (both cloud-to-ground and intracloud) structure of thunderstorms and evolution in time. In addition, the Houston LDAR network's location opens researchers to the opportunity to study the lightning structure of a wide variety of storm types from mesoscale convective systems (MCSs) to typical airmass thunderstorms to tropical storms.

Before analyses are conducted using data from the Houston LDAR network, it is important to understand the basic operation of the sensors and network. This gives insight into understanding w hat and how are LDAR sources detected and determined. In addition, it is necessary to have an understanding of the LDAR network's performance and limitations, such as the LDAR source detection efficiency, network range, and

---

This dissertation follows the style of the *Journal of Geophysical Research.*

location accuracy. Due to the research nature of the Houston LDAR network, the system has undergone adjustments in order to improve its detection capability, which also must be considered when analyzing the LDAR data between different storm days. This also must be taken into account when comparing lightning analyses between different VHF TOA networks. The first part of this paper will be to focus on the LDAR network's design and operation. The second half will focus on the network performance and changes made to improve performance.

2. TIME OF ARRIVAL LIGHTNING DETECTION

2.1. Basics of an LDAR Sensor

Total lightning detection systems map lightning in three dimensions by detecting short impulses of VHF radiation emitted during electrical breakdown and lightning channel propagation. These short, impulsive bursts of VHF radiation have a typical duration of a few microseconds [Mazur et al., 1997]. Utilizing accurate measurements of the time of arrival of VHF pulses at several sensors and based on the fact that VHF signals propagate along line-of-sight, these pulses can be modeled as point sources in three dimensions [MacGorman and Rust, 1998]. The VHF pulses detected by the LDAR network are typically referred to as LDAR or VHF sources. These individual radiation pulses can then be grouped together to map the horizontal, vertical, and temporal extent of lightning flashes (Fig. 2.1).

In order to accomplish this, an LDAR network is normally composed of six or more VHF sensors placed roughly 20 – 25 km apart. Each LDAR sensor is composed of an antenna to detect the VHF radiation from lightning, a GPS antenna to provide highly accurate sensor position and time of arrival (TOA) of the VHF pulse, and a custom Linux PC to digitize, time-tag, and archive the VHF pulse data. The LDAR sensors are typically tuned to a locally unused TV channel (generally 55 - 80 MHz) in order to detect the lightning radiation pulses with minimal man-made interference.

At each LDAR site, the VHF antenna measures the radiation from each source, and an analog to digital (A/D) converter digitizes the logarithmically amplified antenna output. Each LDAR sensor uses an A/D converter with a digitization rate of 20 MHz,

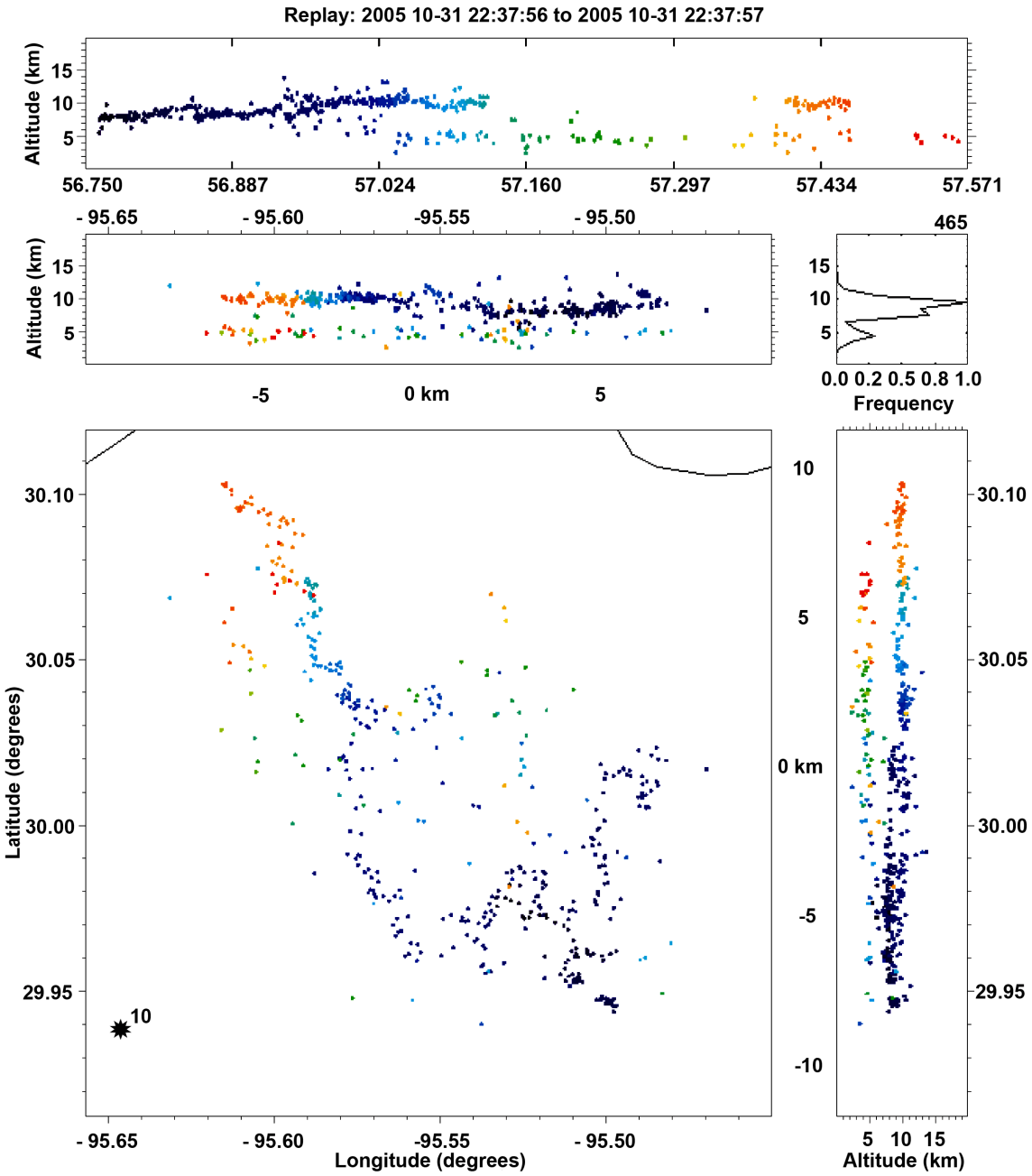

Figure 2.1. A five-panel plot showing VHF sources detected by the Houston LDAR network grouped into a lightning flash. The panels depict a) the time-height, b) longitude-height, c) latitude-longitude, d) latitude-height, and e) height histogram of the VHF sources in the lightning flash. Note: color of points denotes time from oldest (blue) to newest time (red).

which gives a respective time window of 100 μs. This gives each LDAR sensor the possibility of recording a maximum of 10,000 VHF pulses s^{-1}. VHF pulses with the largest peak powers above a designated threshold in each discrete 100 μs time window are saved along with the GPS determined time of the VHF pulse. The peak power received by a sensor is used based on the assumption that these events are related to the peak power produced by a VHF lightning event. However, local noise, such as corona discharges and power line noise, may also exceed the threshold and in some cases mask the received power of the lightning pulse at a given sensor.

2.2. TOA Lightning Solutions

As previously stated, an LDAR network maps lightning in three dimensions by detecting short impulses of VHF radiation emitted during electrical breakdown and lightning channel propagation. With accurate TOA measurements of a VHF pulse at several sensors, the time and location of the VHF pulse can be accurately determined. Figure 2.2 shows the basic geometry of a VHF point source pulse at (x,y,z,t) detected by several LDAR sensors at (x_N,y_N,z_N,t_N), where N is i → m. The geometry of the VHF signal to a sensor is given by the equation:

$$c^2(t-t_i)^2 = (x-x_i)^2 + (y-y_i)^2 + (z-z_i)^2 \tag{2.1}$$

where c is the propagation speed of the VHF signal [Thomas et al., 2004]. Expanding and re-arranging Equation 2.1 and defining $r_i^2 = x_i^2 + y_i^2 + z_i^2$ gives:

$$c^2t^2 + c^2t_i^2 = r^2 + r_i^2 - 2(xx_i + yy_i + zz_i - c^2tt_i) \tag{2.2}$$

To solve the four unknowns (x,y,z,t) for a VHF pulse, a method similar to that demonstrated by Koshak and Solakiewicz [1996] and Koshak et al. [2004] is utilized.

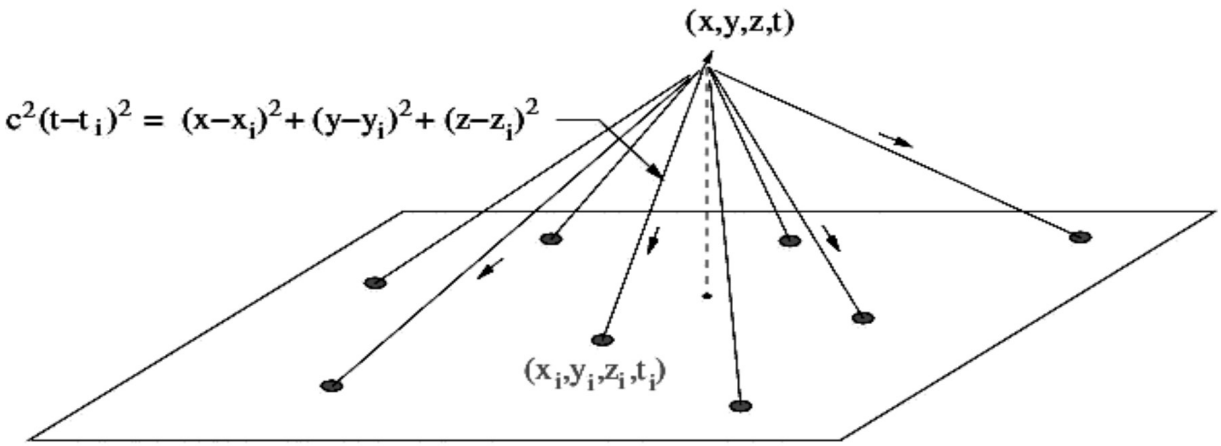

Figure 2.2. Schematic of the basic time-of-arrival technique used in a VHF three-dimensional lightning mapping system. Measurements of the arrival time t_i at $N \geq 4$ sensors are used to determine the location and time of the VHF source (*x,y,z,t*). (Thomas et al. 2004)

This method produces a linear system of equations from the time difference of arrival of the signal of a VHF pulse at five sensors. Therefore we will have four additional equations similar to Eq. (2.2) for each of the four additional sensors:

$$\begin{aligned} c^2t^2 + c^2t_j{}^2 &= r^2 + r_j{}^2 - 2(xx_j + yy_j + zz_j - c^2tt_j) \\ c^2t^2 + c^2t_k{}^2 &= r^2 + r_k{}^2 - 2(xx_k + yy_k + zz_k - c^2tt_k) \\ c^2t^2 + c^2t_l{}^2 &= r^2 + r_l{}^2 - 2(xx_l + yy_l + zz_l - c^2tt_l) \\ c^2t^2 + c^2t_m{}^2 &= r^2 + r_m{}^2 - 2(xx_m + yy_m + zz_m - c^2tt_m) \end{aligned} \tag{2.3}$$

The equation for the difference of the jth sensor from the ith sensor, letting $x_{ij} = x_i - x_j$, $y_{ij} = y_i - y_j$, etc..., yields:

$$\frac{r_i^2 - r_j{}^2 - c^2(t_i{}^2 - t_j{}^2)}{2} = xx_{ij} + yy_{ij} + zz_{ij} - c^2tt_{ij}. \tag{2.4}$$

Subtracting each equation in Eq. (2.3) from the equation for the first sensor (Eq. 2.2) gives four differenced linear equations, similar to Equation 2.4, which can be solved analytically for the event location. The matrix form of the system of equations would be:

$$\begin{pmatrix} x_{ij} & y_{ij} & z_{ij} & ct_{ij} \\ x_{ik} & y_{ik} & z_{ik} & ct_{ik} \\ x_{il} & y_{il} & z_{il} & ct_{il} \\ x_{im} & y_{im} & z_{im} & ct_{im} \end{pmatrix} \bullet \begin{pmatrix} x \\ y \\ z \\ -ct \end{pmatrix} = \begin{pmatrix} Q_{ij} \\ Q_{ik} \\ Q_{il} \\ Q_{im} \end{pmatrix} \tag{2.5}$$

where:

$$Q_{ij} = \frac{r_i^2 - r_j{}^2 - c^2(t_i 2t_j{}^2)}{2}. \tag{2.6}$$

Solving the matrix gives a solution to the LDAR VHF source location and time (x,y,z,t).

2.3. Minimizing Location Error

With five or more sensors, it is possible to reduce the location error by minimizing the non-linear least squares fit of the data. Although only five sensors are required to calculate a VHF source solution and attempt the least squares minimization, it is preferable that at least six sensors contribute to the source solution. The more stations involved in the VHF source solution calculations provides redundancy and acts to filter local noise from the data set. In the case of the Houston LDAR network, a minimum of six sensors are required to detect a VHF source in order for it to be considered valid.

The process of error minimization begins by using the VHF source solution location determined from Equation (2.5) as a first guess. The first guess, along with the position and TOAs from additional sensors are used to solve for the event location using an iterative process called the Levenberg Marquardt method [Bevington and Robinson, 2002]. This method linearizes the equations around successive trial solutions and makes adjustments to the individual timing measurements. This process is repeated until the solution converges, in other words, until the difference in residuals from one iteration to the next, changes by a very small amount.

This method essentially attempts to find the best fit, or minimal error, between the matrix of TOAs, t_i^{obs}, at each station and the matrix of TOA solutions from each iteration, t_i^{fit}. This error or goodness of fit, χ^2, is quantified by:

$$\chi^2 = \sum_{i=1}^{N} \frac{(t_i^{obs} - t_i^{fit})^2}{\Delta t_{RMS}^2}, \tag{2.7}$$

where N is the number of stations in the solution, and Δt_{RMS} is the assumed timing uncertainty in the TOA measurements. In the case that the iterative process does not converge, the VHF source point is considered to be noise and removed from the data. On the other hand, if the iterative process converges, the χ^2, must be below a certain value to be considered a good location. In the case of the Houston LDAR network, the χ^2 value must be less than 40 to be accepted. The entire process (location solution and error minimization) is performed using all reasonable combinations of LDAR sensors. In the event that more than one combination converges and has a χ^2 value below the accepted cutoff, the combination with the lowest χ^2 is kept. TOAs not used in the final combination are reused as possible TOA measurements for a different VHF source.

3. HISTORY OF VHF LIGHTNING DETECTION

The use of time-of-arrival (TOA) measurements in lightning studies was originally pioneered by D. E. Proctor [Proctor, 1971, 1981; Proctor et al., 1988]. The system was built to study the detailed breakdown of individual lightning discharges in thunderstorms over South Africa. The original system utilized a network of five stations arrayed along nearly perpendicular baselines to form a cross with a 30 km east–west (E–W) extent and 40 km north–south (N–S) extent. The four outlying stations transmitted the analog receiver output to the central station, where the data was recorded. Due to the lack of small, cheap computing power at the time, the system was only able to record data for 250 ms at a time. In addition, data analysis to identify times of common VHF lightning events were processed manually, which could take up to 6 months per 250 ms record. The TOA measurements made by the network were made with 5 MHz bandwidth receivers operating at a center frequency of 300 MHz. Proctor estimated timing errors, Δt, of about 70 ns RMS, which gave horizontal and vertical location accuracies of 20 m for and 100 m, respectively, for sources within the boundaries of the network.

Lennon [1975], utilizing Proctors design, implemented a seven station network, named the Lightning Detection and Ranging system, for monitoring lightning over and around Kennedy Space Center (KSC), Florida. The network consisted of an approximately circular array of six measurement stations with a 16 km diameter and a seventh station located in the center of the circle. For processing purposes, the network was considered to consist of two Y-shaped arrays each consisting of three outlying

stations and the central station [Poehler and Lennon, 1979]. Similar to Proctor's system, the logarithmically detected RF signals from the outlying stations were transmitted over microwave links in analog form to the central station. The major improvement in the KSC LDAR network was its ability to digitize the incoming data with a 50 ns time resolution and automatic processing to obtain the lightning sources in real time. In order to reduce noise contamination, the system required that a VHF lightning source be detected by both Y-arrays. Although limited by today's standards, the system typically located several tens of events per lightning flash [Lhermitte and Krehbiel, 1979], which provided an important picture of the overall lightning activity around the Kennedy Space Center (KSC) and the Cape Canaveral Air Force Station [Uman et al., 1978; Lhermitte and Krehbiel, 1979]. Lennon and coworkers at the Kennedy Space Center developed an improved, second-generation version of the LDAR system in the early 1990s [Maier et al., 1995; Mazur et al., 1997]. The updated system had greatly improved detection efficiency and was able to process up to 10,000 VHF lightning sources per second.

In the mid- to late- 90's, New Mexico Tech designed and built a significantly improved TOA system called the New Mexico Tech Lightning Mapping Array (LMA). The largest improvement involved the use of GPS technology at each sensor [Krehbiel et al., 2000; Rison et al. 1999; Thomas et al., 2001]. The use of GPS allowed each sensor to independently record accurate timing information for every VHF pulse detected. Additionally, each sensor was capable of recording and digitizing the VHF pulses locally, which introduced the ability to store data from each sensor locally on a hard drive. These two advances allowed each sensor to essentially run stand-alone and

continuously without intervention. With network data connections, each sensor was able to transmit their data back to a central processor in order to produce real-time VHF source solutions up to a theoretical maximum of 10,000 per second.

In the late 1990's, Vaisala Inc. acquired the rights from NASA to build a commercial version of the KSC LDAR system. Collaboration with New Mexico Tech yielded a system that was functionally similar to the original KSC LDAR system, but incorporated the advances made by New Mexico Tech [Carey et al., 2005]. The commercial version, called LDAR II, added a variable tuner to each sensor. The variable tuner allows the operating frequency to be remotely changed based on changes to noise levels at each site.

4. THE HOUSTON LDAR NETWORK

4.1. The Basics

The Houston LDAR II network is an array of twelve VHF antennas and receivers deployed throughout the greater Houston metropolitan area (Figure 4.1). The Texas A&M Department of Atmospheric Sciences purchased the LDAR II sensors from Vaisala Inc. with the goals to conduct in-depth studies of the effects a major metropolitan city has on thunderstorm electrification [Orville et al., 2001; Steiger et al., 2002] and provide timely lightning threats via the Houston National Weather Service office. The sensors in the Houston LDAR network are functionally similar to the New Mexico Institute of Mining and Technology's Lightning Mapping Array (LMA) described by Rison et al. [1999]. These systems are based on the original Lightning Detection and Ranging (LDAR) system developed at NASA's Kennedy Space Center [Lennon and Maier, 1991].

The Houston LDAR II network began operating in mid July of 2005 with at least seven sensors transmitting real-time lightning data to a central processor on the Texas A&M campus in a network test mode. On August 14, 2005, testing of the network data quality was finished and the archival of lightning data commenced. One week later, the number operational sensors increased to ten. The network remained at ten sensors until January 9, 2007 when the final two sensors were brought online.

The center of the network is located at 29.79°N and 95.31°W, which is slightly northeast of downtown Houston. The network has an average sensor baseline of 25

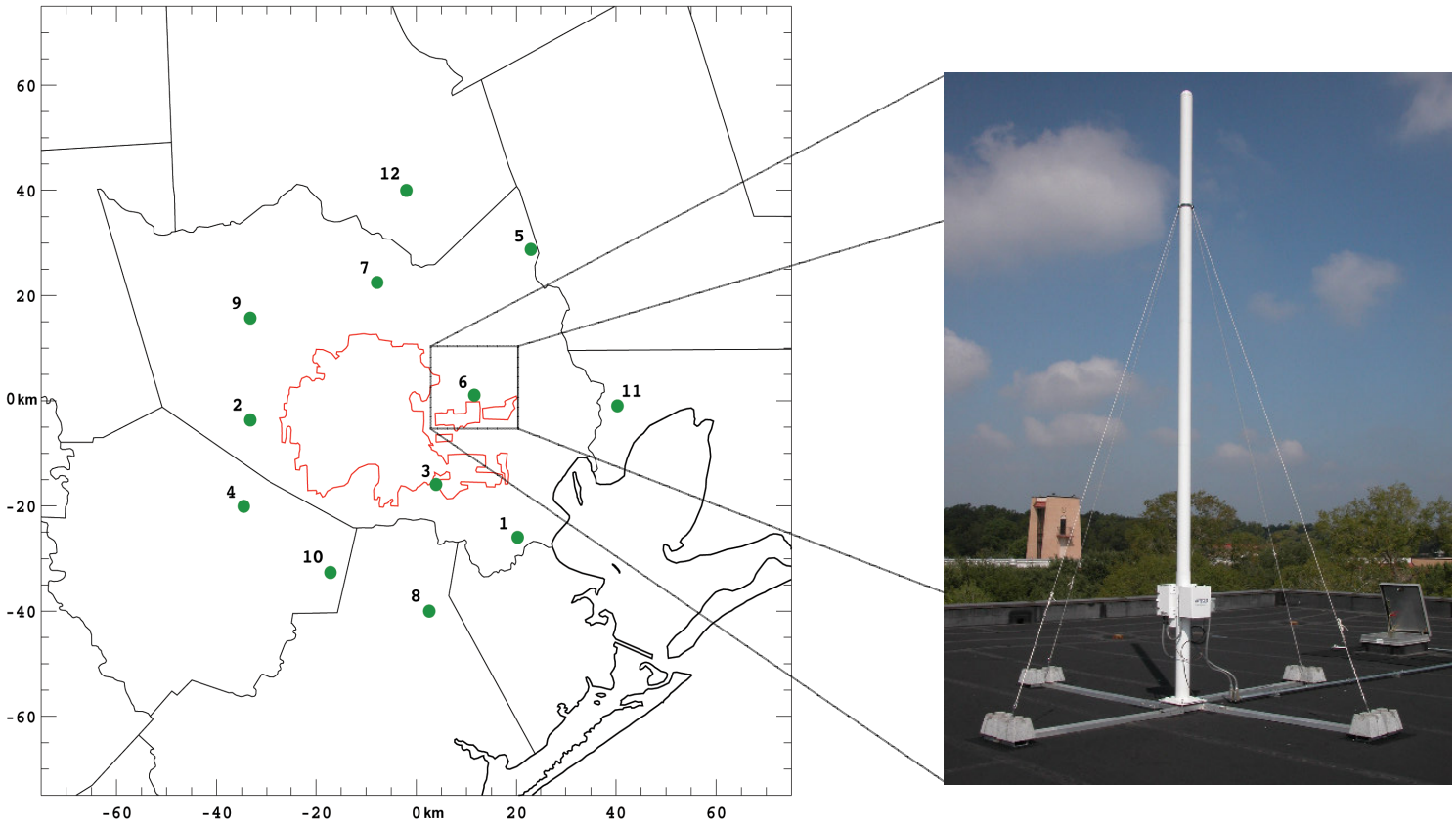

Figure 4.1. Map on left depicts the locations of the twelve Houston LDAR II sensors (green circles). The photo on right side shows the San Jacinto College LDAR sensor. The red outline shows the Houston Urban area and industrial suburbs.

kilometers and an average network diameter of 75 kilometers. Each sensor detects the arrival times of the VHF pulses by demodulating the VHF signal in a 5-MHz base band around a center operating frequency. The operating frequency from October 30, 2005 to March 25, 2007 was around 69.5 MHz depending on RF noise conditions at each antenna site. On March 26, 2007 the operating frequency was changed to 40 MHz in order to improve network detection capabilities.

4.2. Sensor Site Selection

Site selection for an LDAR network around a large metropolitan area is a very tedious, time-consuming affair. There are many requirements that must be considered in laying out the potential configuration of sensors in the network. Rarely are all of the requirements of a perfect site met at any of the potential sites. This requires the site surveyor to weigh the strengths and weaknesses of each site. This means that compromises must be made between the different requirements of a site in order to build the best possible network with what is available.

In order for an LDAR network to produce highly accurate VHF source solutions, the sensors must be spaced out from each other in all directions with a 20 – 30 km baseline between nearby sensors. With twelve sensors to work with in the construction of the Houston LDAR network, the hypothetical layout developed called for a center sensor located within the center area of the city of Houston. Five sensors, each 25 km from the center sensor, forming a pentagon would be then be placed around the center sensor. Around the pentagon, the six remaining sensors would be placed 25 km away

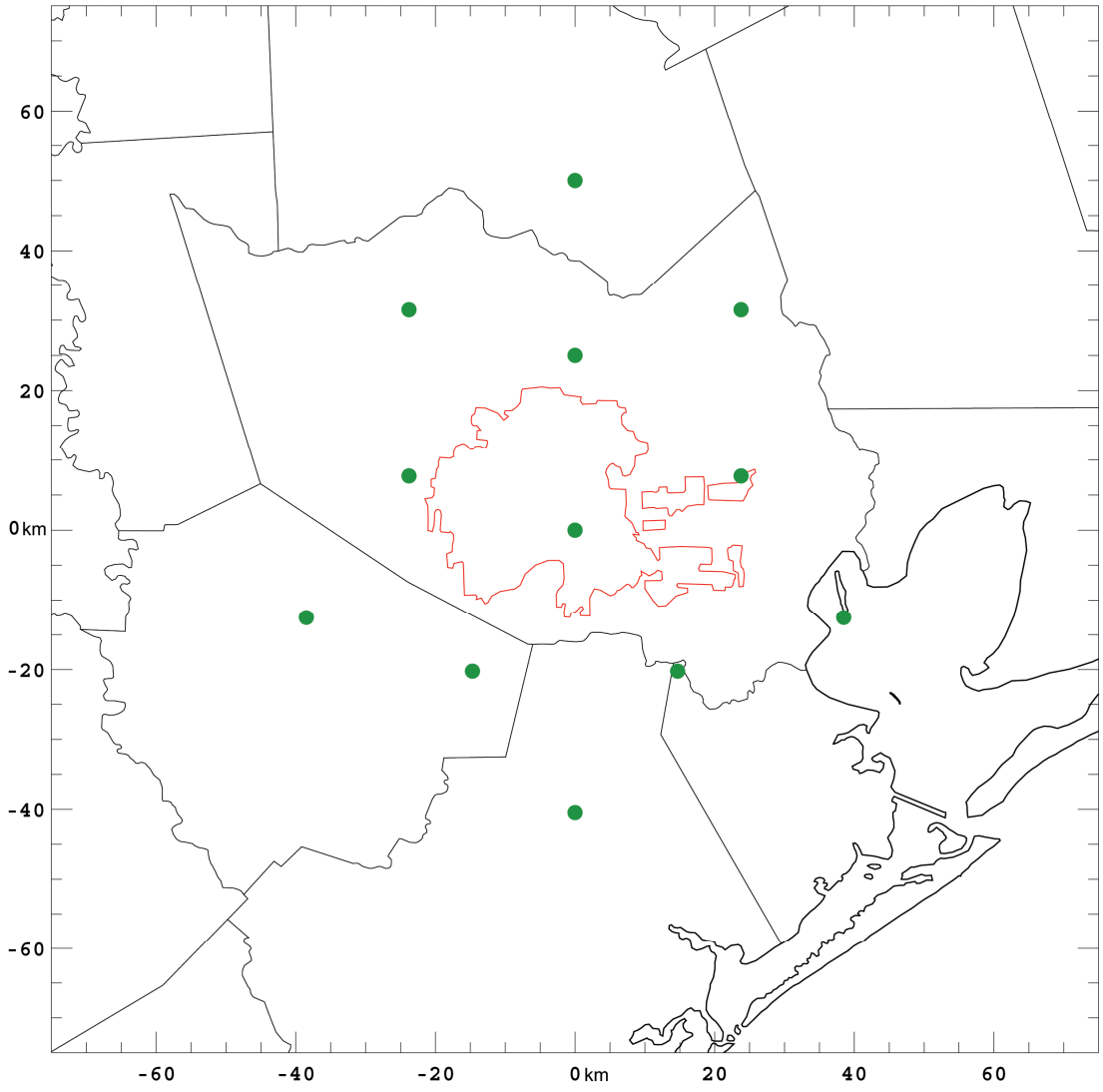

Figure 4.2. Original, theoretical layout of the Houston LDAR network. Each sensor, except the northern most sensor, has a 25 km baseline with at least 2 other sensors.

from two of the corner points of the pentagon. The last remaining sensor was placed directly north in the hope of extended coverage to the north (see Figure 4.2).

Due to the line-of-sight nature of VHF radiation, it is essential to minimize the objects that could obstruct the sensors view of the sky. The general limit followed was that, at each sensor site, obstructions should not block more than 1^{o} above the horizon. This required the sensors be placed in locations with large open fields and short buildings or placed on a building above the nearby obstructions. Places that would most likely fulfill this requirement were airports, school districts, college campuses, and office buildings.

The task at hand was to find potential sites as near as possible to the hypothetical network layout. This was accomplished by obtaining aeronautical maps, researching the locations of school districts and college campuses, and studying aerial photographs looking for large open fields. The preliminary goal was to find at least two potential sites near each hypothetical sensor location. This was necessary in cases the potential sites failed the other site requirements. The additional requirements that needed to be satisfied were: 1) low ambient RF noise level, 2) no nearby (within 150 meters of the sensor) powerlines, radio towers, flood lights, which could cause intermittent periods of high RF noise, 3) access to some form of high-speed internet connection.

Before extensive noise surveys were conducted, all potential sites were visited in order to rule out sites that did not meet the visibility, no nearby noise sources, and high-speed internet requirements. The high-speed internet requirement proved to be most difficult for many of the sensor sites in the outer ring, which were in rural, farm areas.

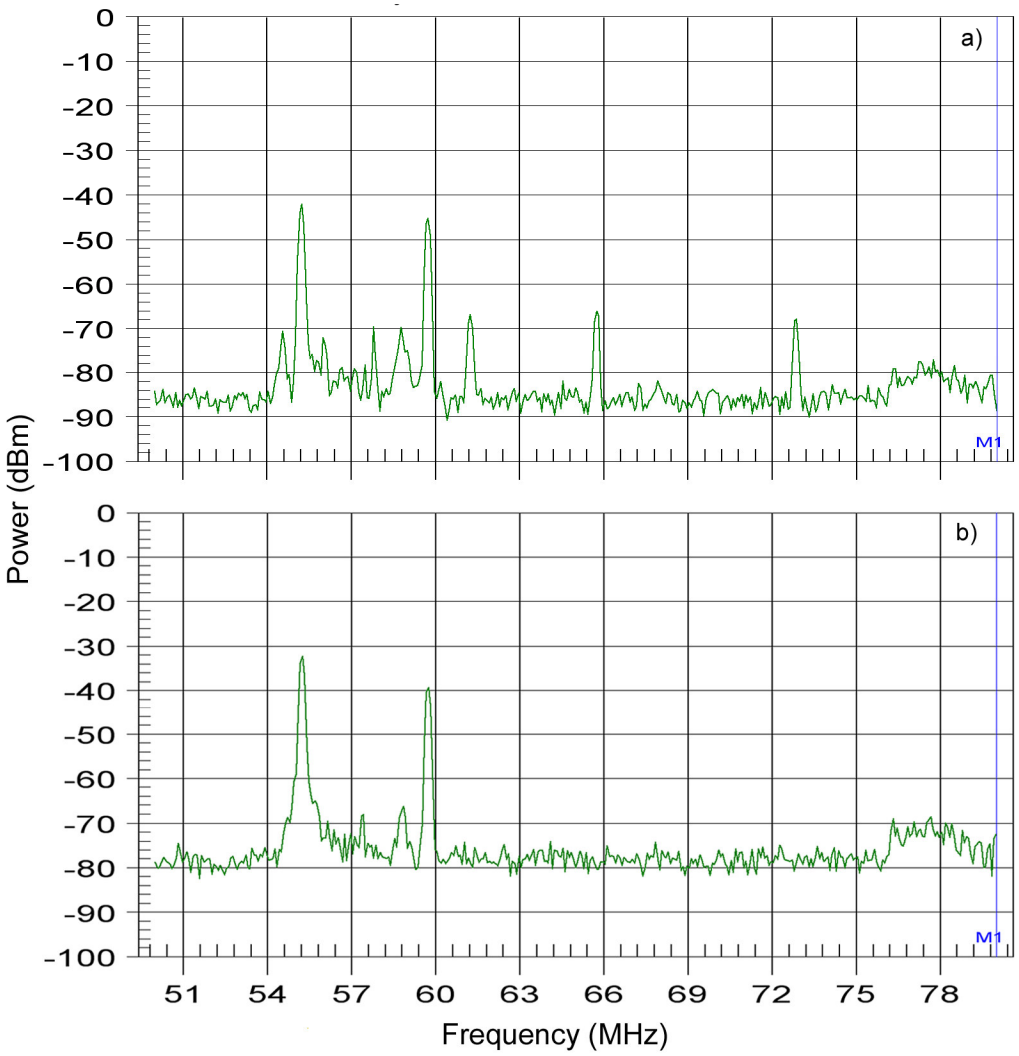

Figure 4.3. Spectrum analyzer results for two sensor sites a) Cypress-Fairbanks and b) Impact Weather during preliminary site selection. Note the lack of signal peaks at 61, 65, & 73 MHz at the Impact Weather site.

Each sensor required a high-speed internet connection to relay VHF pulse triggers back to the central server at Texas A&M for real-time data processing and sensor monitoring. For the maximum data rate of 10,000 VHF data sources per second, minimum internet upload rate of 600 kbps is needed. It was determined that at most sites 300 kbps was the maximum data rate achievable, which limited the real-time data analysis to a maximum of 5,000 VHF sources per second.

Once the preliminary site inspections had been conducted and the list of potential sites refined, full noise surveys were conducted. At each site, the first thing done was to use a hand held spectrum analyzer to look for obvious, continuous manmade RF noise. Figure 4.3 shows the spectrum analyzer results at two of the potential sensor sites. Figure 4.3a shows a noise floor of roughly -85 dBm and several spikes in noise associated with TV channel audio and video carriers. Figure 4.3b shows a noise floor of roughly -78 dBm and only a couple of TV channel noise spikes compared to Figure 4.3a. If the spectrum analyzer results showed a noise floor at or above -70 dBm, the sites was considered noisy and rejected as a possible sensor site.

If a site passed the initial test with the spectrum analyzer, a series of noise surveys were conducted with an LDAR sensor. The results of the noise surveys show how local RF noise actually affects an LDAR sensor at the site. The surveys were performed using a routine built in to the LDAR sensor. This routine steps through the frequency spectrum, in this cases 55 – 80 MHz, with a fixed step size (0.5 MHz). At each frequency the gain (AGC value) of the sensor is set to 80, which is roughly equivalent to a minimum detectable signal (MDS) of -57 dBm (see section 5.3.1 for

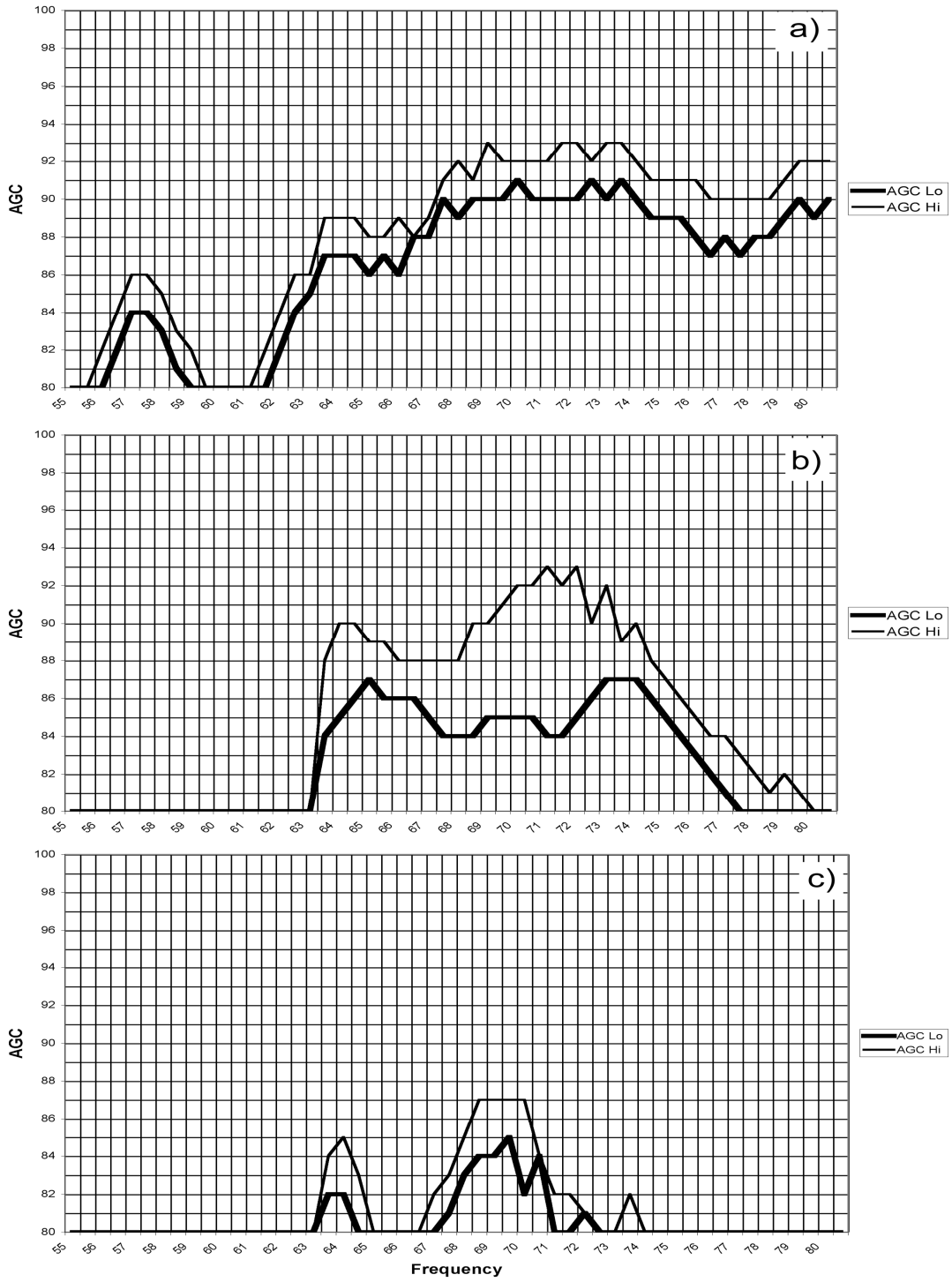

Figure 4.4. LDAR site noise surveys for three potential sites. Each plot shows an example of a) an acceptable site, b) marginally acceptable site, and c) unacceptable site. Note: AGC low label is equivalent to 3% noise rate and AGC high is equivalent to 50% noise rate.

information on AGC to MDS conversion). The program then increments the AGC value by 1 until the local noise is amplified enough to produce a rate of 5,000 data points per second (50% data rate). The program records the AGC values at a noise rate of 3% and 50%. This is repeated three times throughout the day for each frequency.

To make the final decision on a site's noise level, the AGC values for the 3% and 50% data rate were graphed (Figure 4.4). Under clear sky conditions, the gain of an LDAR sensor is set to a point where roughly 300 noise points per second exceed the detection threshold. This was felt to be a reasonable compromise between maximizing a sensor's gain setting but minimizing noise contamination in the data. Therefore, when analyzing the graphs of AGC versus frequency, the best sites would have a frequency band with higher AGC values for the 3% contour. The distance between the 3% and 50% contour provides information on how rapidly a sensor would be saturated by noise if the noise floor increased slightly. Therefore, the larger the distance between the 3% and 50% data rates, the better the site.

For a given frequency to be even potentially useful, the distance between the 3% & 50% contour must be at least 2 AGC values (roughly 2dB). From there, any sites that had a frequency band with AGCs for the 3% data rate above 90 were considered acceptable. Sites with a frequency range where the 3% data rate AGC was above 85 and the 50% data rate AGC was above 89 were considered marginally acceptable. Any site with a 3% data rate AGC below 85 was considered unacceptable.

Due to the abundance of locally generated noise around the Houston major metropolitan area, a majority of the sites fell into the last two categories. The potential

sites with the worst noise problems were the sites for the downtown sensor. All of the downtown locations required the sensor to be placed on top of high-rise office buildings or dormitories. Unfortunately, the test results showed all sites in the downtown area were far too noisy due to the large air handlers and other mechanical systems located on their roofs. As one would expect, the remote sites faired much better in the noise tests, but often times failed the requirement of high-speed internet access. In the end, balance was struck between the strengths and weaknesses of each site and the final network configuration was chosen (Figure 4.1).

Comparing the theoretical network configuration to the actual configuration, the overall design remained similar. However, due to the noise problems previously mentioned, the center sensor was drastically shifted 15 km southeast creating a sizeable gap near the center of the network. In addition most of the outermost sensors were moved closer to Houston in order have access to high-speed internet access.

4.3. Typical Sensor Site

The standard LDAR II sensor used in the Houston LDAR network is designed to be relatively self-sufficient when properly configured. The general design consists of a central mast of 30 ft in height. The top 18 ft consists of three vertically stacked VHF antennas topped by a small GPS antenna (Figure 4.5.). Attached to the mast near the base are two enclosures. The first enclosure houses the main electronics for the sensor, including the receiver, processor, basic communication connections, and onsite data storage (Figure 4.5). The second enclosure contains a battery backup for continuous sensor operation during a power failure of less than 3 hours.

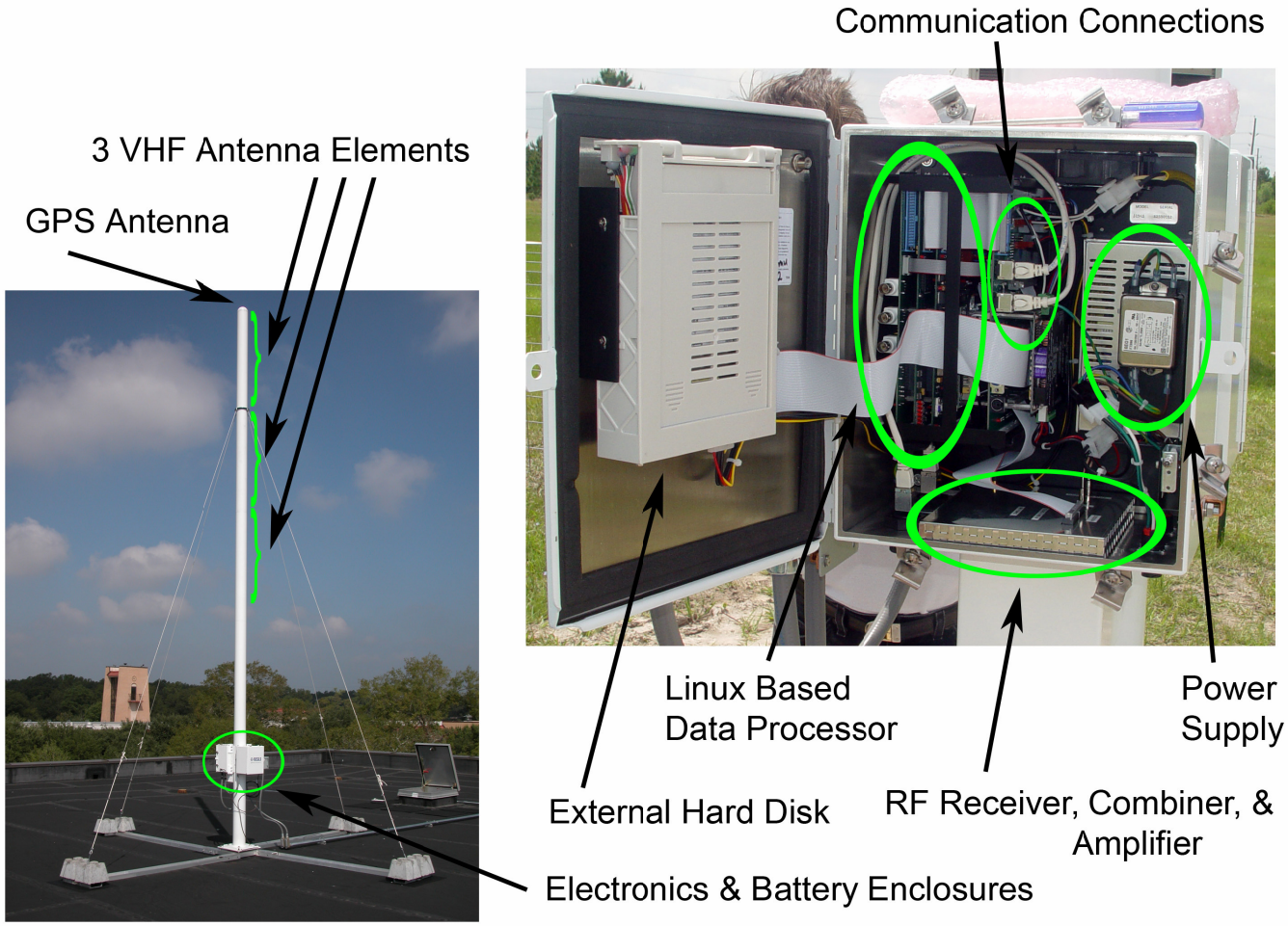

Figure 4.5. Images showing a typical LDAR sensor installation (left) and the inside layout of the electronics enclosure (right) showing the major parts of an LDAR sensor.

Most sites are located in fields well over 100 m from any buildings. This means that running Ethernet cable from sensor to an internet connection is not possible. In the most extreme cases, the sensor is located roughly 800 meters from the closest internet connection. For those sites, an 802.11g wireless bridge device is added inside the battery backup enclosure. An external directional antenna is added to the mast just below the main antenna elements. The other end of the wireless bridge is installed in the closestline-of-sight building with an internet connection. For all other cases, Cat 5 ethernet cable is run through sealed conduit between the sensor and building.

The LDAR sensor has two mounting options depending on the location. Ground mount sites use a circular concrete pad with four anchor bolts that the mast assembly connects to. Roof mounts use four aluminum I beams attached to form a cross. The mast is attached at the center of the cross and 45 kg (100 lb) weights are placed at the end of each beam. In both mounting options, guy wires are installed on the mast to add stability. With guy wires installed properly, the sensor mast is able to withstand up to 240 km hr^{-1} (150 mph) or Category 4 hurricane force winds.

4.4. Real-time Operation

The Houston LDAR network is capable of processing VHF lightning source solutions in real-time. Previous TOA systems used a wireless communications array linking each sensor in order to relay data back to the central server. This method was generally much more expensive and required additional maintenance. In addition, if one of the critical wireless relays broke, real-time data for nearly half the network would be lost. In order to cut operating costs, the Houston LDAR network's data is transmitted

over the internet using a variety of connections from dedicated T1 lines to DSL modems back to the central workstation at Texas A&M.

Data packets from the LDAR sensors are sent in 1 second intervals. Each data packet contains the time and peak strength of all VHF radiation pulses that exceeded the sensor's threshold setting for the previous second along with a GPS timing correction. An LDAR sensor is capable of detecting a VHF pulse every 100 μs, which produces a maximum detection rate of 10,000 VHF sources per second and a corresponding data rate of 600 kbps. Due to bandwidth constraints at most of the sensor sites, the upload rate to the central server is limited to a maximum of 384 kbps. In order to deal with the bandwidth limitation, each sensor is configured to transmit the strongest VHF pulse during a 200 μs interval, essentially cutting the data and data rate in half.

The central processor is responsible for analyzing the incoming data for VHF lightning source solutions. The central workstation processes the data in the same 1-second increments as the data is received. To deal with potential time delays from a slow internet connection, the workstation waits 5 seconds to allow data from all sensors to arrive. All detected VHF sources are then transmitted to a real-time display system for monitoring purposes. In addition, the VHF sources are grouped into 2 minute increments, which are sent to the League City National Weather Service office and used for the Houston LDAR real-time webpage (www.met.tamu.edu/ciams/ldar).

4.5. Data Processing

For research purposes, it is usually desirable that the dataset has the best time resolution possible. As stated above, each LDAR sensor is capable of recording VHF

pulses every 100 μs. Due to communications bandwidth issues, it is not possible to transmit this much data back to the central computer for processing and storage. However, each sensor is equipped with an 80 GB external removable hard drive capable of storing the 100 μs resolution raw data. This data is physically retrieved every couple of months and processed to produce the research quality VHF source solution data set. In the event of a hard disk failure, the real-time decimated 200 μs data for that sensor can be incorporated into the research dataset to partially replace the lost raw data.

Once the raw data has been retrieved and loaded on the central computer's data storage system, all data from time periods without radar echoes within 350 km and / or VHF source solutions detected by the real-time data set. For time periods where storms were present, an automated data processing program sifts through the raw data set, extracts all relevant data, and keeps a list of the operational sensors. Next, the program scans through the real-time, decimated data archive and determines which sensors were transmitting data during the specified time period. The program then compares the operational sensor lists from the two different data sets to determine if raw data was lost from any sensors. If data was lost, the decimated data for that sensor is extracted from the real-time data archive.

The data extracted from the raw dataset and, if necessary, real-time data archive are merged into a storm event archive file and moved to a Network Attached Storage (NAS) device for permanent storage. Once the backup of the storm event file is made, the file is processed to determine the GPS timing correction for each LDAR sensor. The proper timing corrections are fed into the VHF source location algorithm configuration

file along with each stations three-dimensional position. Now that the location algorithm configuration file is set, the data in the storm event file is passed to the LDAR VHF source location algorithm. Any VHF source solutions meeting the following criteria:

- Minimum of six sensors in solution
- VHF source $\chi^2 < 40$
- Source altitude > 0 km and < 20 km

are considered valid sources. All valid source solutions are recorded in a new data file containing the following information:

- Date and time to the nanosecond
- Latitude and Longitude out to 4 decimal places
- Altitude in meters
- Estimated VHF source power in dBm
- Number of sensors involved in solution
- Degrees of freedom for location optimization (# sensors – 4)
- χ^2 value

for each detected VHF source. Once all raw data has been processed, the VHF source solution file is moved to the same NAS archive for permanent storage. The final step of the program examines the storm event archive file for any time periods of 1 second or greater with missing data. If gaps in the data are present, the time periods are recorded to a separate text file and stored along with the VHF source solution file.

5. NETWORK PERFORMANCE – DATA AND METHODS

5.1. Network Tuning and RF Noise

Since the network became operational in mid July of 2005, several noise surveys have been conducted at the various sites in order to improve the network's overall sensitivity to weaker amplitude and more distant VHF sources. The extensive changes in sensor operating frequencies and gain settings over the past two years are expected to significantly affect the network performance. Below is a detailed description of changes in sensor tuning that were made and the reasoning behind the changes.

The first seven sensors were originally tuned to a center frequency near 74 MHz in an attempt to avoid interference from television channels (Fig. 5.1). After continuous monitoring of the sensors, it became clear that the noise level at this frequency varied greatly throughout a 24-hour period. This required a daily routine of monitoring noise levels and adjusting the sensitivity of the sensors downward by several dBm during the afternoon. Through additional, continuous noise surveys and sensor monitoring, a combination of aviation communications and local industrial communications were most likely responsible for the daily increase in noise and associated reduction of network sensitivity at 74 MHz.

In early October 2005, once the nearly constant thunderstorm activity subsided, a new round of noise surveys were conducted for the ten operational sensors. Figure 5.2 is a plot of noise surveys from three sensors showing the variation in noise levels in the frequency range of 50 MHz – 80 MHz at different locations around Houston. The

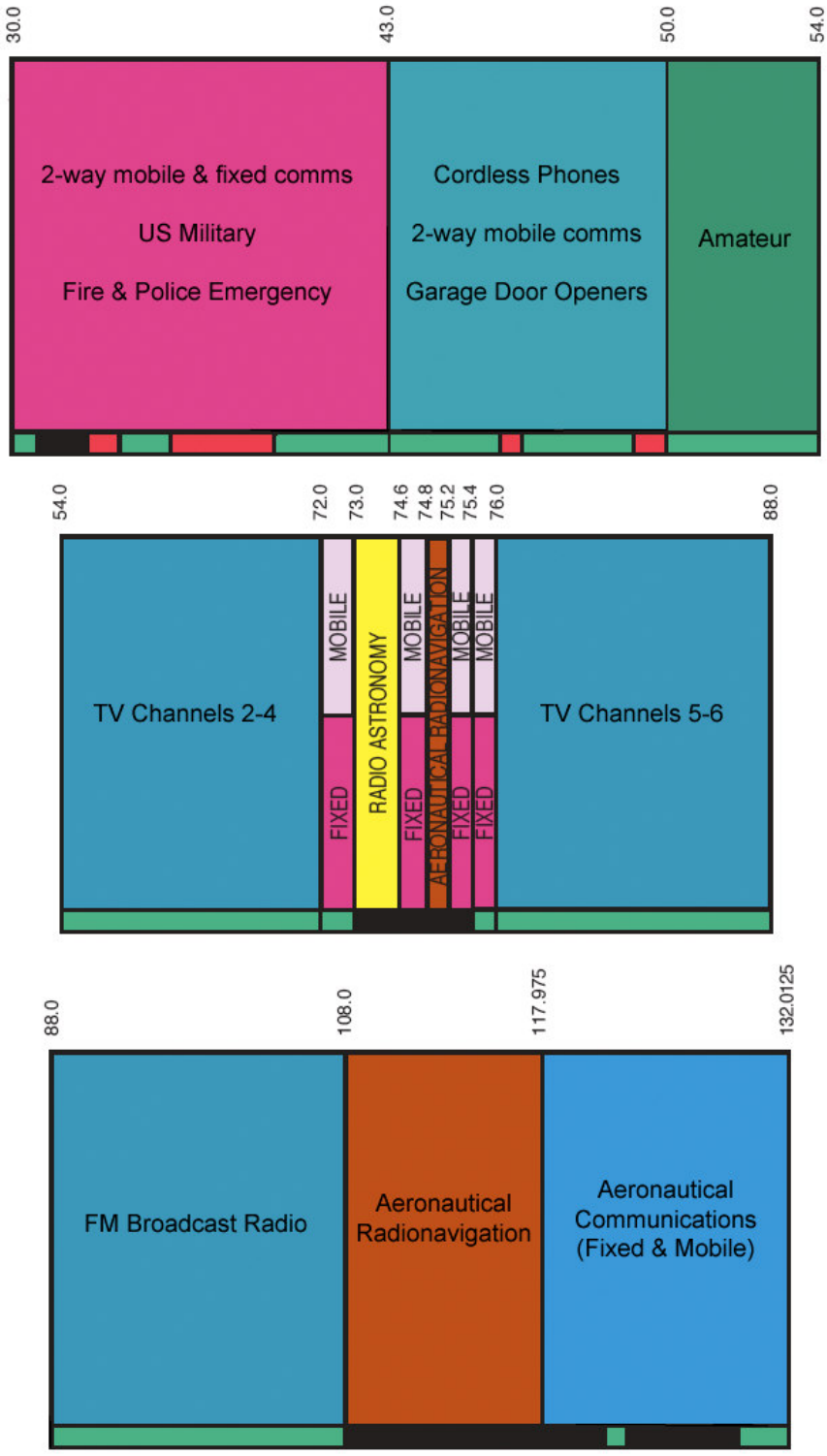

Figure 5.1. United States VHF frequency spectrum from 30 – 132 MHz. Adapted from http://www.ntia.doc.gov/osmhome/allochrt.html

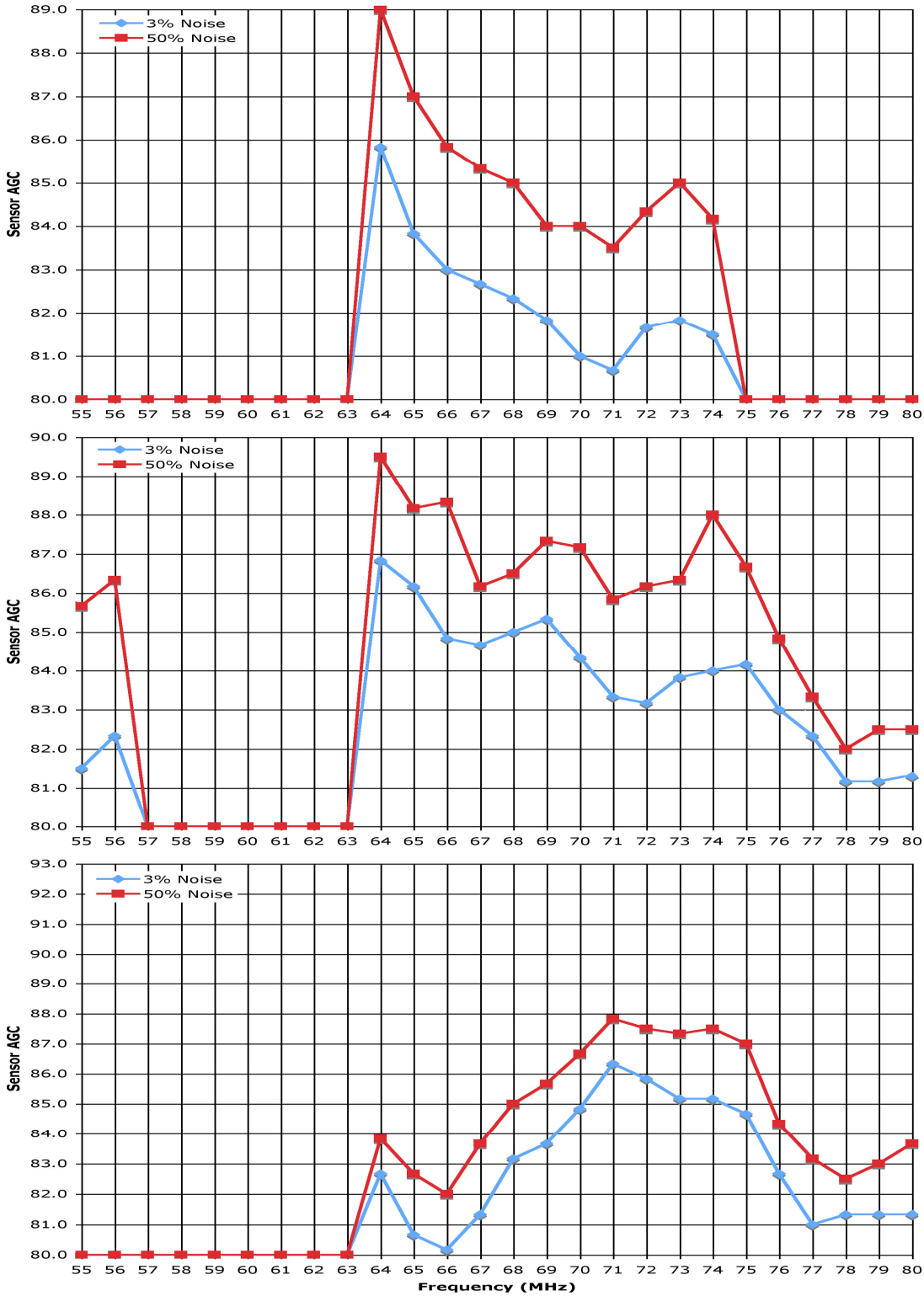

Figure 5.2. Noise surveys conducted at sensors located at: a) Impact Weather, b) Sugarland Airport, c) Cypress - Fairbanks High school for the 55-80 MHz frequency range. Note: A higher Sensor AGC indicates a higher sensor sensitivity / lower noise floor.

results from the noise surveys suggest the range from 65 – 74 Mhz was usable. From the spectrum analysis conducted during the original site surveys (Fig. 4.3), there are strong signals at 65 MHz and 73 MHz with a quiet region in-between centered at 69 MHz. With this information, all operational sensors were tuned to a center frequency of 69 MHz. The change in frequency did have the desired effect of greatly reducing the daily variation in noise levels. However, the change did not improve the overall sensitivity of the network. Unfortunately, a new but less frequent noise problem was introduced to the system.

Anomalous propagation of TV channel 4 occurs when a strong temperature inversion at the top of a shallow, cold front causes ducting of VHF radio transmissions. This causes the sudden increase in the number of non-lightning related VHF pulses to cross above sensor threshold settings. This rapid increase in noise levels, on the order of minutes, generally saturates the sensors causing them to output the maximum of 10,000 potential data points per second. With a large increase in random noise being detected by every sensor, the likelihood of false VHF lightning source detection increases. This would not be too much of a problem if it were not for the fact that most cold season thunderstorm systems are along the leading edge of cold frontal boundaries. Due to the general southeast to eastward propagation of cold fronts in SE Texas the increased noise levels are from San Antonio, TX approximately 350 kilometers away. Sensor noise levels are regularly monitored and their gains are adjusted as required to minimize noise contamination and thus sensor sensitivity may vary from day to day.

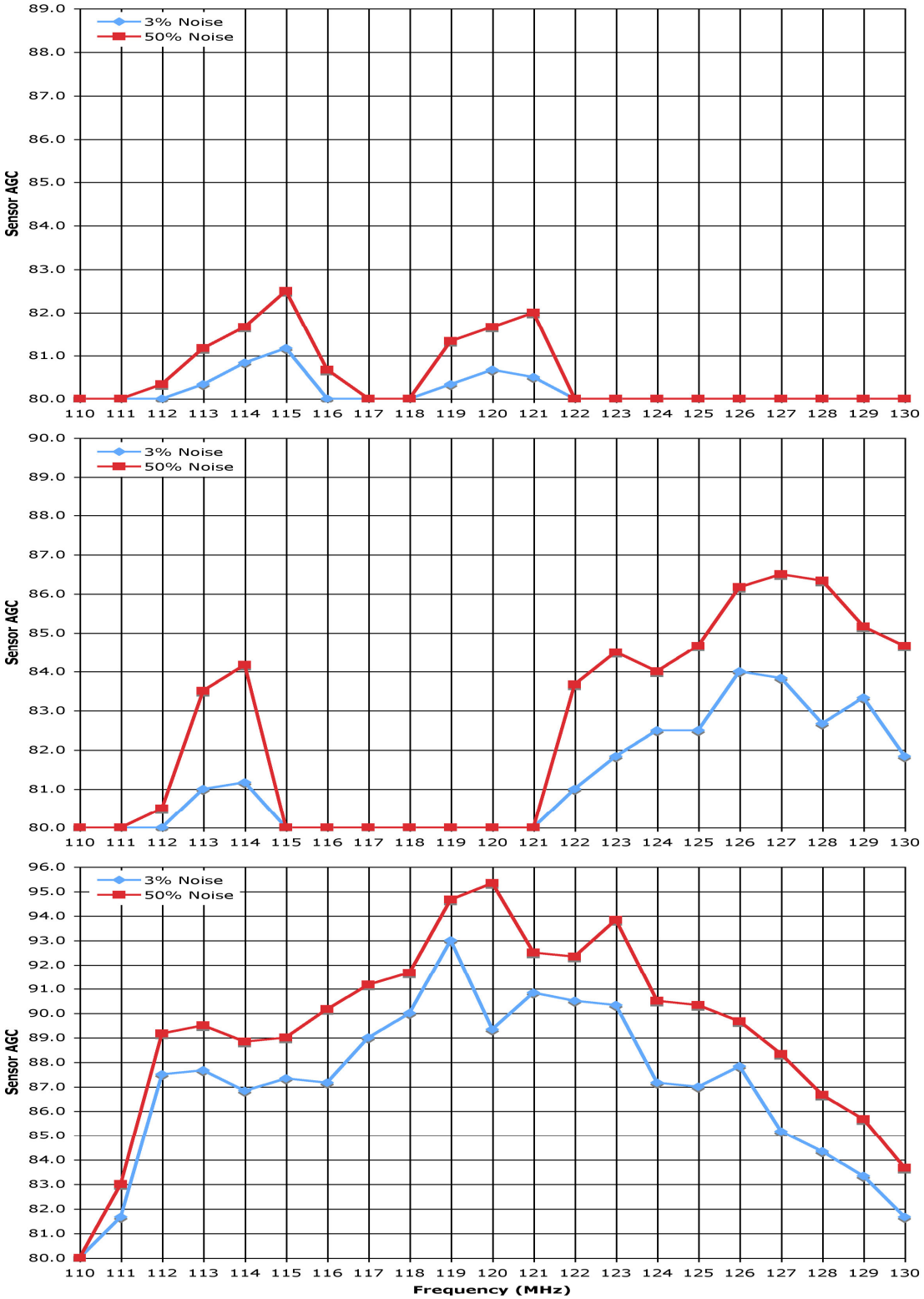

Figure 5.3. Same as Figure 5.2, except for the 110 – 130 MHz frequency range.

The LDAR sensors were originally designed to operate in the frequency range of 55 MHz to 80 MHz (TV Channels 2 – 5). For nearly one and half years, the Houston LDAR network remained operating at a center frequency of 69 MHz within the suggested operational frequency range. In early 2007, personal communications with Vaisala Inc. employees revealed the variable tuner was capable of operating from 30 MHz to 140 MHz, but had never been tested.

In an attempt to improve network performance, a new series of noise surveys were conducted on the fully operational, twelve sensor network in the aviation communication section of the VHF band (110 – 130 MHz). Figure 5.3 shows selected noise survey results from three sensors, which show that each sensor had different usable frequencies. Examination of noise surveys for all twelve sensors yielded a small frequency range near 114 that was common to all sensors. Unfortunately, the noise surveys indicated that a majority of the sensors would have significantly reduced gain settings (AGC) compared to 69 MHz.

The noise surveys were then conducted for the 30 – 55 MHz range. This frequency range is used by a wide variety of technology such as: cordless phones, pagers, and garage door openers. With this knowledge, the noise survey results presented in Figure 5.4 were quite surprising. For nearly every sensor, the noise floor was dramatically lower yielding higher sensor sensitivities (higher AGC values). In late March 2007, the operating frequency was switched to 40 MHz. Constant monitoring of noise levels for several months revealed little variation. This allows the network to run

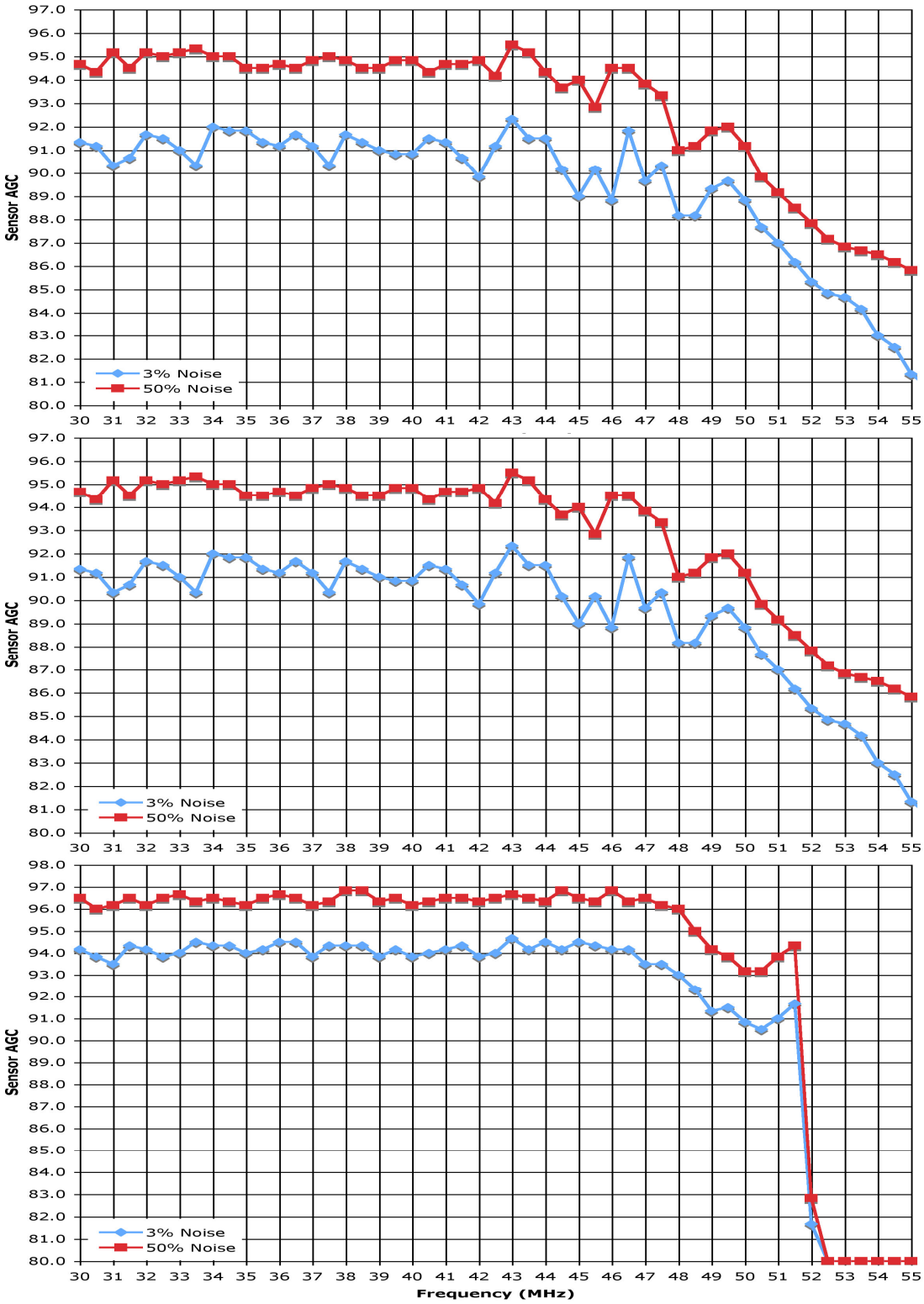

Figure 5.4. Same as Figure 5.2, except for the 30 – 55 MHz frequency range.

at fairly constant network performance, which should allow comparisons of storms from different days.

Before the Houston LDAR total lightning data is used for research purposes, it is necessary to analyze the networks performance. The three important performance metrics to be examined are the Houston network's VHF source detection efficiency, location accuracy, and effective range. The network performance will be examined for both the 69 MHz and 40 MHz frequencies in order to demonstrate changes in performance that occurred.

5.2. Location Accuracy

5.2.1. Network Timing Error

As noted by Thomas et al. [2004], the VHF source solution algorithm essentially solves the simple equation:

$$\Delta \text{ distance} = \text{velocity} * \Delta \text{ time} \tag{5.1}$$

From this simple equation, it is possible to lump all inaccurate measurements of sensor positions and imprecise estimates of the VHF pulse propagation velocity into the timing error. Obtaining the network's timing error and utilizing basic geometric models, reasonable estimates of the Houston LDAR network's VHF source location accuracies can be easily determined.

Recall from Section 2.3 that an LDAR network uses the arrival time of a VHF pulse detected by at least five sensors to determine the location and time (x,y,z,t) of the VHF pulse. By requiring at least six sensors involved in a VHF lightning source solution, it is possible to minimize the location uncertainty of the detected VHF sources

and eliminate most noise sources. This is accomplished by using the timing information from the additional sensors to minimize the chi-square goodness of fit value for the VHF source location given by the following equation:

$$\chi^2 = \sum_{i=1}^{N} \frac{(t_i^{obs} - t_i^{fit})^2}{\Delta t_{RMS}^2} \tag{5.2}$$

where t_i^{obs} is the measured arrival time at the i^{th} station, t_i is the predicted arrival time for each trial solution, and Δt^2_{RMS} is the uncertainty in the timing measurements [Thomas et al., 2004].

Although the actual Δt_{RMS} timing error is not known in advance, the timing error value determined by Carey et al. [2005] for the Dallas LDAR network of 75 ns is used as a good first guess. One method to determine a more precise value of the timing error is to plot the reduced chi-square errors, χ_v^2, of the VHF source solutions versus the theoretical reduced chi-square error distribution [Bevington and Robinson 2002]. The reduced chi-square error is simply given by the following equation:

$$\chi_v^2 = \chi^2 \Big/ \#\, df \tag{5.3}$$

where the *df,* degrees of freedom, is given by *df* = # of sensors – 4. The theoretical chi-square distribution is given by the equation:

$$\chi^2(x, df) = \frac{(1/2)^{df/2}}{\Gamma(df/2)}\, x^{(df/2)-1}\, e^{-x/2} \tag{5.4}$$

where Γ is the gamma function.

By adjusting the timing error value used in Equation (5.2), the reduced chi-square error values of the VHF source solutions can be adjusted to fit the theoretical distribution. This is accomplished by simply multiplying χ_ν^2 by (75 ns)^2 / (new Δt_{RMS})^2. The timing error value that produces the best fit to a theoretical chi-sqaure distribution is the best estimate of the LDAR network timing error. Because different sensors can have different magnitudes of positional and timing errors and not all sensors are functional during every storm and/or contribute to a VHF source solution, the timing error may differ day to day. However, it is expected that any change in the timing error should be relatively small.

5.2.2. Inside Network Location Accuracy

Estimates of location errors within the perimeter of the Houston LDAR sensors can be determined through simple geometric models and assumptions. The basic equation relating time ,t, and distance ,d, between the VHF source and sensor is simply:

$$d = \nu * t. \tag{5.5}$$

This basic equation, along with the estimate of the RMS timing error, Δt_{rms}, is the basis for determining the horizontal location accuracy. Inside the network perimeter, the uncertainty of the VHF source location is constrained by measurements of the VHF source location by several sensors from several different directions (Figure. 5.5a). With enough sensors, the location uncertainties from all of the sensors essentially produce a crude circle with a diameter of 2Δd around the VHF source. From this result and using the basic equation above, we get the estimated horizontal location error:

$$\Delta d = \nu * \Delta t_{rms}. \tag{5.6}$$

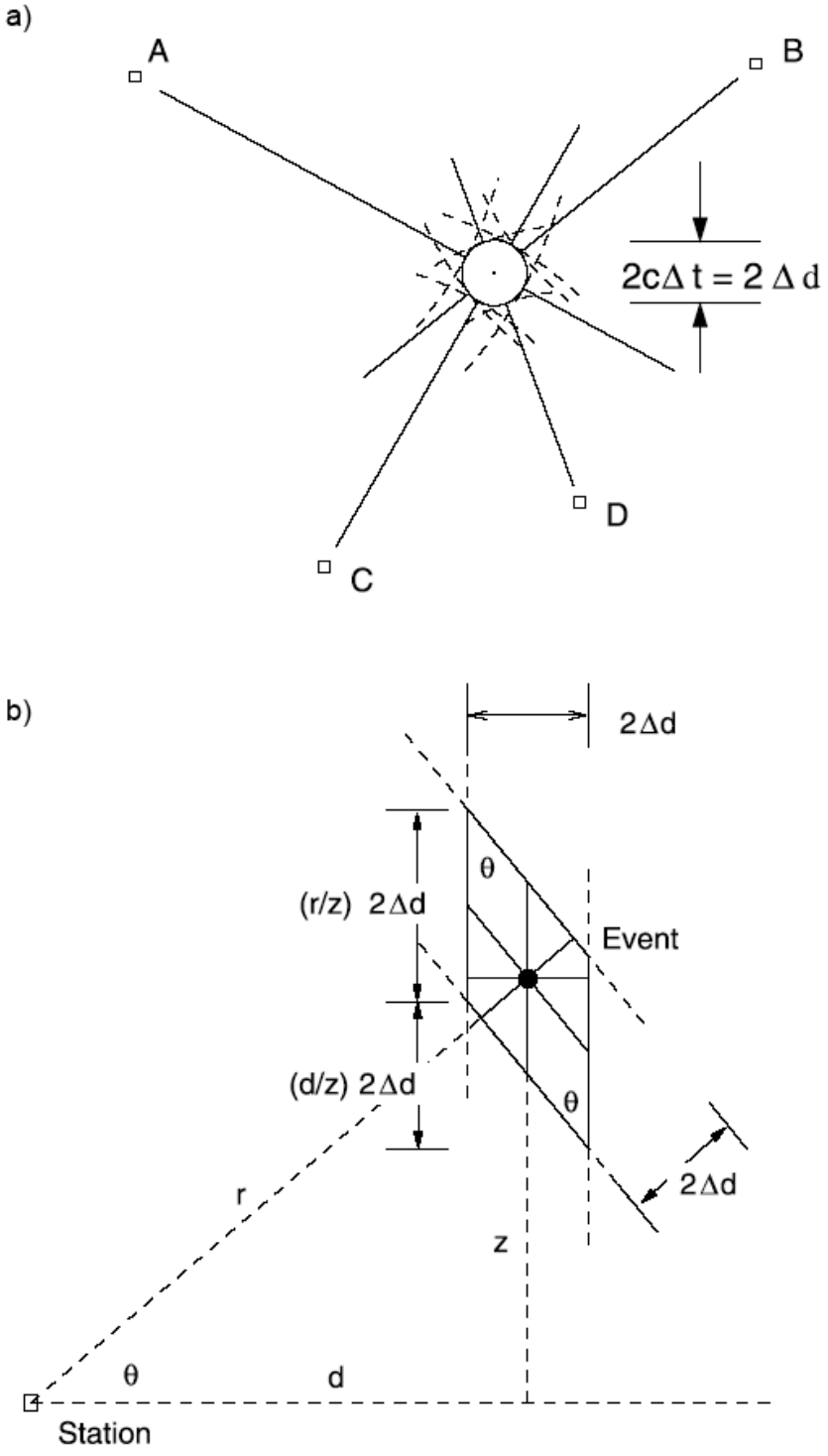

Figure 5.5. Graphical depictions showing the basic geometry used in determining the a) horizontal and b) vertical location accuracy of a VHF source within the boundary the Houston LDAR network (Adapted from Thomas et al. 2004).

Inside the network perimeter, the sensor closest to the VHF source is the primary sensor in determining the height of the VHF source. Figure 5.5b shows the basic geometry involved in estimating the VHF vertical location accuracy. From the determination of the horizontal location accuracy discussed above, the range uncertainty along the horizontal distance, d, is $2\Delta d$. In addition, the location uncertainty outward along the radial distance, r, from the sensor to the VHF source is $2\Delta d$. The parallelogram produced by these uncertainties around the VHF source allows the height uncertainty to be determined. Solving for the total vertical extent of the parallelogram gives the following equation:

$$\Delta z \cong \nu \Delta t_{rms} \left(\frac{d + r}{z} \right) \tag{5.7}$$

for the vertical uncertainty of the VHF source.

Thomas et al. [2004] tested the validity of these simple geometry models using a balloon born VHF transmitter and onboard GPS. Their analysis found that the simple model errors were generally in good agreement with the measured errors. The location uncertainties can also be determined from an error analysis of the original equations used to obtain the VHF source solutions (Eq. 2.5). Koshak et al. [2004] conducted a detailed study of these error estimates. Thomas et al. [2004] compared the results to the simple geometry solution and found fairly good agreement in the error estimates.

5.2.3. Outside Network Location Accuracy

Outside the network, there are three main errors to determine: range, azimuth angle, and elevation angle errors. A simple network layout of five sensors in the form of

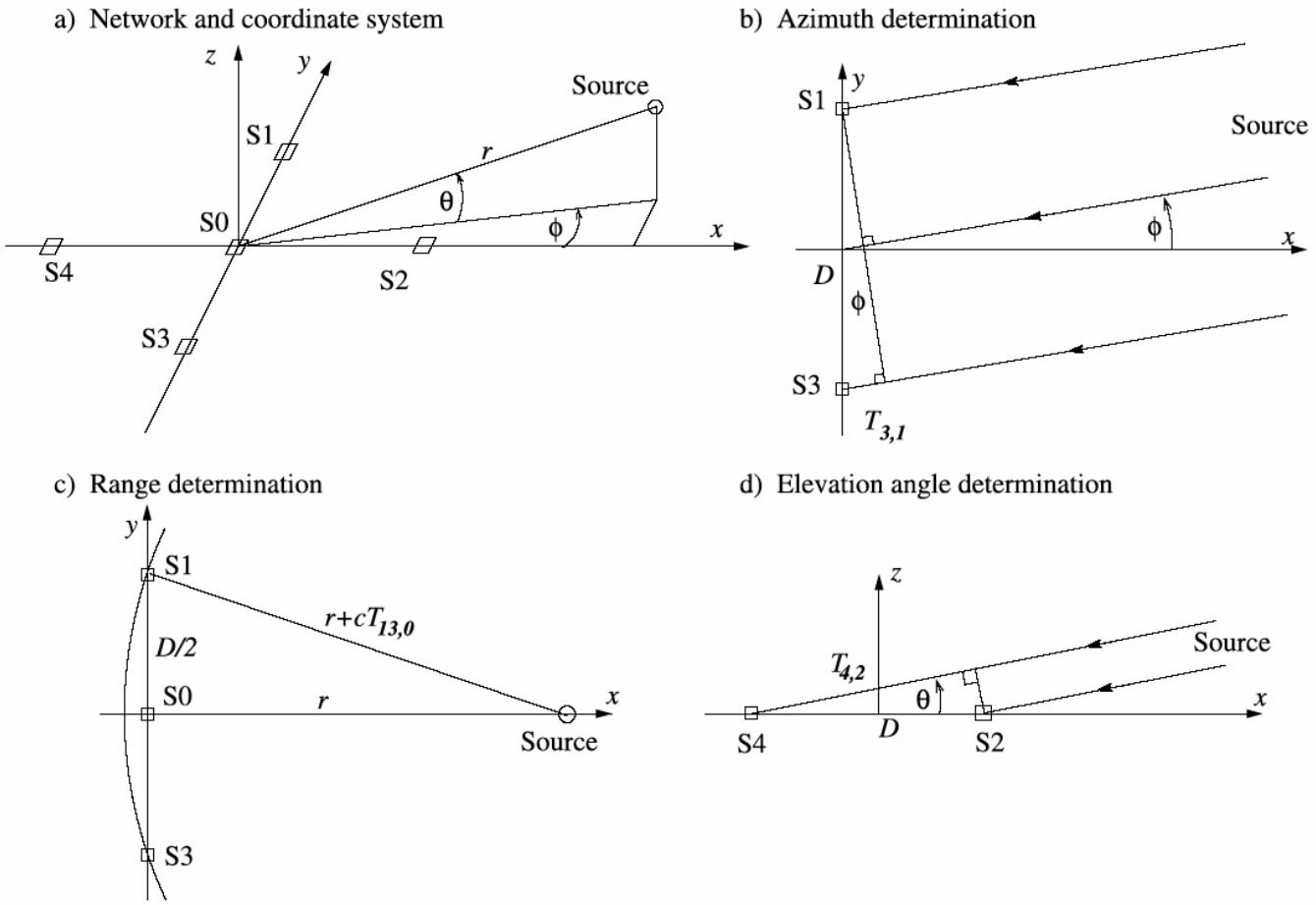

Figure 5.6. Graphical depictions showing a) the sensor and coordinate system layout and the basic geometry used in determining the b) azimuthal, c) horizontal range, and d) vertical location accuracy of a VHF source outside the perimeter of the Houston LDAR sensors (Adapted from Thomas et al. 2004).

a plus symbol is used to determine the estimates of these three errors (Fig. 5.6a). The results of this model should hold true for larger networks, as the geometry involved in the error analysis generally utilize the distance between the most distant sensors (essentially the network diameter).

In an LDAR network, the azimuth angle and associated error are determined by the pair of stations with the greatest separation and is closest to being perpendicular to the incoming signal. For a first order approximation the incoming signal is assumed to have a planar wavefront (Fig.5.6b). Using the simple network model the azimuth angle is given by:

$$\sin\phi = \frac{v\, t_{13}}{D}. \tag{5.8}$$

From this equation and assuming a small angle, ϕ, we obtain the following azimuth angle uncertainty, $\Delta\phi$, relationship with the arrival time difference, Δt_{13}:

$$\Delta\phi = \left(1/D\right) v\, t_{13}. \tag{5.9}$$

The resulting error in the y-direction would be:

$$\Delta y = r\Delta\phi = \left(r/D\right) v\, \Delta t_{13}. \tag{5.10}$$

Assuming ϕ is a small angle, the error in the y-direction is roughly the location uncertainty perpendicular to the VHF source's range.

The range of a VHF source is essentially determined by the curvature of the wavefront of the VHF pulse (Fig. 5.6c). To achieve a simple, easy to determine approximation for the curvature, it is assumed that the VHF source lies along the x-axis. This setup means that the wavefront from the VHF source will first be detected by

sensor S0, then later in time by sensors S1 & S2. The time difference between S1 & S0, Δt_{15}, (or S2 & S0) gives a measure of the wavefront's curvature. The distance from S0 to the VHF source is, r, the distance from S1 to the VHF source is, $r + \nu t_{01}$, and the distance between the two sensors is half of the network diameter, D/2. This forms a right triangle that when solved for the radial distance, r, gives:

$$r \cong \frac{D^2}{8\nu t_{01}} \tag{5.11}$$

and the differential of equation (5.11) gives the equation for the estimate of the range uncertainty:

$$\Delta r = 8\left(\frac{r}{D}\right)^2 \nu \Delta t_{01} \tag{5.12}$$

where $\Delta t_{01} = \sqrt{2}\Delta t_{rms}$.

The elevation angle and associated angle uncertainty is obtained in a similar manner as the azimuth angle. Using the simple network model, the elevation angle is determined using the stations with the greatest separation along the direction of the VHF source (Fig. 5.6d) and the radiation wavefront is again assumed to be planar. Knowing the difference between the arrival times at the two stations and the horizontal distance between the two stations, the elevation angle is given by the following:

$$\cos\theta = \nu t_{24} / D. \tag{5.13}$$

From this the uncertainty in the elevation angle is given as:

$$\Delta\theta = \frac{\nu \Delta t_{24}}{D\sin\theta} \cong \frac{r\nu\Delta t_{24}}{Dz}. \tag{5.14}$$

Notice that, unlike the azimuth angle, small errors in the time difference will produce a relatively large error in the elevation angle error.

The height uncertainty, Δz, is composed of the elevation angle and range uncertainties. The height uncertainty associated with the elevation uncertainty is:

$$\Delta z_\theta = r\Delta\theta = \frac{r^2}{Dz} v\Delta t_{42} \tag{5.15}$$

and the height uncertainty due to the range error is given by:

$$\Delta z_r = \sin\theta\Delta r = \frac{8zr}{D^2} v\Delta t_{01}. \tag{5.16}$$

Given that the diameter of the Houston LDAR network is roughly 75 km, it can be determined that the relative contributions of each of these height uncertainties. For a VHF source at a height of 10 km and range of 120 km, Δz_θ is roughly 11 times greater than Δz_r. Therefore it is reasonable to use only Δz_θ as the height uncertainty for a VHF source outside the network.

5.3. Detection Efficiency

5.3.1. Sources of an LDAR Network's Detection Efficiency Profile

There are three main contributors that can reduce the network's detection efficiency. The first is due to the line of sight nature VHF radiation propagation. This implies that any solid objects in the path between VHF source and the sensor blocks the VHF signal. In the case of an LDAR sensor, this means that objects, such as buildings or rows of trees that are blocking the horizon near the sensors will limit the minimum detectable height of a VHF pulse. Figure 5.7 Illustrates how objects blocking line of sight contribute to the loss in detection of low altitude VHF sources.

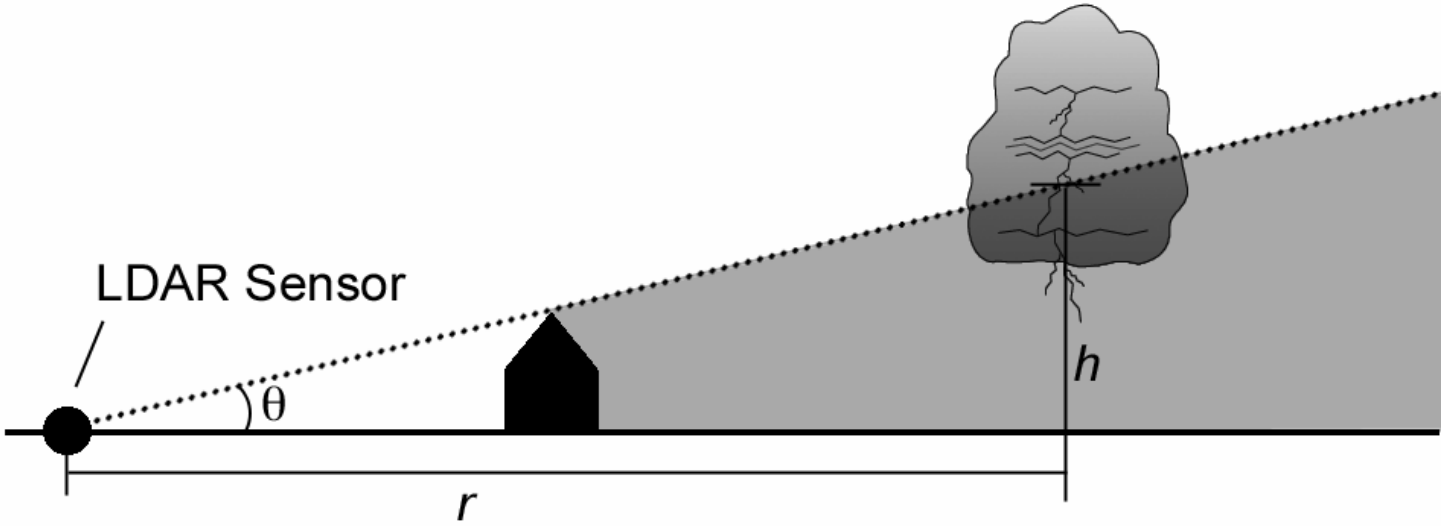

Figure 5.7 Illustration depicting the blockage of low altitude detection of VHF lightning sources in a thunderstorm due to nearby obstructions. VHF lightning sources occurring in the gray shaded region can not be detected by the LDAR sensor.

Sensor sites for the Houston LDAR network were selected to minimize this by limiting line of sight blockage to no more than 1^{O} above the horizon. Basic geometry shows that at a distance of 100km (200 km), the network would be unable to detect sources below 1.7 km (3.4 km) in height. Observations of storms over the network show that roughly 90 – 95% of sources detected by the Houston LDAR network are located above 4 km in altitude. This suggests that line of sight should not hinder the network's detection efficiency, except for very distant (> 300 km) storms.

The next contributor is based on each LDAR sensor's minimum detectable signal (MDS). The local level of VHF noise at each sensor site determines the minimum detectable signal. Each sensor has a configurable detected power threshold setting that marks the division between noise and a possible VHF lightning pulse. Therefore, less local VHF noise at an LDAR site leads to an increase in ability to detect weaker VHF lightning sources. In the case of an LDAR sensor, the minimum detectable signal (minimum received power detectable at the antenna) is determined by the sensor's AGC gain setting (Figure 5.8). The equations for determining a sensor's MDS (in units of dBm) are as follows:

$$\begin{array}{ll} \mathrm{AGC} \le 90 & \mathrm{MDS} = -32 - 0.6(\mathrm{AGC} - 40) \\ 90 < \mathrm{AGC} \le 110 & \mathrm{MDS} = -62 - 0.9(\mathrm{AGC} - 90) \\ 110 < \mathrm{AGC} & \mathrm{MDS} = -80 - 0.5(\mathrm{AGC} - 110) \end{array} \qquad (5.17)$$

Recall from Section 4.1 that a sensor's AGC is set to a value that positions the sensor's pulse detection threshold at or slightly above the local noise floor, therefore the MDS can be determined directly by the gain setting.

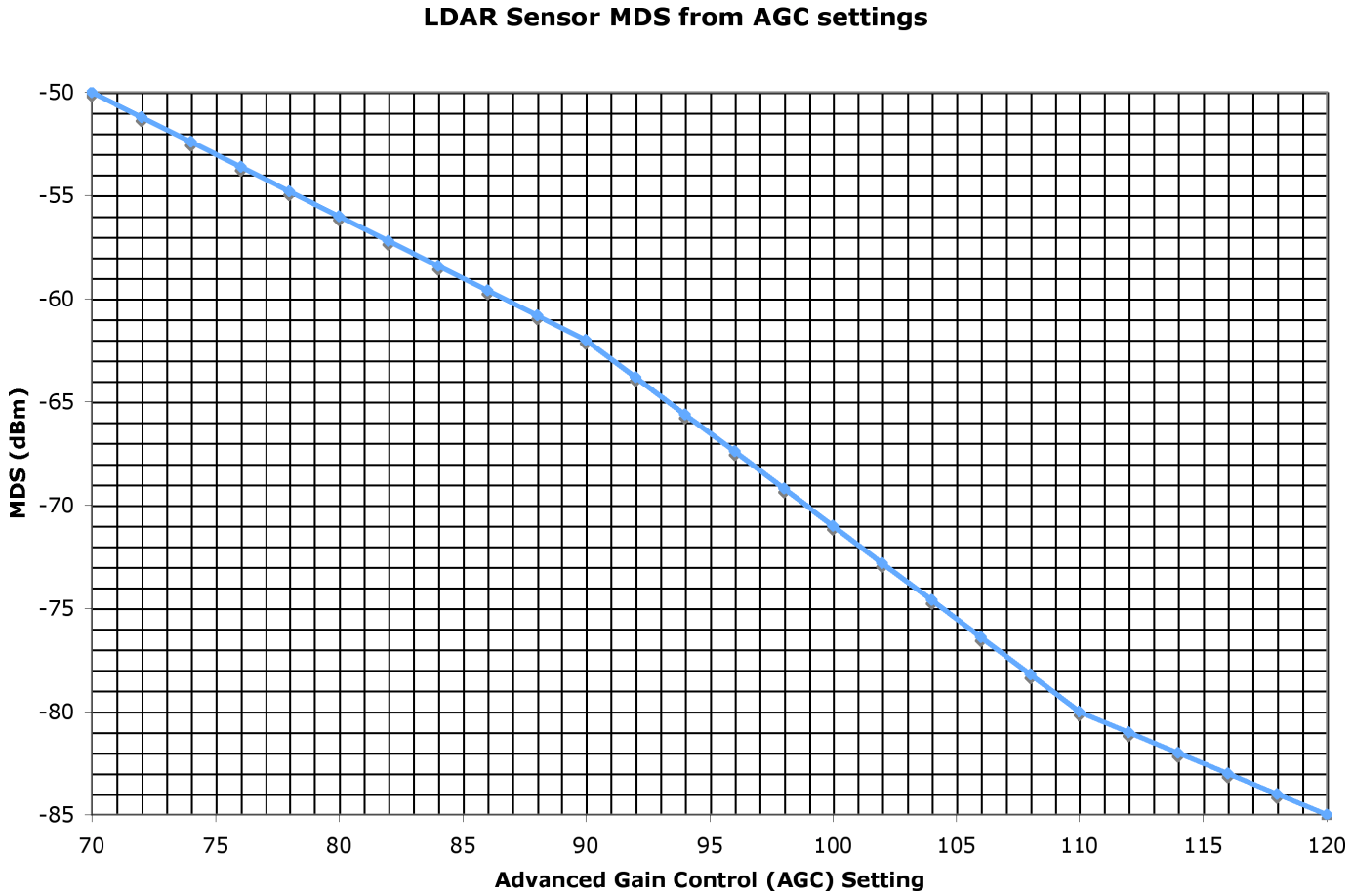

Figure 5.8. Plot of LDAR Advanced Gain Control (AGC) versus the LDAR antenna's minimum detectable signal in dBm.

The last major contributor to any change in detection efficiency is due to VHF signal attenuation. A VHF lightning pulse is treated as an isotropic radiator and the power per unit area at a distance, *r*, from the pulse is given by $P_s/4\pi r^2$, where P_s is the VHF source power at the pulse's origin. The received power at the antenna is a function of the effective area of the antenna, A_{eff}, and the power per unit area of the original VHF pulse at the antenna:

$$P_r = A_{eff}\frac{P_s}{4\pi r^2}. \tag{5.18}$$

Knowing that each sensor has a minimum detectable signal at the antenna, P_{min}, equation (5.18) can be rearranged to show that the minimum detectable VHF source power increases at a rate of the distance, r, squared.

$$P_s = P_{\min}\frac{4\pi r^2}{A_{eff}} \tag{5.19}$$

This equates to the loss in detection of weaker VHF lightning sources at distant ranges. Using equation (5.19) for each functional sensor, it is possible to map the minimum detectable VHF source power by at least six LDAR sensors at any location. Producing these maps for different network configurations (frequency and/or AGC) provide useful insight to changes in detection sensitivity that can be expected.

5.3.2. Detection Efficiency / Network Sensitivity

From the previous section, knowing the received power, P_r, at the antenna and the antenna's effective area, it is possible to calculate the VHF lightning source's power. The antenna's effective area is related to the antenna gain, *G*, and wavelength of the radiation, λ, by:

$$A_{eff} = G\left(\frac{\lambda^2}{4\pi}\right). \tag{5.20}$$

Combining equations (5.18) and (5.20), the resultant equation for the VHF lighting source power is:

$$P_s = P_r \frac{(4\pi r)^2}{G\lambda^2}. \tag{5.21}$$

The Houston LDAR network performs this calculation automatically for every LDAR source detected and takes into consideration the antenna gain pattern. This allows the examination of the distribution of VHF source powers.

One method of estimating the detection efficiency of the Houston LDAR network is to examine the VHF source power distribution. As previously stated, the value minimum detectable VHF source power will increase the further out a storm is from the network. Therefore, as distance from the network increases, it is expected that the lower end of the power distribution will be lost. Utilizing the same method used by Carey et al. [2005], it is possible to estimate the detection efficiency at any range from the center of the network. The method examines the source power distribution in specific range rings of a width corresponding to no more than 1 dB of minimum source power detection loss and a ring spacing corresponding to a 2 dB detection loss.

Within the perimeter outlined by the sensor locations, the network detection efficiency is rather uniform [Carey et al., 2005]. Any range rings within the perimeter can be grouped together to form a composite distribution and make the assumption that the effective detection efficiency over the network is 100%. To determine the effective

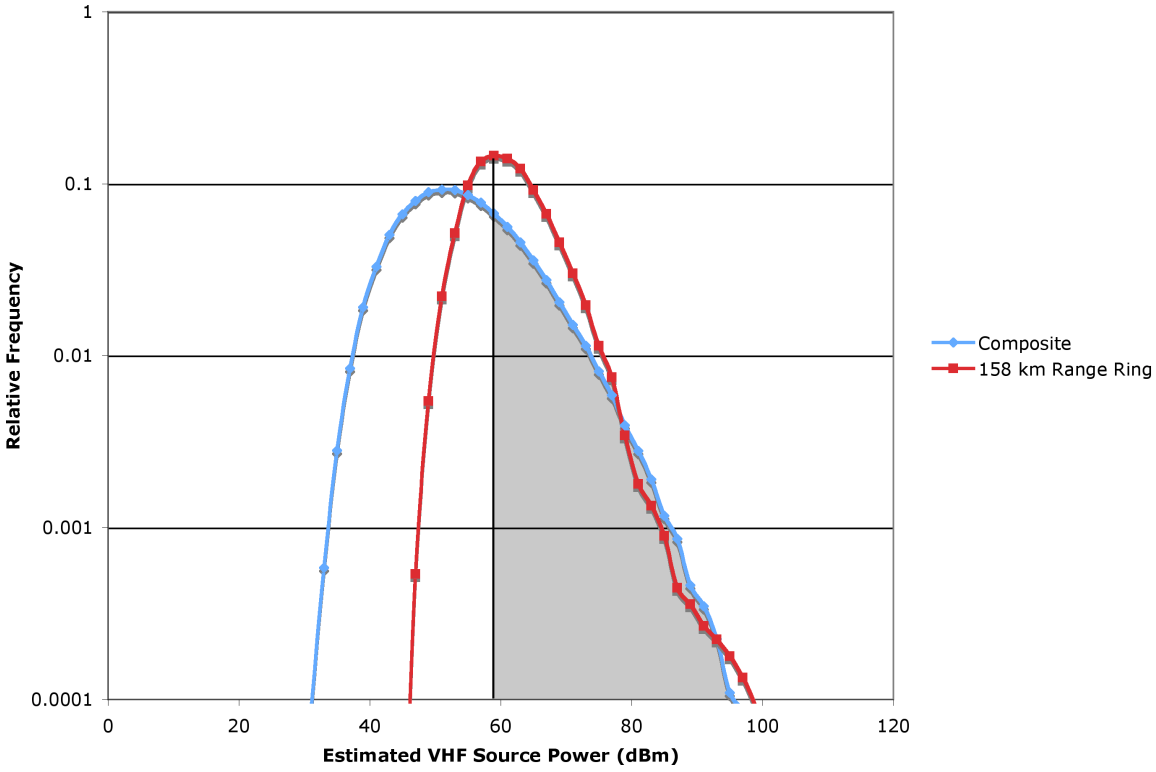

Figure 5.9. Example showing the method of integration used to estimate network detection efficiency. The area under the composite curve is integrated from the mode outer range ring distribution.

detection efficiency outside the network perimeter, the composite distribution is integrated for all powers at and above the mode of the distant range ring (Figure 5.9).

A variation of the method listed above can be used to examine the change in detection efficiency due to the various changes in sensor tuning detailed in Section 5.1. In this case, source power distributions composed of all detected VHF sources from 0 – 30 km from the center of the network. Using the power value of the mode of each distribution, the effective change in the network detection efficiency can be determined. In theory, given source power distributions from two LDAR networks, it would be possible to evaluate the relative difference in detection efficiency. Due to differing assumptions in calculating VHF source powers, this method can not be used to compare the Houston LDAR system to other VHF TOA systems.

Caution to the accuracy of this method must be mentioned. Boccippio et al. [2001] used the fall-off in source density over a long period of time (over 1½ years) to infer the distribution of source amplitudes. The inferred distribution disagreed significantly with the source power distribution determined from the measurement of received power at the antenna. The discrepancy suggests an unknown signal loss that must be taken into account. Carey et al. [2005] noted that although the distributions did not agree, the general decrease in detection efficiency with range from both methods were generally in good agreement. The Houston LDAR network does not currently have data from a sufficiently long enough period of time at a consistent network configuration to perform a source density analysis to determine the fall off in detection efficiency.

Until a suitable data set has been accumulated, the source power distribution method can be used to give a reasonable estimate of the network detection efficiency.

5.4. Network Range

Depending on the intended use of the LDAR data, the network range limit can be based on a specific loss in detection efficiency or upper limit in location accuracy. For real-time use, forecasters are interested in changes in intensity / frequency of lightning. In this case, a network range limit based on detection efficiency is logical. For research purposes, the location accuracy of sources is also important to compare the three-dimensional lightning structure with other storm related structures. Therefore a network range limit that considers both detection efficiency and location accuracy is required. To date, a concrete method or calculation of a LDAR network's range is not known to exist. General discussions between various scientists have yielded opinions that have been incorporated into a simple guideline used by researchers at Texas A&M.

The first limit on network range is based on the median location accuracy (median value for sources located between 3 – 12 km in altitude at a fixed horizontal location) at a specific network range. The upper limit of the median location accuracy used for the Houston network is 1 km. The second limit is not set by a specific value of effective detection efficiency, but does produce similar results. The reason for not using detection efficiency is due to the fact that, in the past, source powers were not regularly determined for the Houston LDAR network. Instead, storm systems that traverse the network and remain at nearly constant radar intensity throughout the time period are examined. The method uses the same range rings from the detection efficiency analysis.

However, only the total number of VHF sources is examined for each range ring is analyzed. These total source count values are then compared to the area of each range ring. Following the assumption that nearly constant radar intensity equals nearly constant lightning activity, the total VHF source count curve should follow the same trend as the range ring area. The range ring where the total source count no longer follows this trend by exhibiting a sharp decrease in total sources defines the second limit to the network range.

5.5. Houston LDAR & Radar Data

The Houston LDAR system became operational in mid July 2005. Due to the inexperience in operating the LDAR network, some configuration settings, for the first several months, needed for network performance analysis were not routinely kept. The first available LDAR data that can be used to analyze network performance is 2005 October 31. The data from this day is particularly useful due to the nature of the storm system. The system in question was a linear mesoscale convective system (MCS), which developed several hundred kilometers away from the Houston LDAR network and traveled across the center of the network. This storm system type became the standard for all network performance analysis for each of the main LDAR frequency / gain configurations over the last couple of years. The other storms day that will be used occurred on 2006 April 21 and 2007 April 25.

Level-II WSR-88D reflectivity data from KHGX, which is available from the National Climatic Data Center (NCDC), was used to analyze the reflectivity structure of the MCSs in our area of interest around the Houston LDAR network. In all cases, the

KHGX was operating under Volume Coverage Pattern 11 (VCP-11) as the MCS passed within range. VCP-11 makes 14 unique elevation scans (0.5 – 19.5) in five minutes [Crum et al., 1993; Brown et al., 2000]. Using REORDER software [Oye and Case, 1995], the radar reflectivity data were converted from radar coordinates to Cartesian coordinates with a horizontal and vertical grid spacing of 1.0 km [Miller et al., 1986]. Interpolation was accomplished with a Cressman weighting scheme [Cressman, 1959]. After multiple tests, a horizontal and vertical radius of influence of 2.0 km was used. The radar for the entire life of each MCS was grouped together to produce plots of mean radar reflectivity as a function of range from the center of the LDAR network. This type of plot is useful in comparing the changes in LDAR VHF source density with changes in storm reflectivity changes.

6. NETWORK PERFORMANCE RESULTS

6.1. Location Accuracy

The first step in determining the location accuracy of the Houston LDAR network is plot the distribution of the χ_ν^2, reduced goodness-of-fit, values against a theoretical χ^2 distribution. Recall from Section 5.2 that the reduced chi-square error is simply:

$$\chi_\nu^2 = \chi^2 \Big/ \#\, df, \tag{6.1}$$

where df = # of sensors involved in solution – 4. This means that a plot of the χ_ν^2 distribution is required for 6, 7, & 8 sensor solutions. It is noted that solutions involving more than 8 sensors does occur, however the numbers are too small to create meaningful distributions.

The original results of the reduced chi-square error distributions for 31 October 2005 (Figure 6.1) show that 6 sensor solutions have an RMS timing error, Δt_{RMS}, of approximately 90 ns. VHF sources detected by 7 sensors had a significant reduction in timing error to 70 ns and 8 sensor solutions had the best timing error of 60 ns. Using the RMS timing error for the 6 sensor solutions to determine the worst-case location accuracy, plots of the radial (Figure 6.2), azimuthal (Figure 6.3), vertical location accuracy at 3 km (Figure 6.4) and 12 km (Figure 6.5), and the three-dimensional median location accuracy (Figure 6.6) between 3 – 12 km are made. Figures 6.4 and 6.5 show that the vertical location accuracy increases with increasing altitude, as is expected from Equation (5.15).

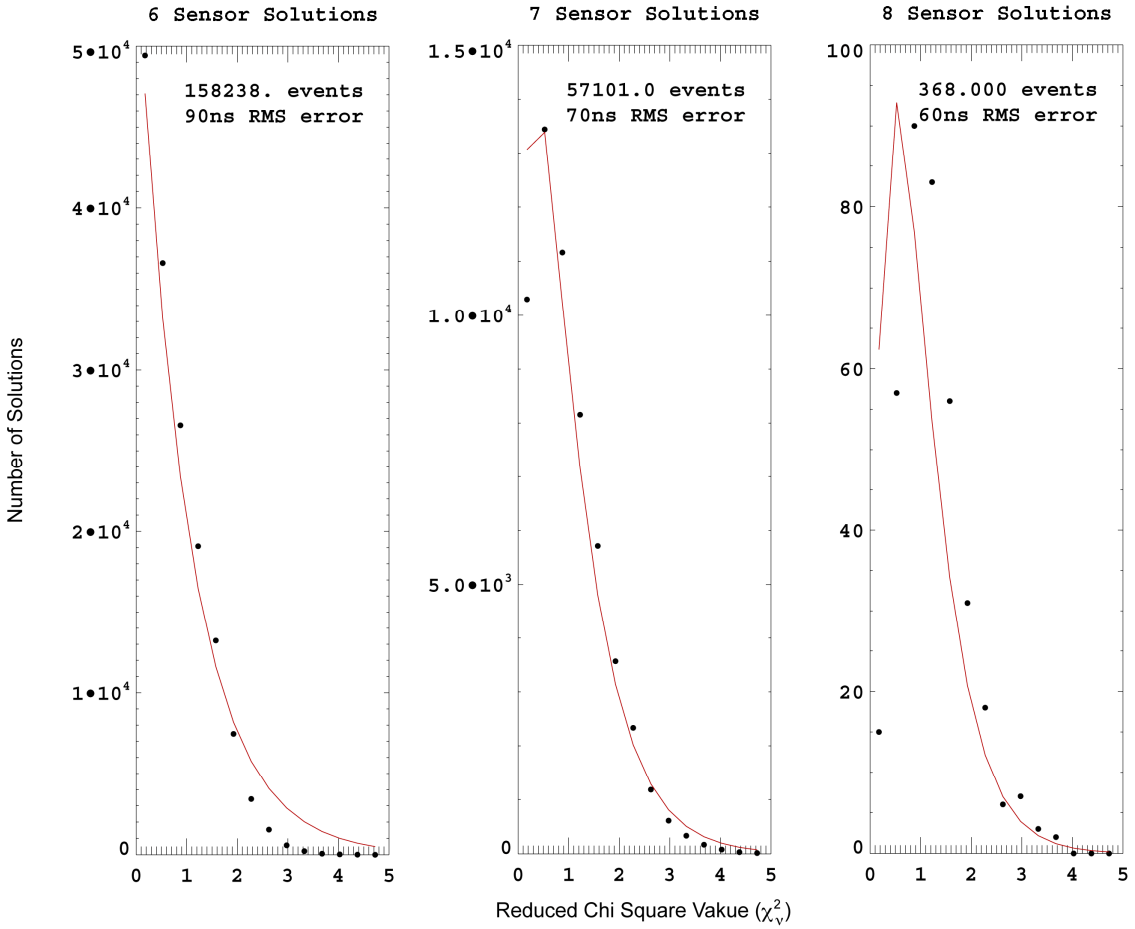

Figure 6.1. Histograms of χ^2 values for 6, 7 & 8 sensor solutions (black dots) fitted to theoretical χ^2 probability distributions (red lines) for October 31, 2005 before LDAR sensor site location adjustments.

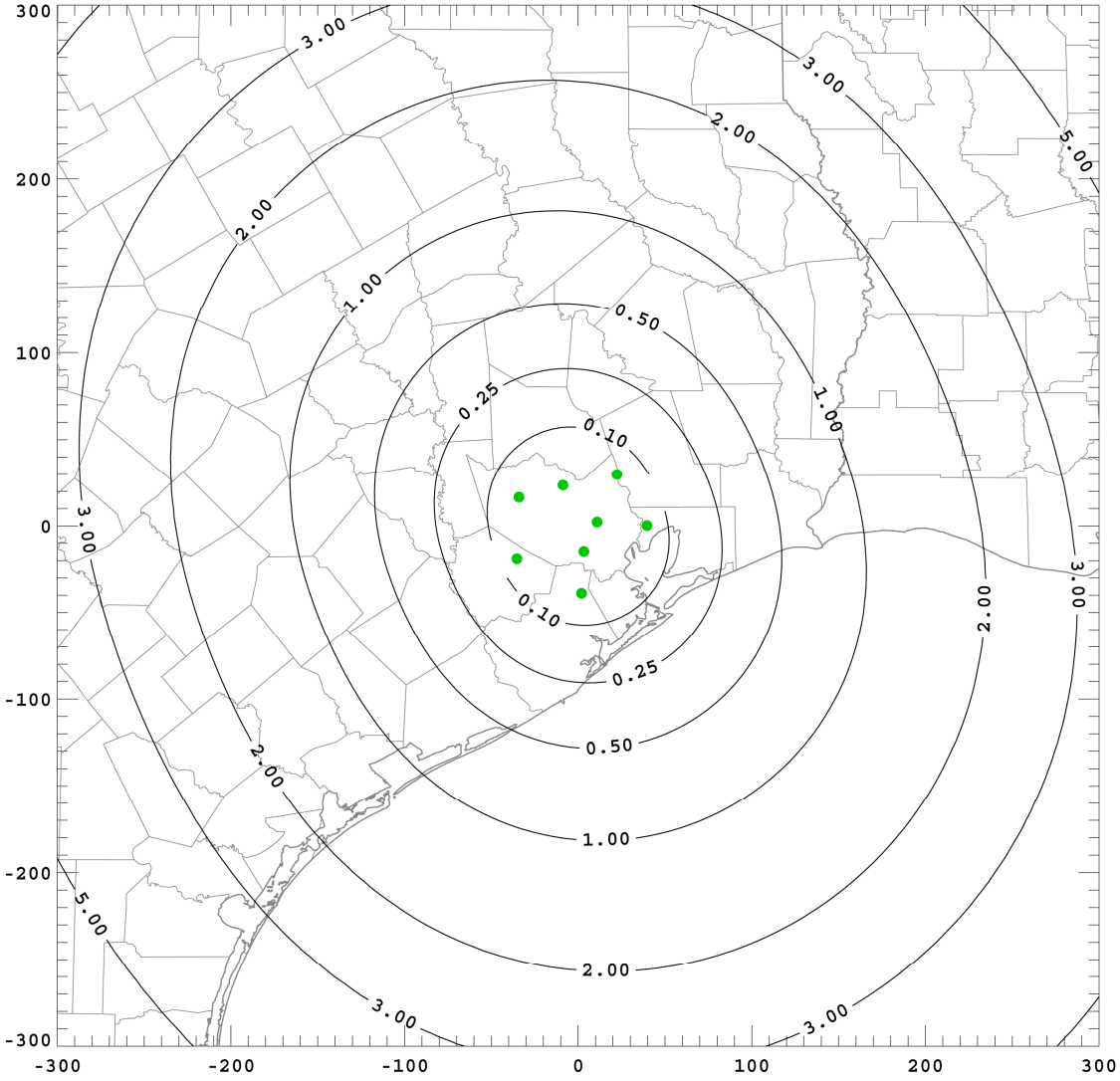

Figure 6.2. Radial location accuracy of VHF sources on October 31, 2005 with a network RMS timing error of 90 ns. Units and distances are in kilometers.

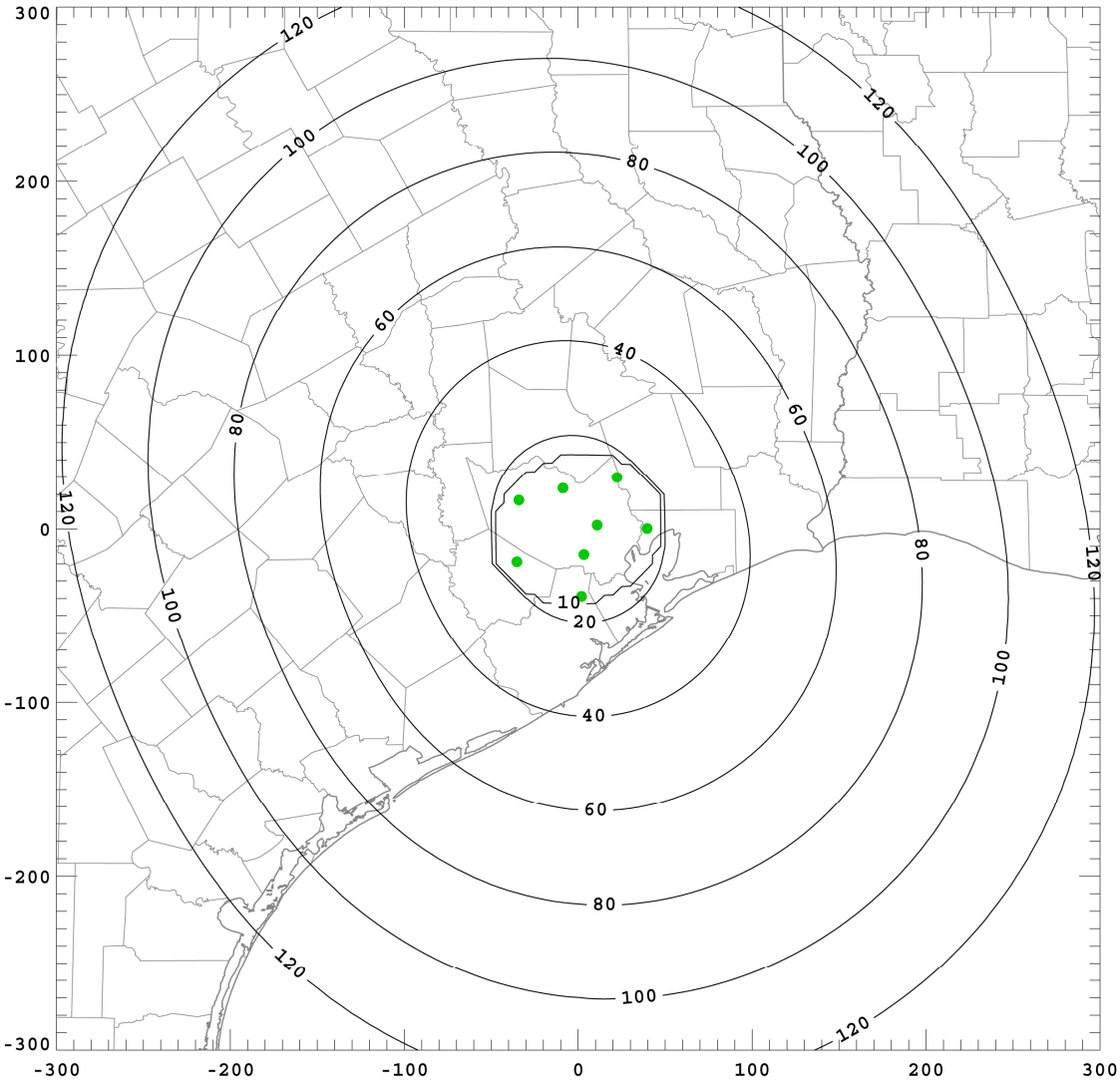

Figure 6.3. Azimuthal location accuracy of VHF sources on October 31, 2005 with a network RMS timing error of 90 ns. Units and distances are in kilometers.

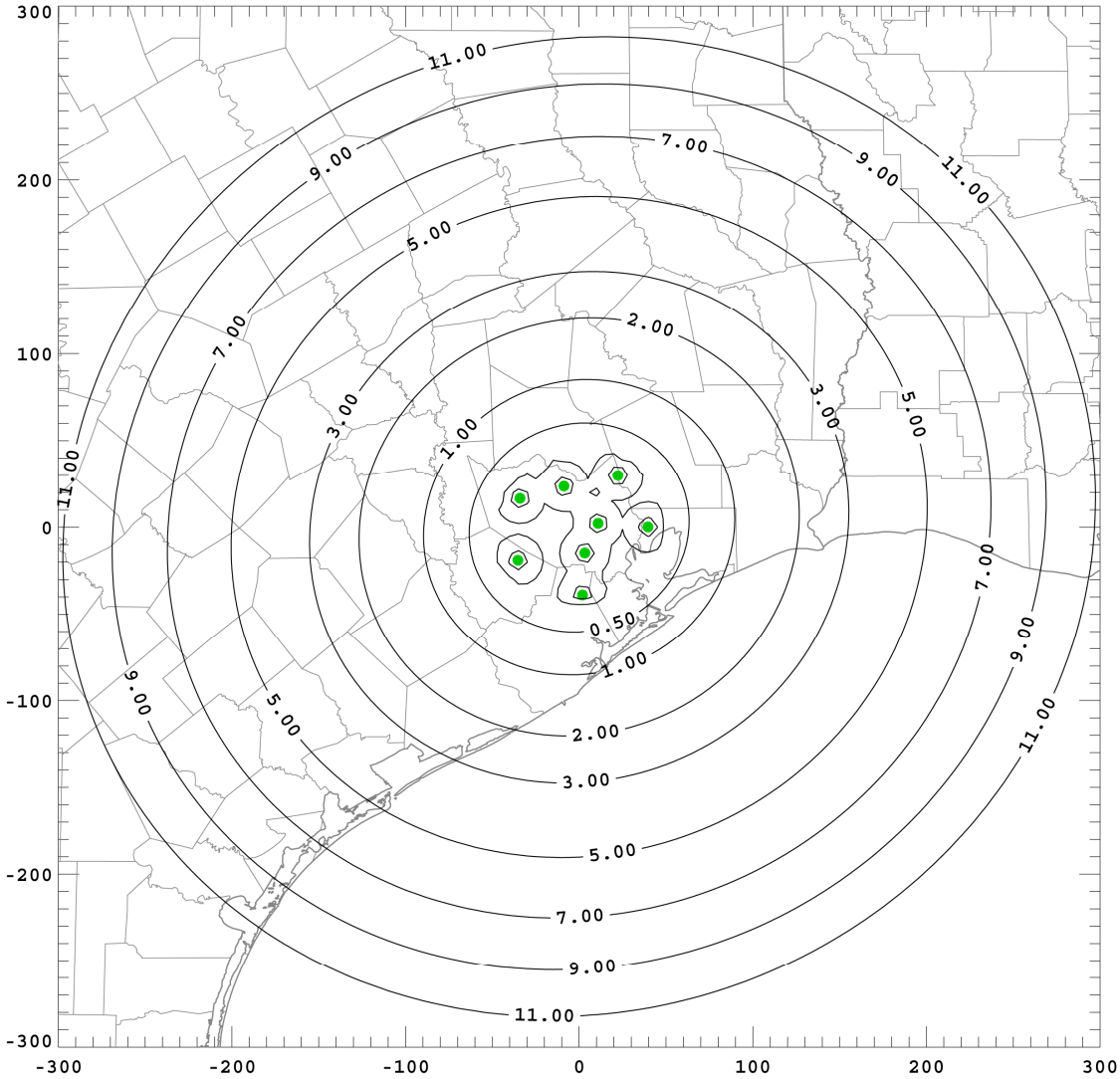

Figure 6.4. Vertical location accuracy of VHF sources on October 31, 2005 at an altitude of 3 km and a network RMS timing error of 90 ns. Units and distances are in kilometers.

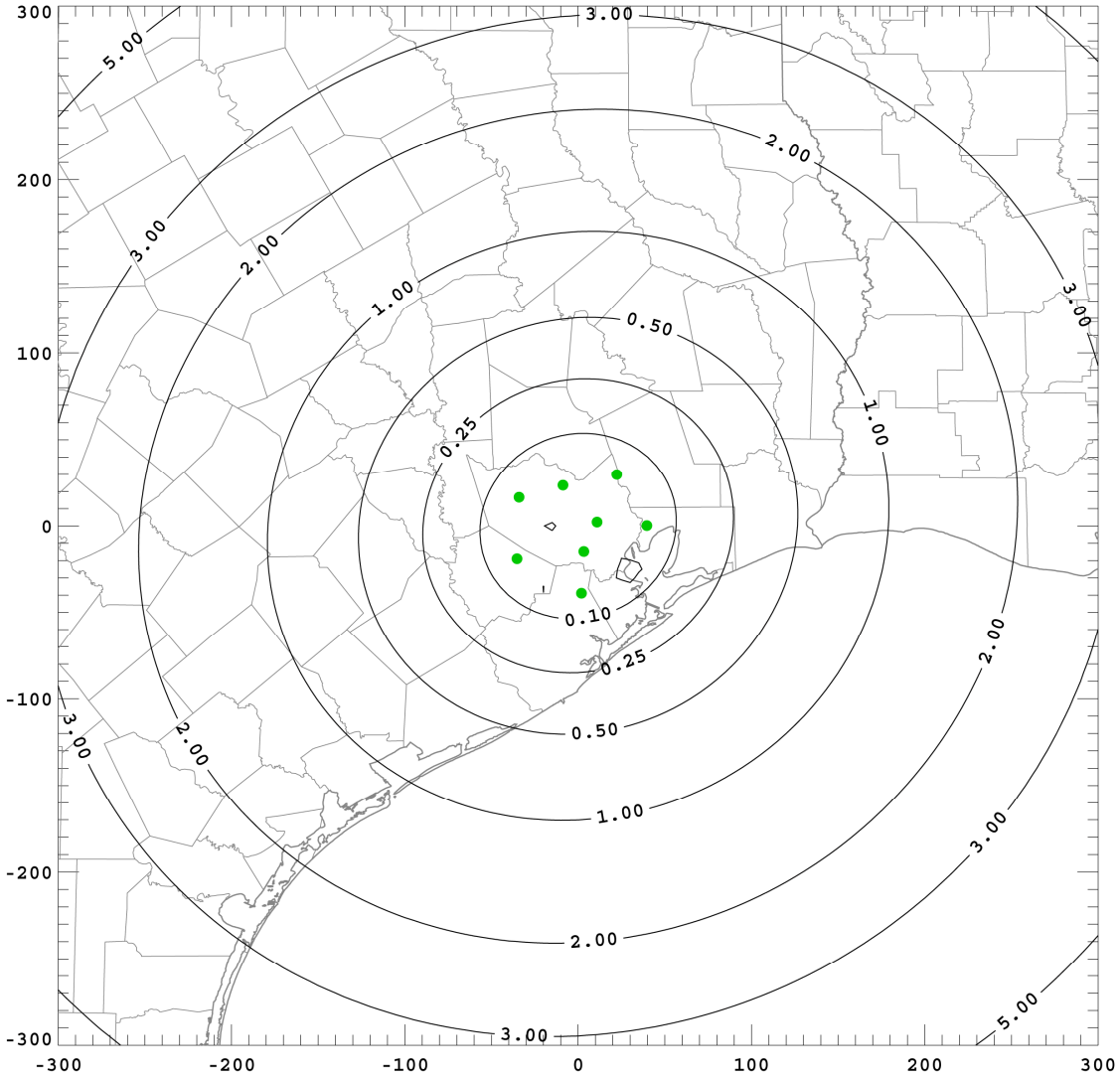

Figure 6.5. Vertical location accuracy of VHF sources on October 31, 2005 at an altitude of 12 km and a network RMS timing error of 90 ns. Units and distances are in kilometers.

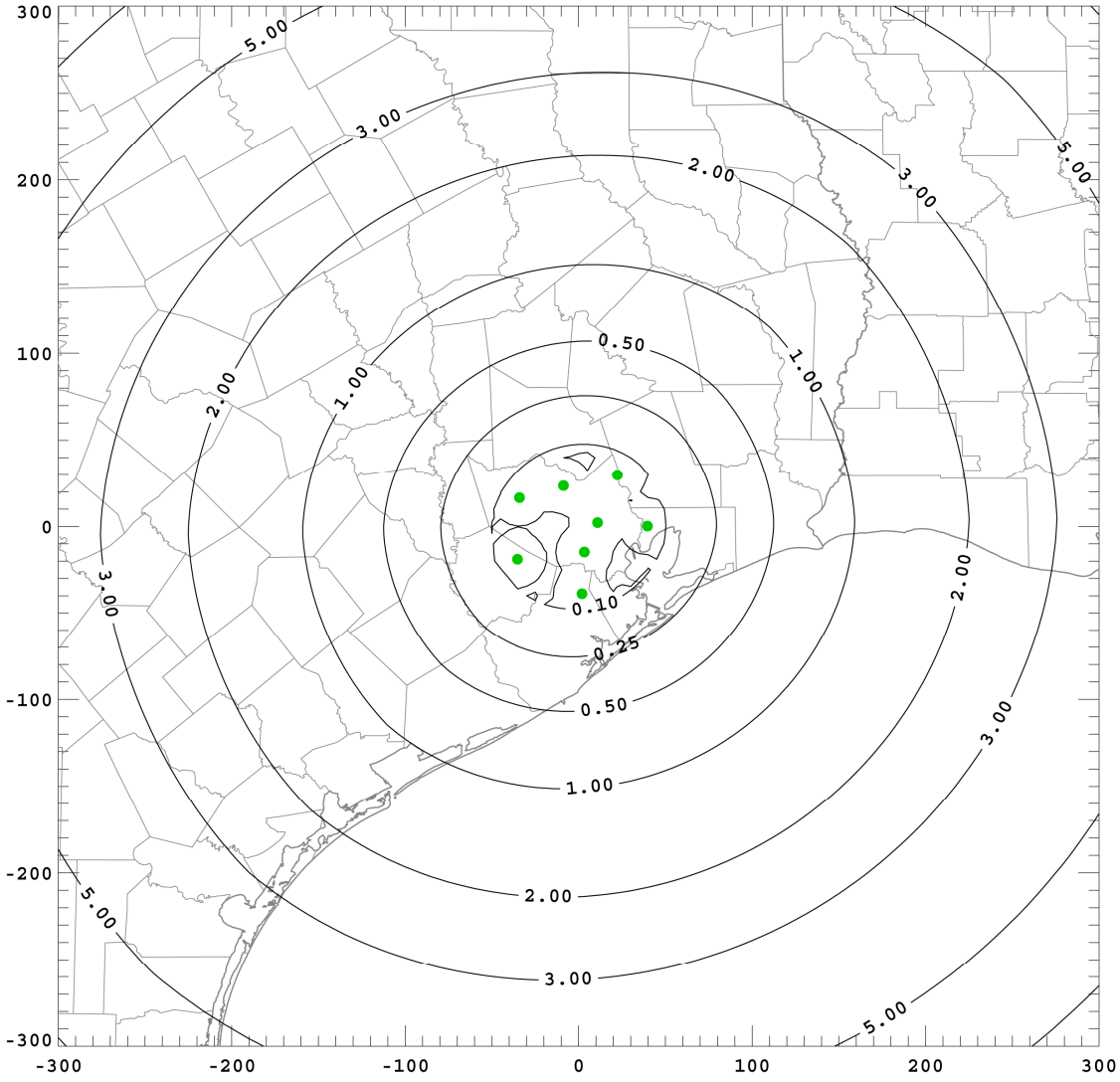

Figure 6.6. Median three-dimensional location accuracy of VHF sources on October 31, 2005 with a network RMS timing error of 90 ns. Median value is of location accuracies for points between 3 – 12 km in altitude. Units and distances are in kilometers.

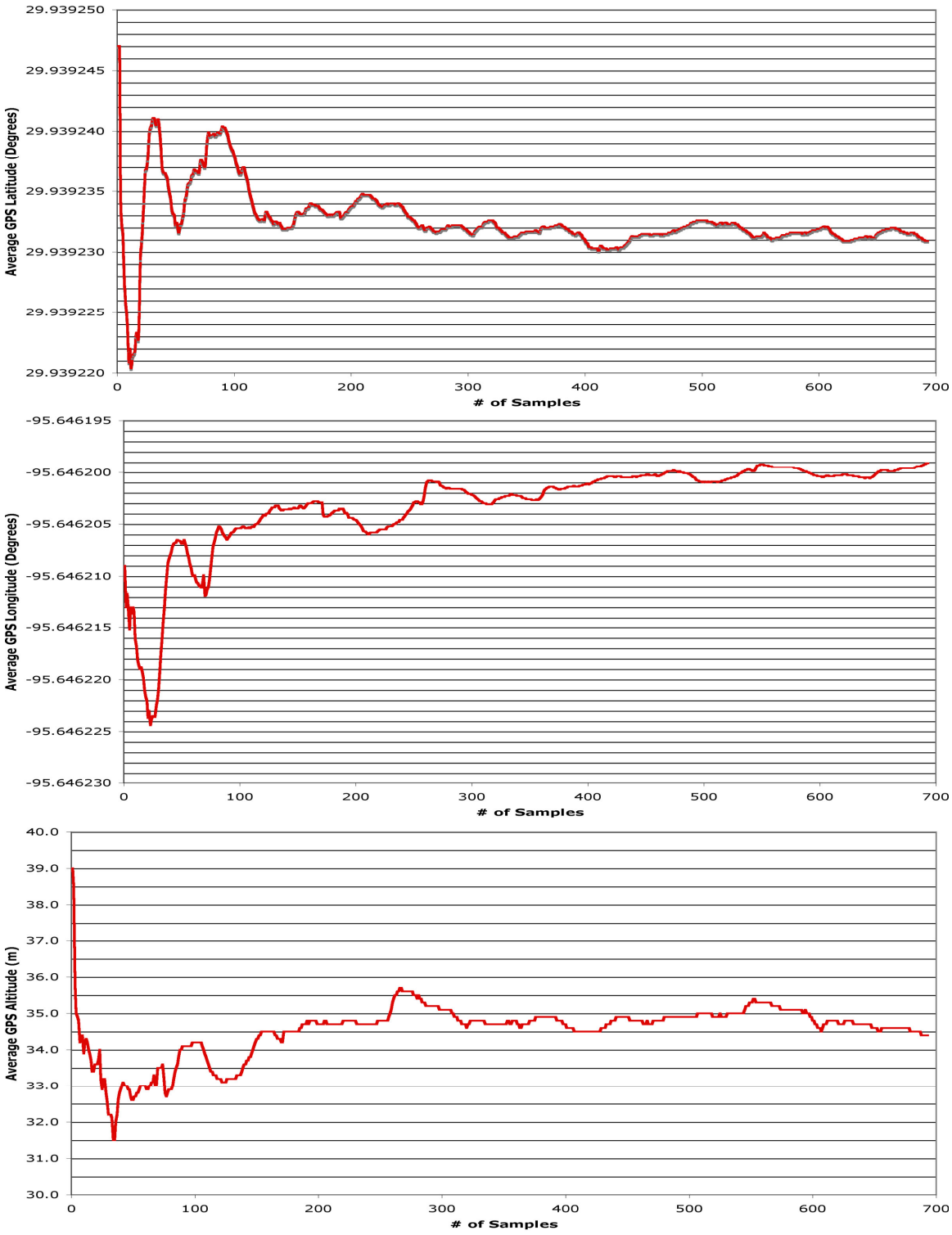

Figure 6.7. Plots showing the running average of GPS measured a) latitude, b) longitude, and c) height for an LDAR station based on 700 samples taken over the course of 2½ days.

Recall that the χ^2 values are originally calculated by the LDAR network location algorithm using 75 ns as a good first guess. The value used is based on the results of the timing error analysis of 6 sensor solutions from the DFW LDAR II network [Carey et al., 2005]. Due to the fact that the two networks use the exact same hardware, it is expected that similar timing errors are achievable.

From the simple equation for measurement errors, $\Delta d = \nu \Delta t$, all errors associated with distance and time measurements are lumped into the timing error. Using GPS based timing measurements that are adjusted every second, any error in time measurements should already be minimized. This suggests that the increased timing error of the Houston network compared to the DFW LDAR II network is due to distance measurement errors (ie. sensor location measurement error). Using a value of 2.99792×10^8 m s^{-1} for the VHF radiation propagation velocity, ν, the effect a position measurement error has on the RMS timing error is easily calculable (Table 6.1).

To reduce the LDAR sensor positional errors, a script was written to record the GPS position information every 5 minutes for 2½ days. The intended goal is to reduce the measurement uncertainty to less than 0.00001 degrees latitude/longitude and less than 1 m in height. Plots of the running averages for the latitude, longitude, and height at each were made. Figure 6.7 shows the results for the Cypress-Fairbanks sensor. The variability between each measurement can be very large, but, with enough samples, the average location eventually converges to a small uncertainty range. These plots were repeated for every sensor and new latitude, longitudes, and altitudes were entered into the configuration file for the LDAR VHF source location algorithm.

Table 6.1. Network timing error from inaccurate sensor positions.

	Latitude / Longitude (degrees)			Height (m)	
	0.001	0.0001	0.00001	10.0	1.0
Error (ns)	320.65	32.07	3.21	33.36	3.34

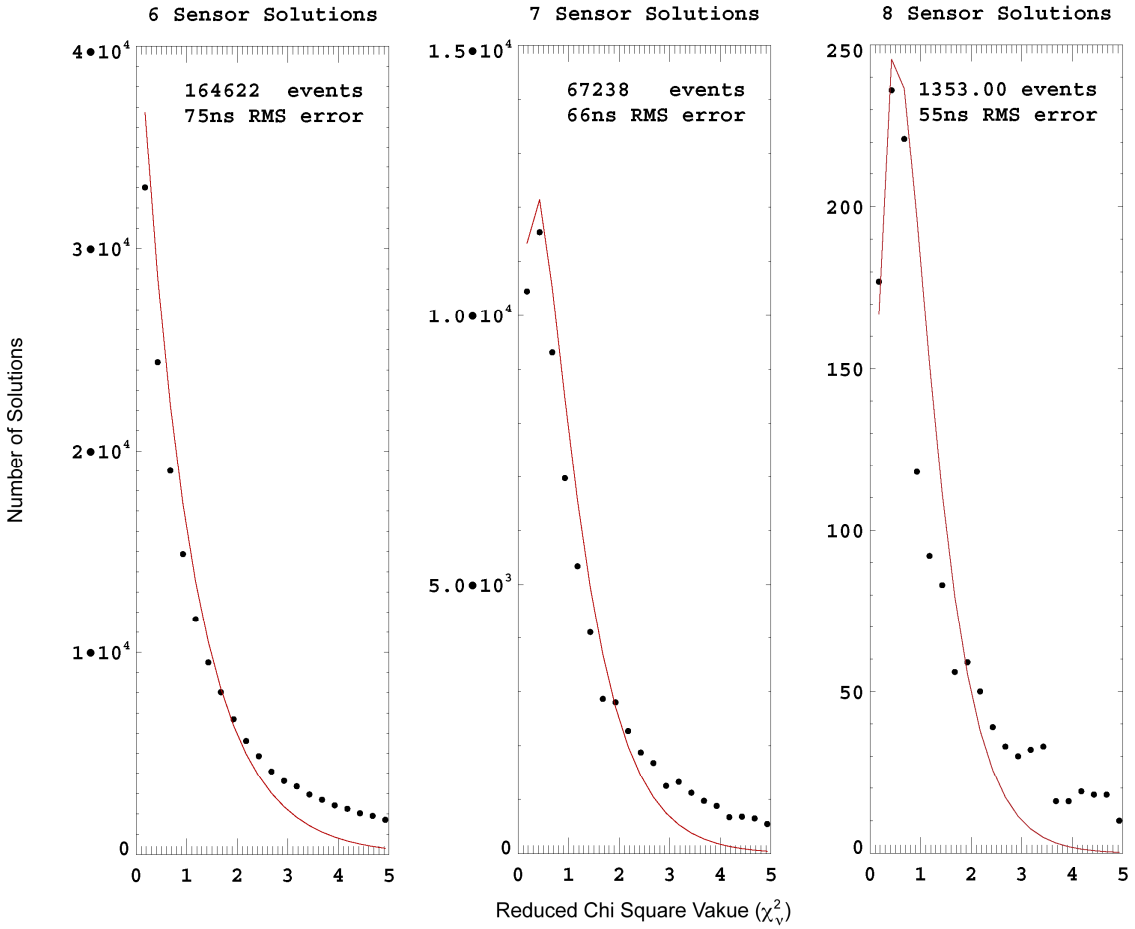

Figure 6.8. Histograms of χ^2 values for 6, 7 & 8 sensor solutions (black dots) fitted to theoretical χ^2 probability distributions (red lines) for October 31, 2005 after LDAR sensor site location adjustments.

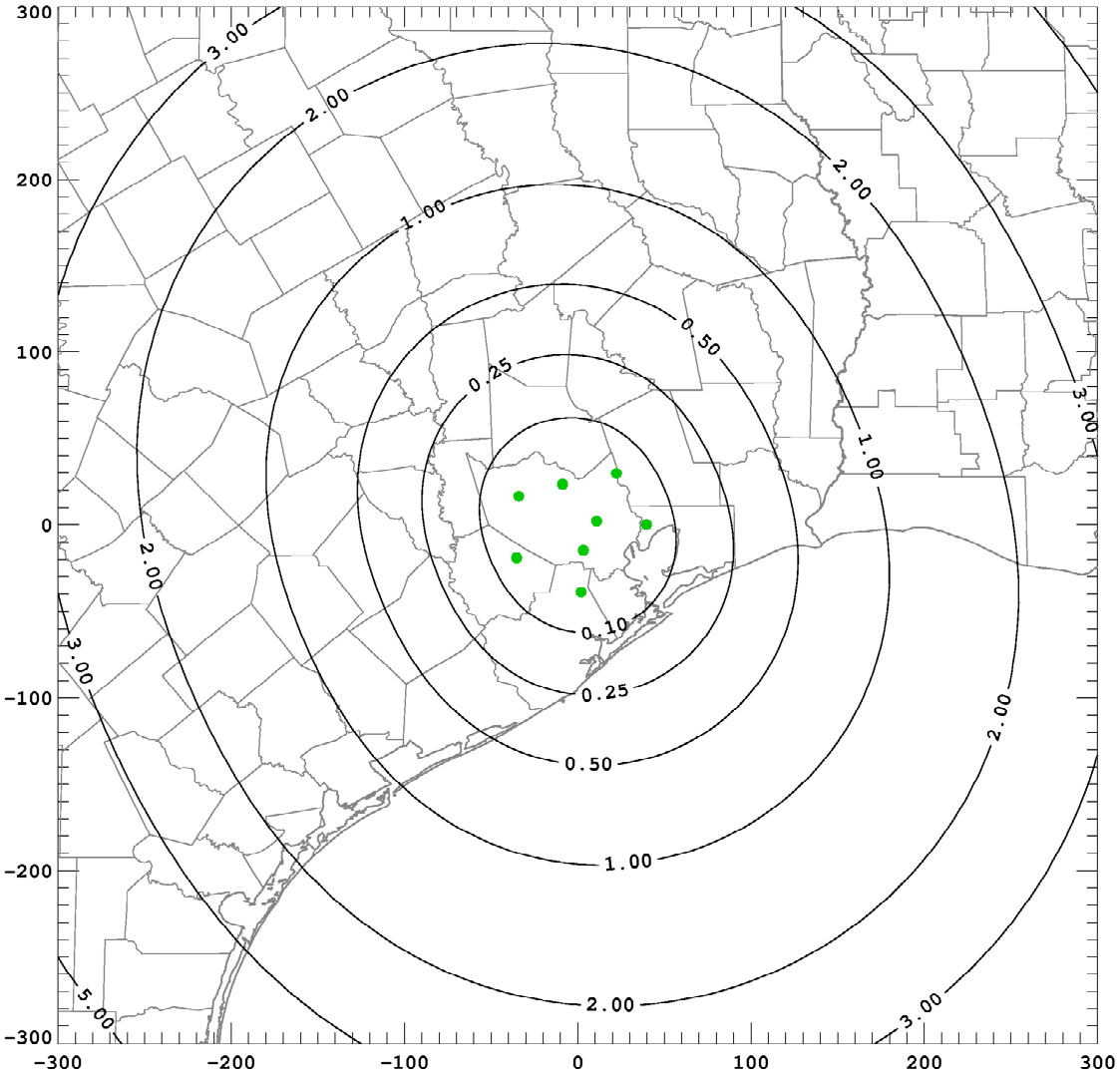

Figure 6.9. Radial location accuracy of VHF sources on October 31, 2005 with a network RMS timing error of 75 ns. Units and distances are in kilometers.

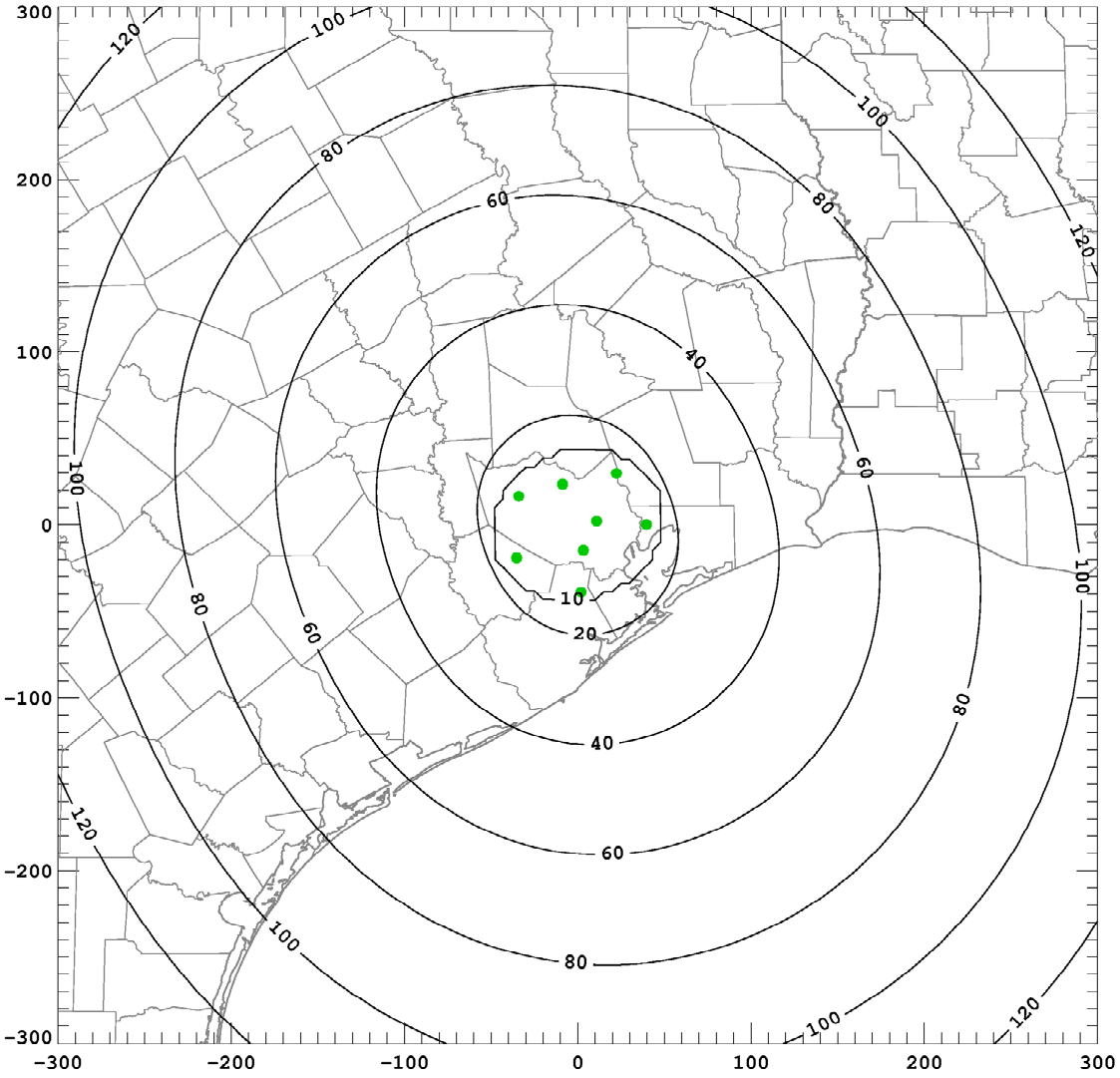

Figure 6.10. Azimuthal location accuracy of VHF sources on October 31, 2005 with a network RMS timing error of 75 ns. Units and distances are in kilometers.

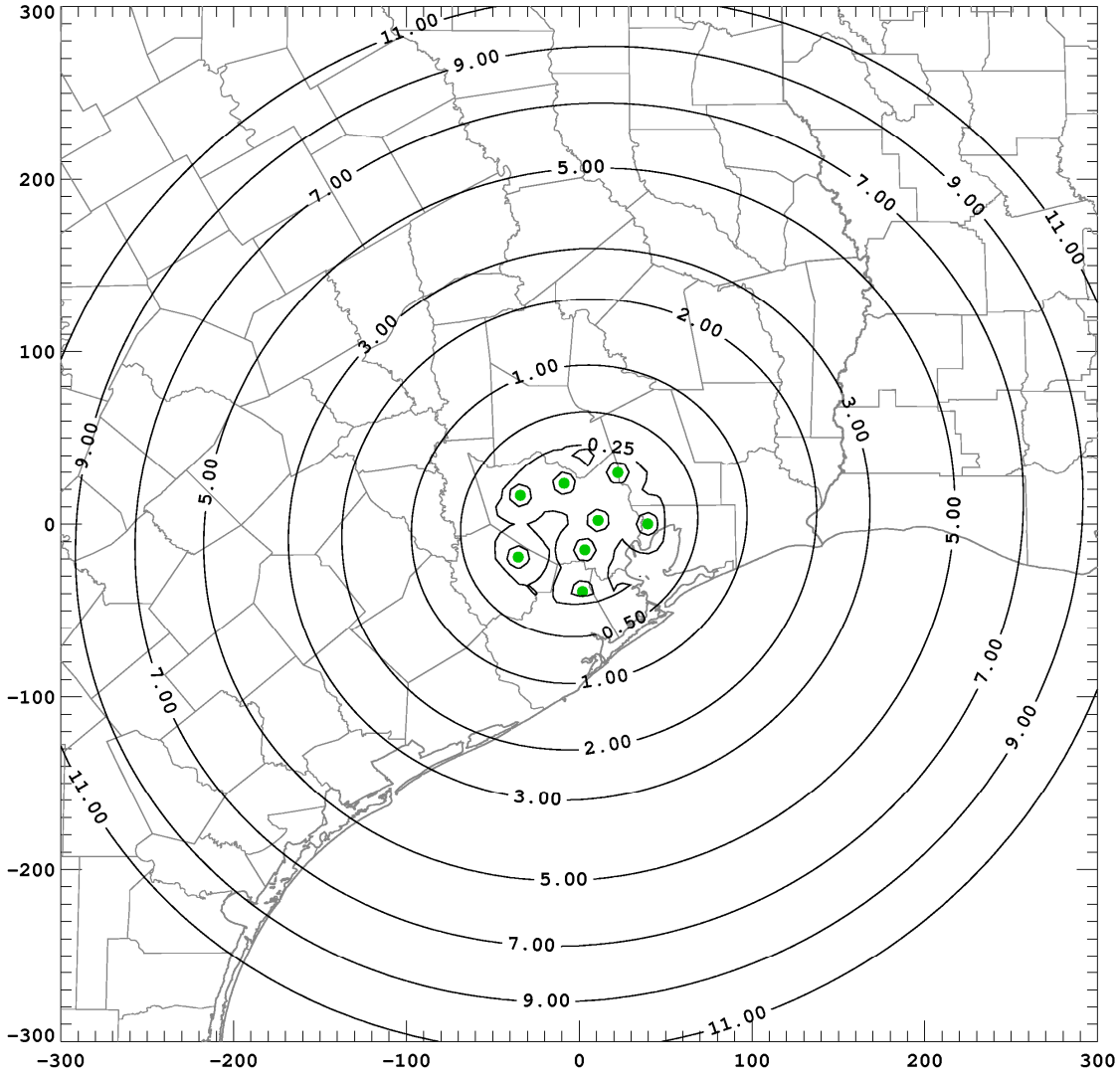

Figure 6.11. Vertical location accuracy of VHF sources on October 31, 2005 at an altitude of 3 km and a network RMS timing error of 75 ns. Units and distances are in kilometers.

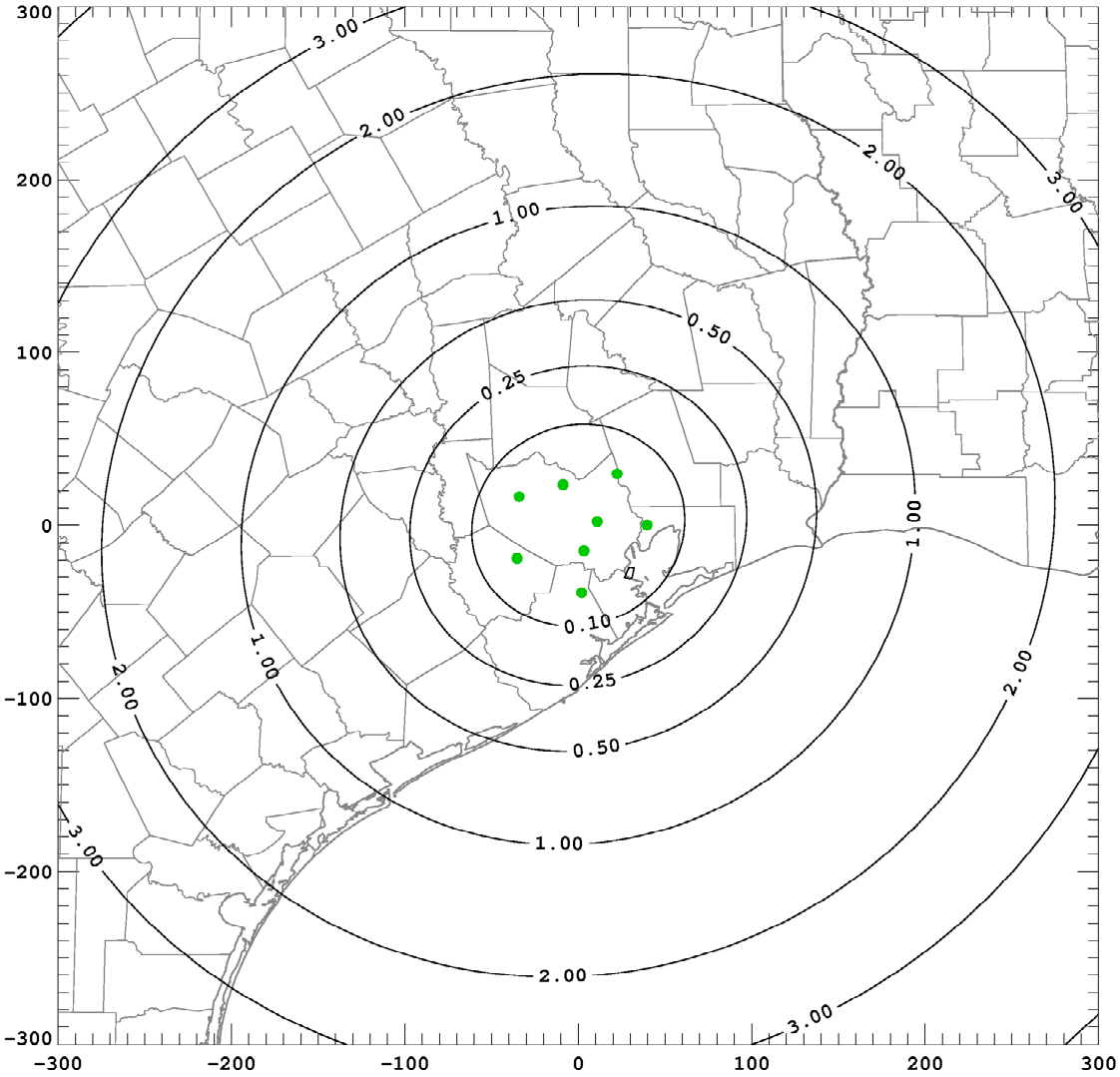

Figure 6.12. Vertical location accuracy of VHF sources on October 31, 2005 at an altitude of 12 km and a network RMS timing error of 75 ns. Units and distances are in kilometers.

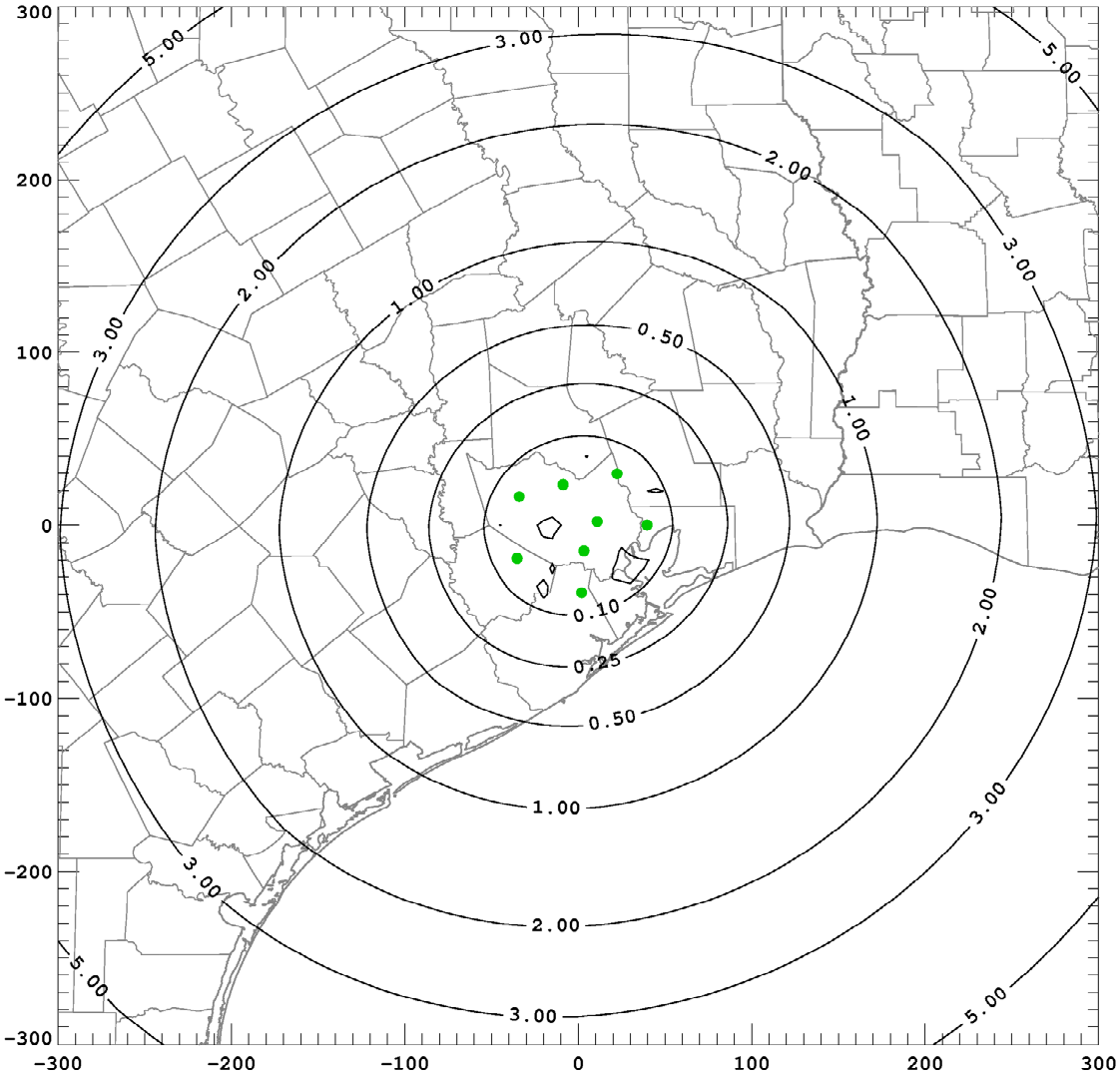

Figure 6.13. Median three-dimensional location accuracy of VHF sources on October 31, 2005 with a network RMS timing error of 75 ns. Median value is of location accuracies for points between 3 – 12 km in altitude. Units and distances are in kilometers.

With the updated configuration file, the data for 31 October 2005 was re-analyzed. New reduced chi-square error distribution plots were generated for 6, 7, and 8 sensor VHF source solutions. As shown in Figure 6.8, the new sensor locations reduced the network RMS timing error to 75, 65, and 55 ns, respectively. The improvement in the network timing error for the 6 sensor solutions is now identical to the DFW LDAR II network timing error of 75 ns. Again, using the RMS timing error for the 6 sensor solutions to determine the worst-case location accuracy, plots of the radial (Figure 6.9), azimuthal (Figure 6.10), vertical location accuracy at 3 km (Figure 6.11) and 12 km (Figure 6.12), and the median three-dimensional location accuracy (Figure 6.13) in the range of 3 to 12 km are made.

Overall, the improvement in the RMS timing error by 15 ns has improved the overall location accuracy for the entire network. In order to easily quantify the increase in location accuracy from a 15 ns improvement the timing error, plots showing the difference between the 90 and 75 ns location accuracy results for the vertical location accuracy at 3 km (Figure 6.14), vertical location accuracy at 12 km (Figure 6.15), and the median three-dimensional location accuracy (Figure 6.16) were plotted. Figure 6.14 and 6.15 show that the largest increase in location accuracy are for locations that have a small elevation angle with respect to the center of the network, meaning low altitude sources and radially distant sources. Figure 6.16 shows the median location accuracy improved by 100 m at the 100 km range and 500 m at the 250 km range.

The network RMS timing error was again analyzed for the 21 April 2006 and 25 April 2007 MCSs. For the 21 April 2006 MCS, the reduced chi-square error distribution

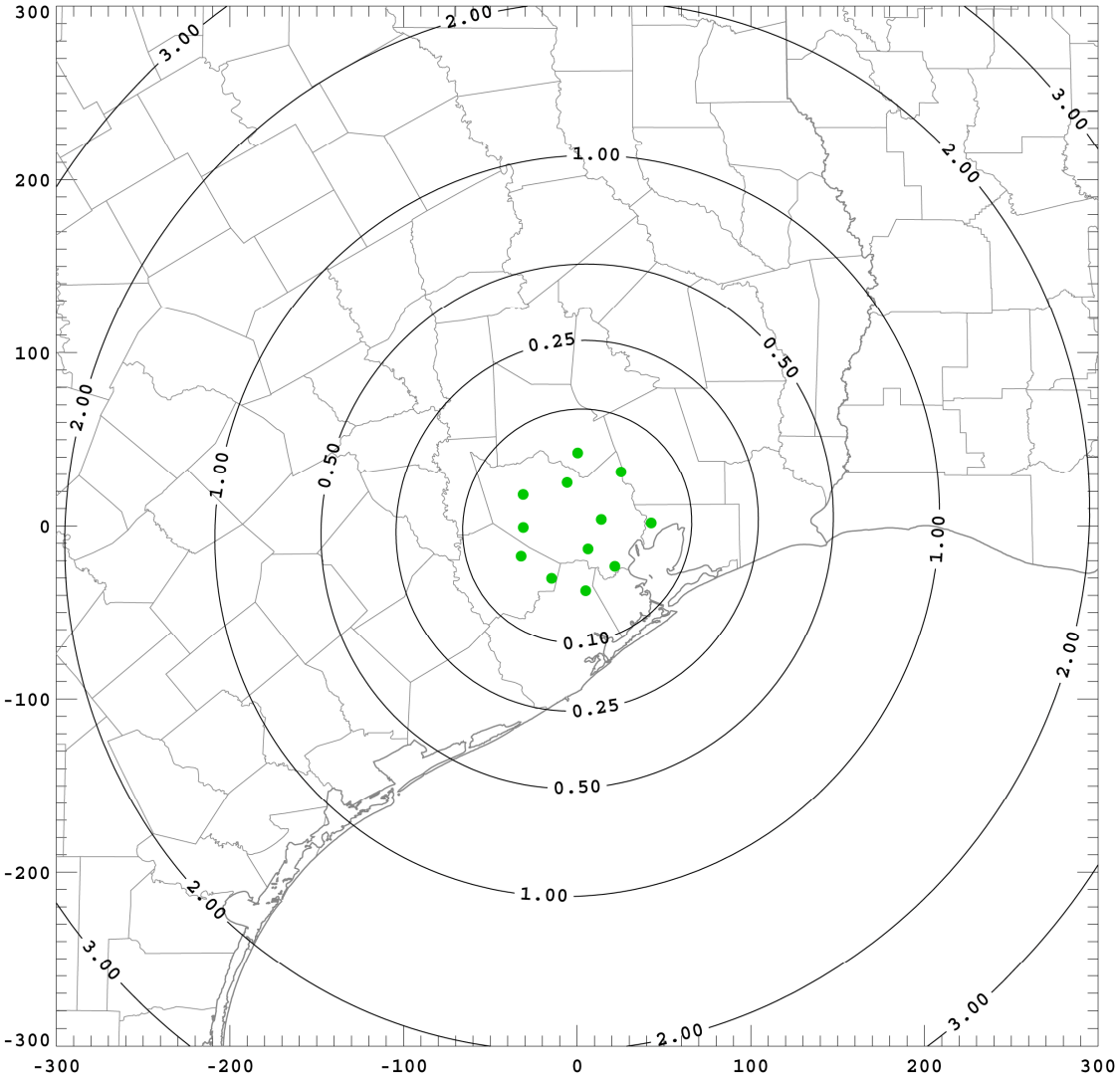

Figure 6.14. Increase in VHF source location accuracy for sources at an altitude of 3 km due to an RMS timing error decrease from 90 ns to 75 ns.. Note all distances are in kilometers.

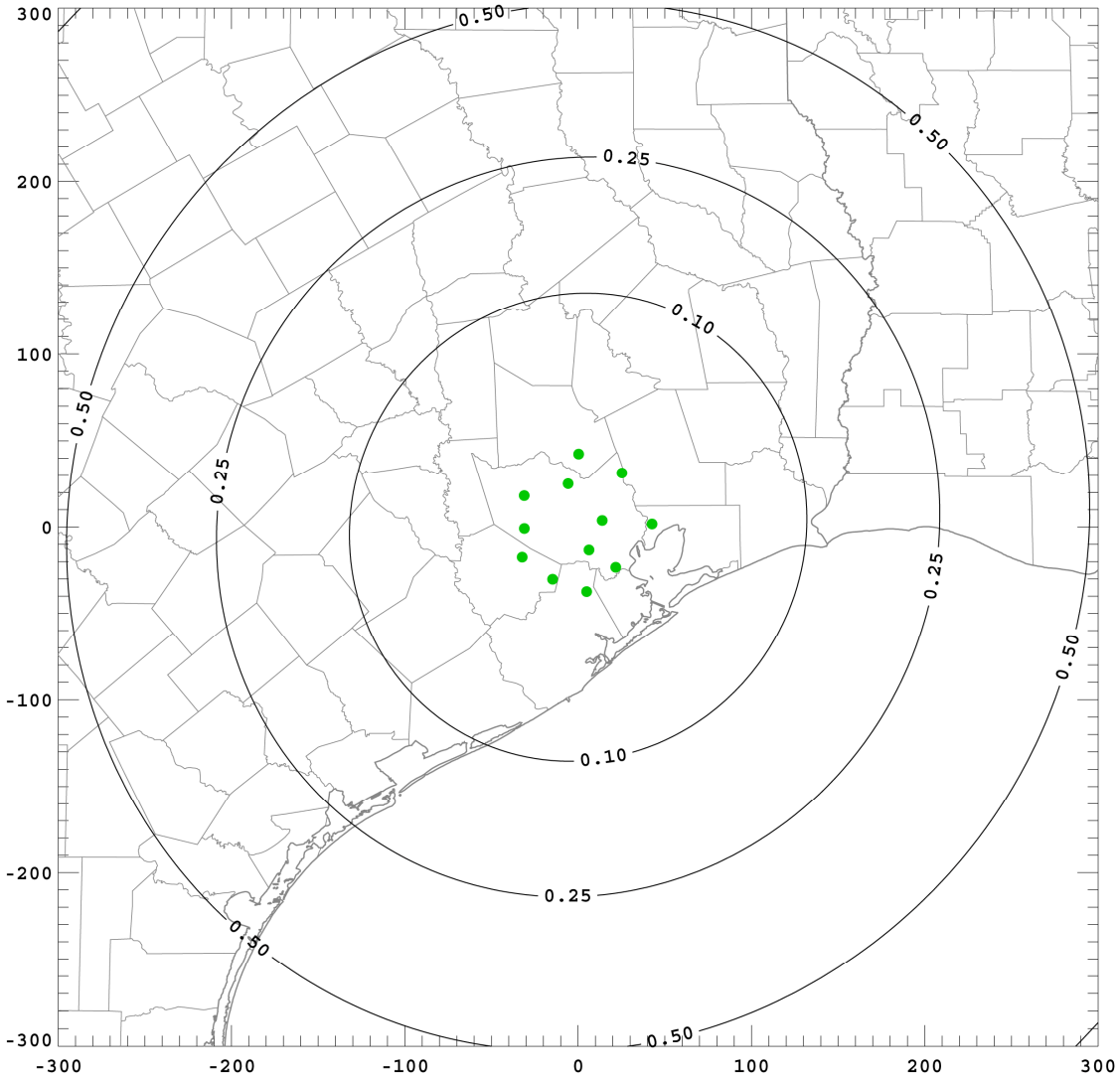

Figure 6.15. Increase in VHF source location accuracy for sources at an altitude of 12 km due to an RMS timing error decrease from 90 ns to 75 ns.. Note all distances are in kilometers.

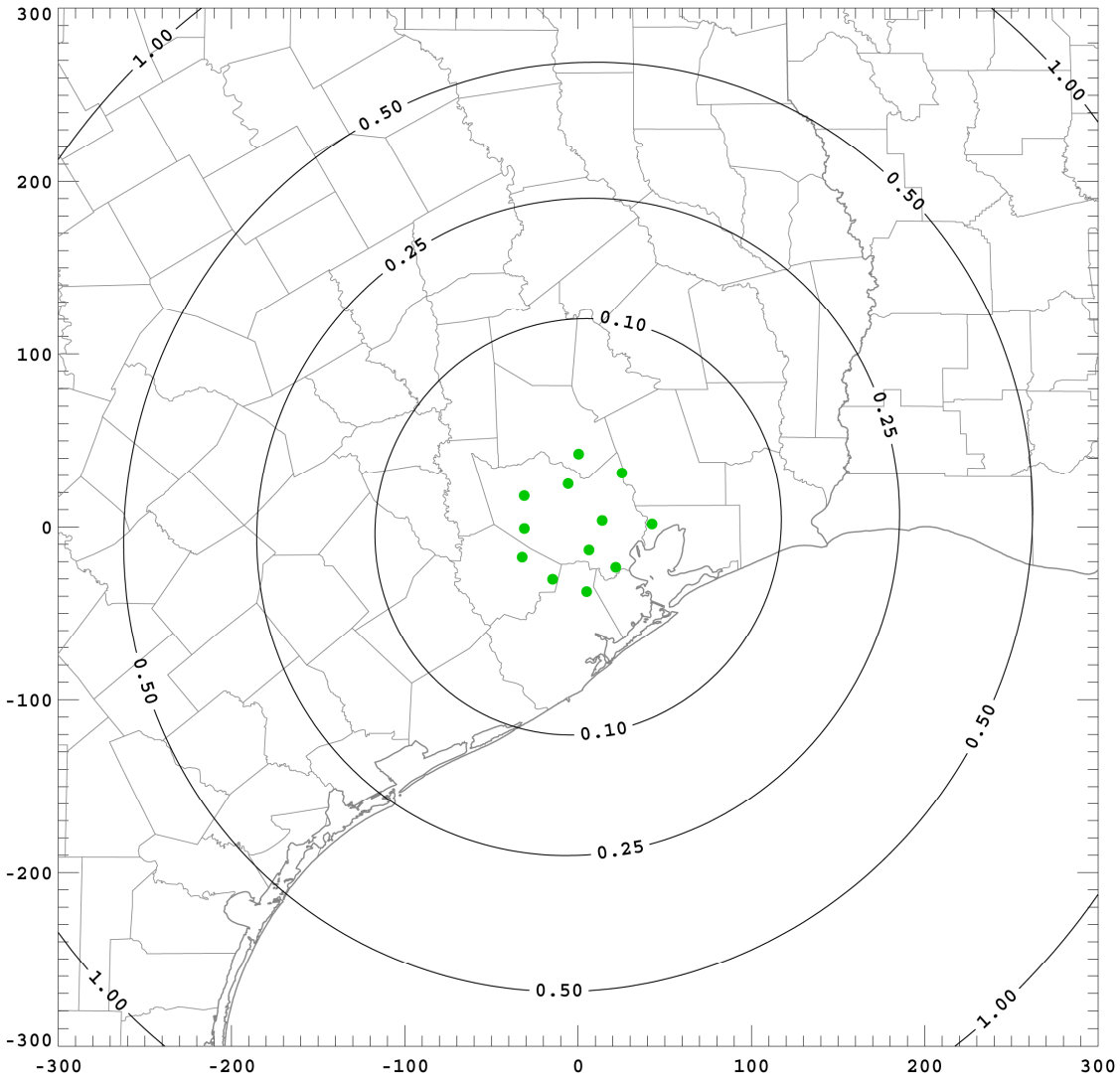

Figure 6.16. Increase in the median three dimensional VHF source location accuracy for sources between 3 – 12 km in altitude due to an RMS timing error decrease from 90 ns to 75 ns. Note all distances are in kilometers.

plots show similar RMS timing error values to the 31 October 2005 MCS of 72 ns, 58 ns, and 50 ns for 6 sensor, 7 sensor, and 8 sensor solutions (Figure 6.17). For the 25 April 2007 MCS, the RMS timing errors relapsed back to the higher values observed in the original analysis for the 31 October 2005 MCS (Figure 6.18 and 6.1). Even though the network operating frequency had been switched from 70 MHz to 40 MHz, the RMS timing error of the network should not have changed. With the error in sensor locations already minimized, the only other possible cause of the increased error is from a problem in the GPS timing measurements.

The GPS antenna provides the precision timing needed to correlate pulses detected at each sensor site and determine VHF lightning sources. Each sensor emits a VHF test pulse at the start of every second based on the GPS timing measurements. This test pulse is detected by the VHF antennas, processed, and time stamped. This is used to measure the amount of time between when the antenna receives a VHF pulse to the time it is digitized and time stamped. These timings are different for each sensor based on the length of cabling and additional noise filters in the system, but should remain steady for each sensor. Extracting 40 seconds worth of timing correction data from the 25 April 2007 data for the Cypress Fairbanks gave an average timing correction of 5,753 ns, but with a standard deviation of 37.8 ns. Similarly large standard deviations were found in two other sensors for that day. Remotely accessing the Cypress Fairbanks sensor revealed that even weeks after 25 April 2007, the timing corrections were still drifting wildly. A simple command to reset the GPS system brought the timing corrections back to a constant value of 5650 ns and a standard deviation of 0.

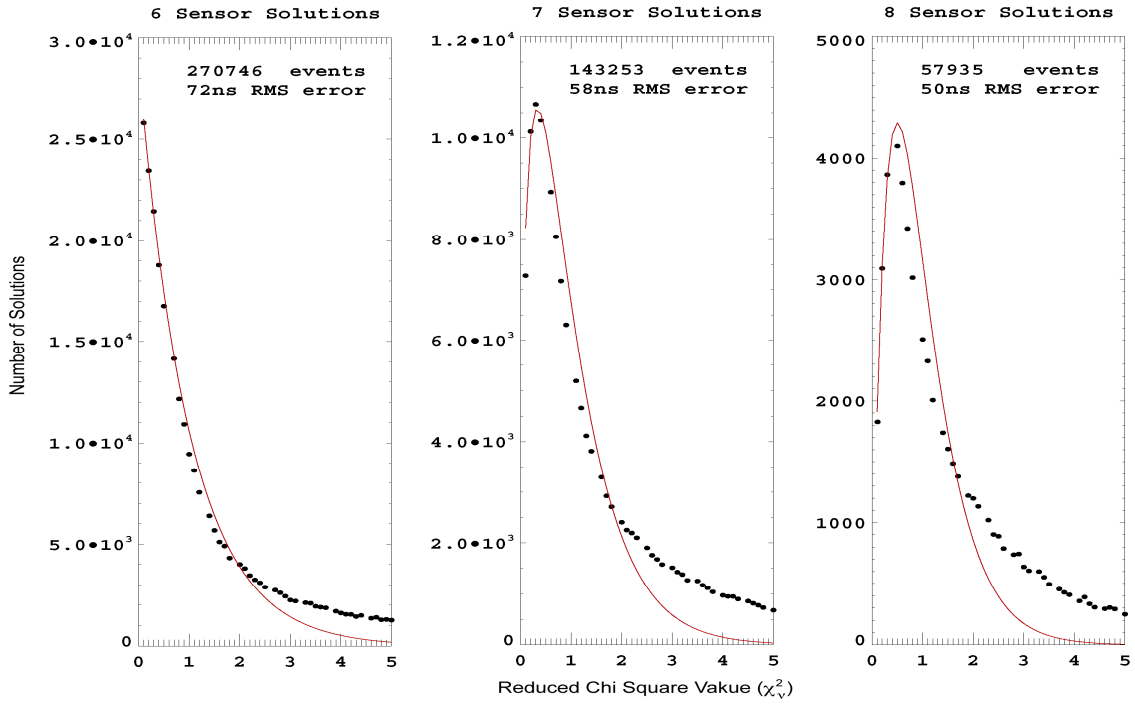

Figure 6.17. Histograms of χ^2 values for 6, 7 & 8 sensor solutions (black dots) fitted to theoretical χ^2 probability distributions (red lines) for April 21, 2006.

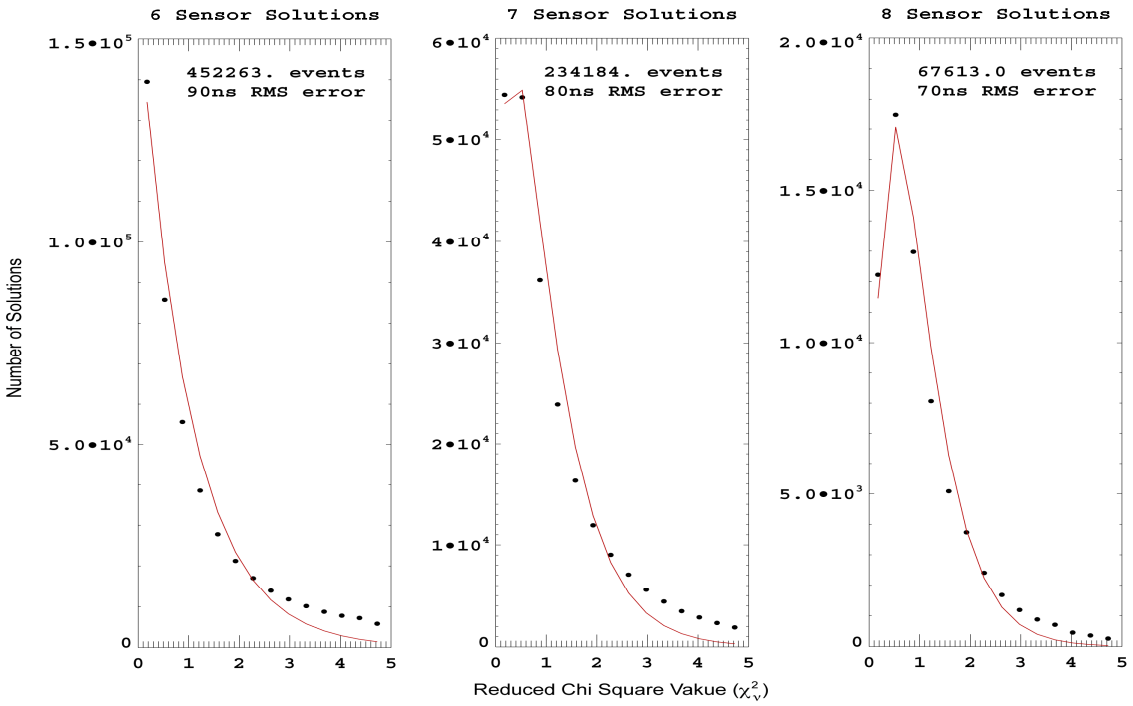

Figure 6.18. Histograms of χ^2 values for 6, 7 & 8 sensor solutions (black dots) fitted to theoretical χ^2 probability distributions (red lines) for April 25, 2007.

6.2. Detection Efficiency

6.2.1. Theoretical Minimum Detectable Signal

The possibility of mapping a network's minimum detectable VHF source power at any point would be useful in diagnosing directional weaknesses in VHF source detection based on current network operational status and configuration. In addition, it can be used to quantitatively show the change in network sensitivity based on proposed changes in network configurations, such as frequency and sensor gain changes. The MDS at any point would be the minimum signal detectable by at least 6 sensors based on their respective gain and frequency settings. All calculations for the minimum detectable source power maps assume an isotropic antenna with a uniform gain of 1. In reality, the antenna gain pattern is much more complex, however the actual gain pattern had not been obtained in time to be accounted for in the following analysis.

Recall from Section 5.1 that the three main changes in the network configuration involved changing the operational frequency of the network. The goal behind the change was to find the frequency range with the lowest noise floor highest sensor sensitivity. Table 6.2 shows the individual sensor sensitivities based on their individual frequency and gain settings. These values are used in the simple minimum detectable VHF source power model for the following analysis. The map of the network for 21 April 2006 (Figure 6.19) shows the minimum detectable source power (in dBm) at an altitude of 8 km for the time period when the network was operating at a frequency of 70 MHz.

Table 6.2. The minimum detectable signal (in dBm) of each sensor's antenna based on the sensor gain setting (AGC).

Frequency (MHz)	Minimum Detectable Signal (dBm) Sensor # 1	2	3	4	5	6	7	8	9	10	11	12
70.0	N/A	N/A	-61.4	-62.0	-61.4	-62.0	-59.6	-61.4	-58.4	-56.0	-58.4	-64.7
114.0	N/A	N/A	-54.8	-54.2	-56.0	-60.2	-60.2	-56.6	-57.8	-45.8	-61.4	-55.4
40.0	-56.6	-61.4	-54.8	-63.8	-72.8	-59.0	-61.4	-60.8	-64.7	-57.8	-64.7	-68.3

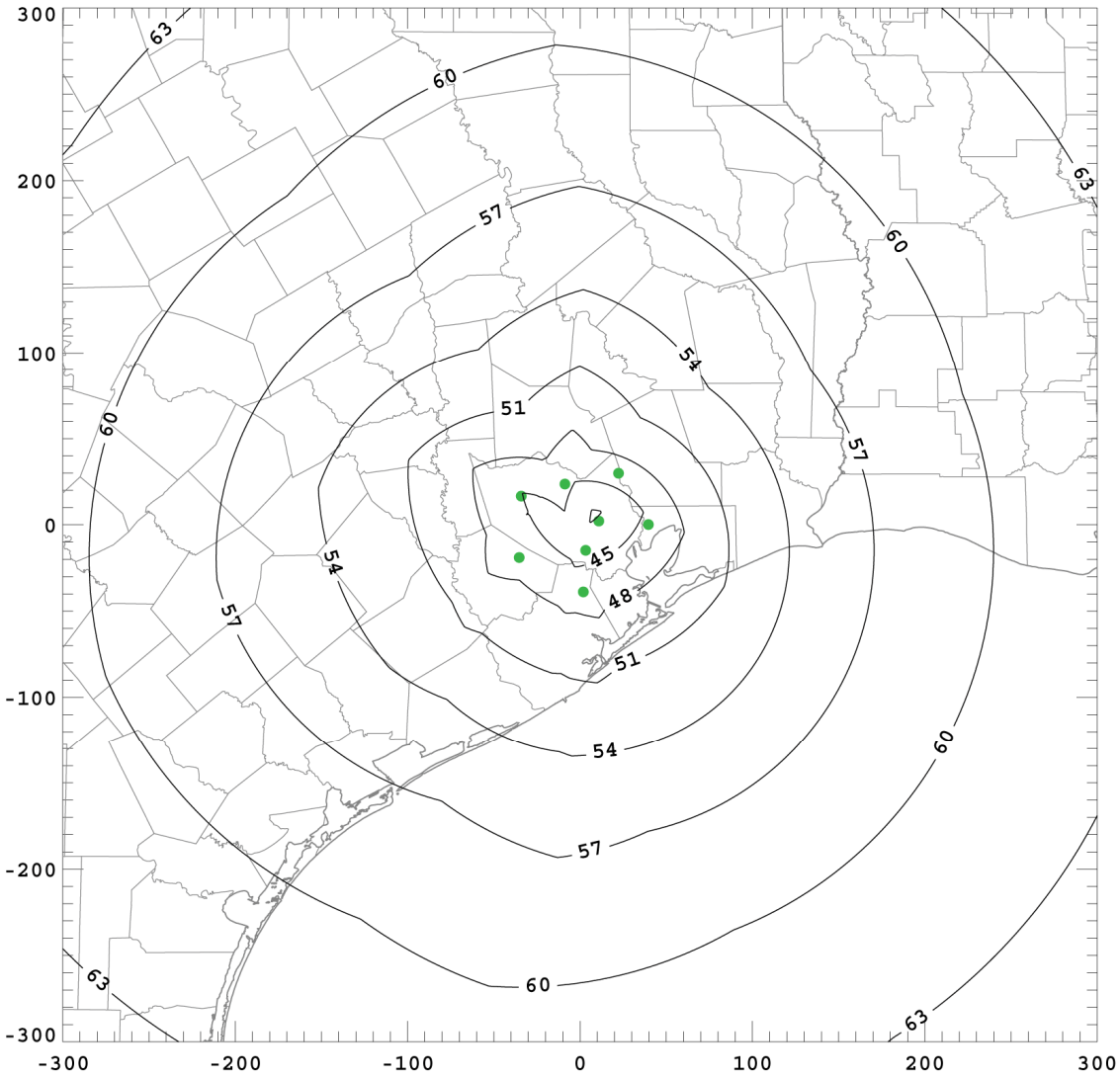

Figure 6.19. Theoretical minimum detectable source power (in dBm) based on sensor AGCs and an operating frequency of 70 MHz.

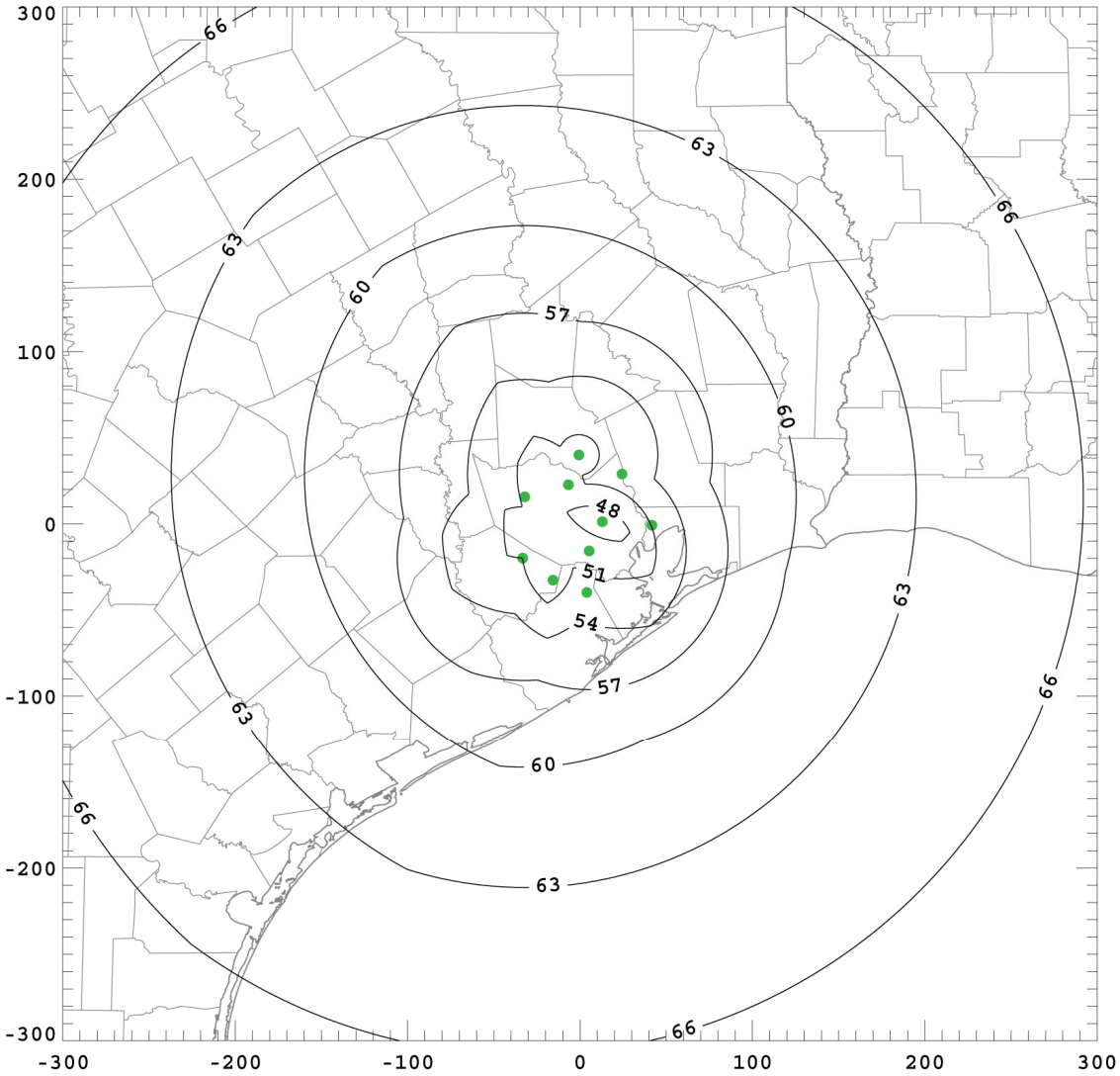

Figure 6.20. Same as Figure 6.19 but for an operating frequency of 114 MHz.

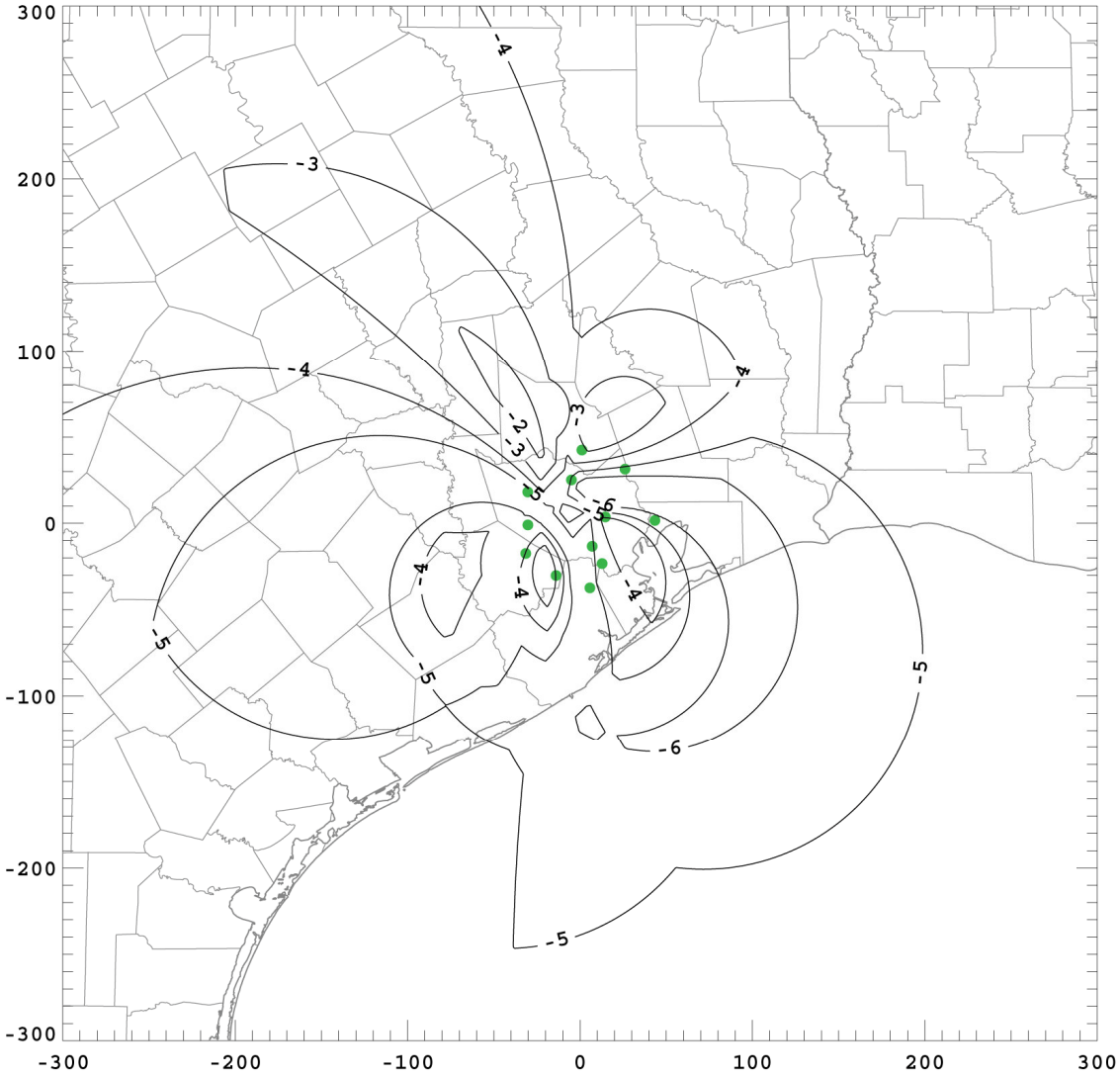

Figure 6.21 Estimated change in the minimum detectable source power due to a change in operating frequency from 70 to 114 MHz. Source power values are in dBm.

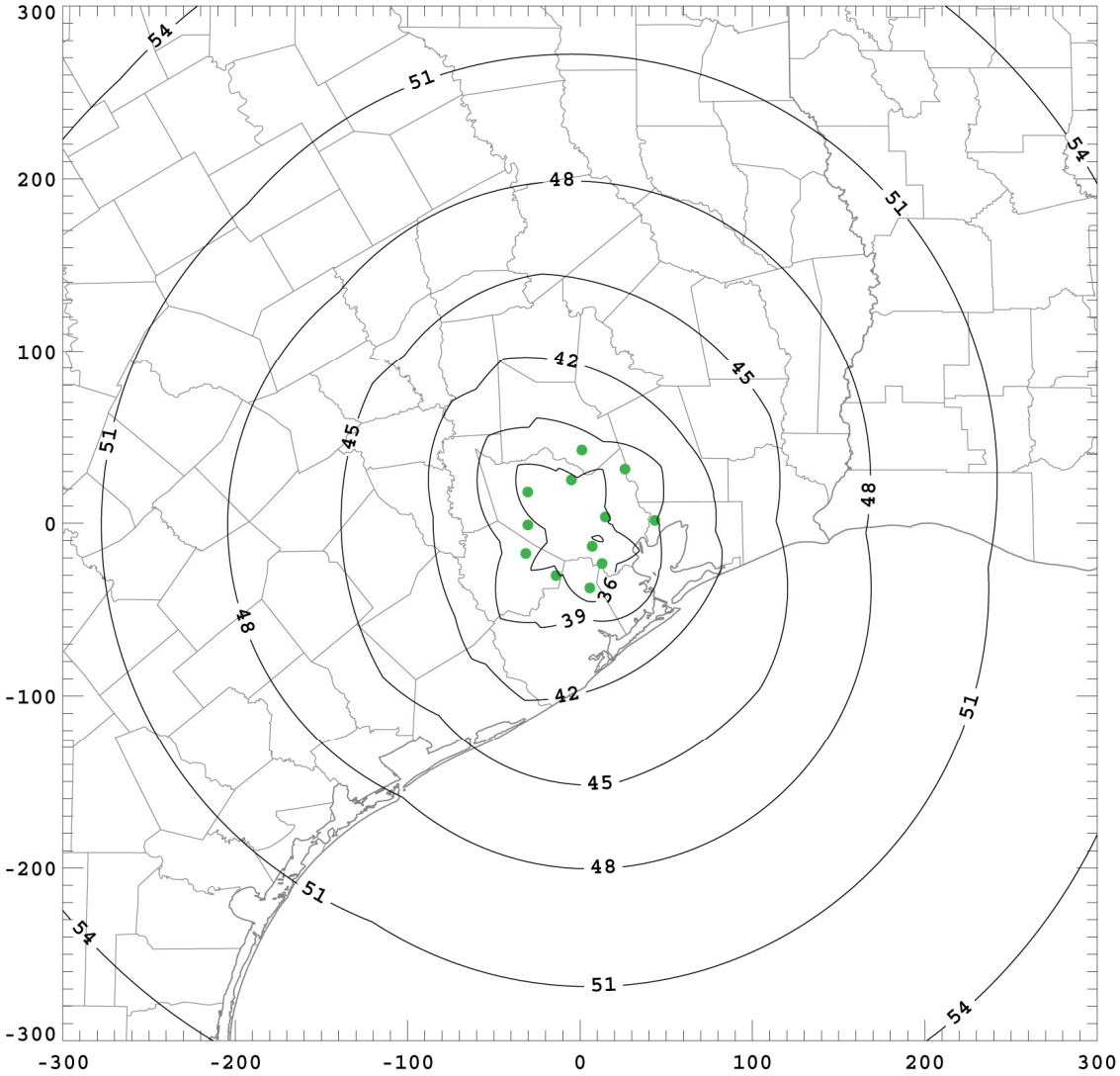

Figure 6.22. Same as Figure 6.19 but for an operating frequency of 40 MHz.

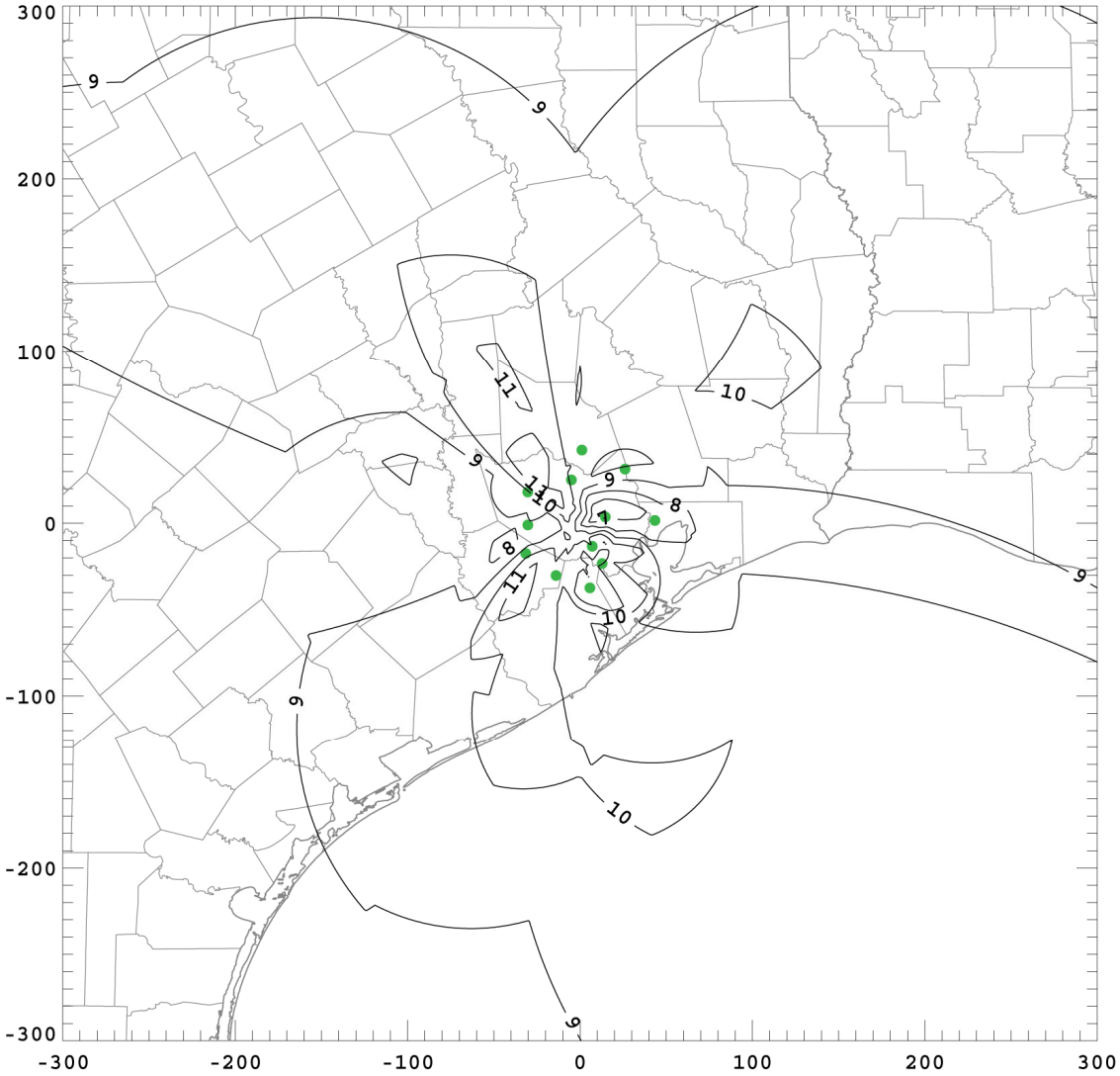

Figure 6.23 Estimated change in the minimum detectable source power due to a change in operating frequency from 70 to 40 MHz. Source power values are in dBm.

In early January 2007, different operating frequencies were being investigated. Sensor gain surveys suggested that the 114 MHz frequency setting would result in a slight decrease in sensitivity. Inputting the new frequency and sensor AGC values into the minimum detectable power mapping program produced the results seen in F igure 6.20. A map plotting the change in minimum detectable source power between the 70 MHz and 114 MHz configurations shows a network wide decrease of 3 – 4 dB (Figure 6.21).

Additional sensor surveys in early 2007 focused on the 30 – 55 MHz range. This range is used for cordless telephone, military & emergency communications, and mobile communications (taxi cabs, buses), and various other uses. Despite all of those uses, the noise surveys show that frequencies around 40 MHz permit much higher AGC (gain) settings. Using the new frequency and gain settings gives a minimum detectable source power map with much higher sensitivity (Figure 6.22). Mapping the change between the 70 MHz and 40 MHz settings (Figure 6.23), the simple model predicts an increase in sensitivity by 9 – 10 dB across the entire network coverage area.

To test the model results, the change in VHF source power distributions are compared for two separate days that were operating at 70 MHz and 40 MHz. Distributions of VHF source powers for storms occurring over the central region of the network on 21 April 2005 (70 MHz) and 25 April 2007 (40 MHz) are plotted (Figure 6.24). The distributions show a definite offset in the mode and lower limit of detectable powers. In both cases, the difference is roughly 8 – 9 dB, with the 25 April 2007 (40 MHz) case having the higher sensitivity. Although the model predicted change agrees

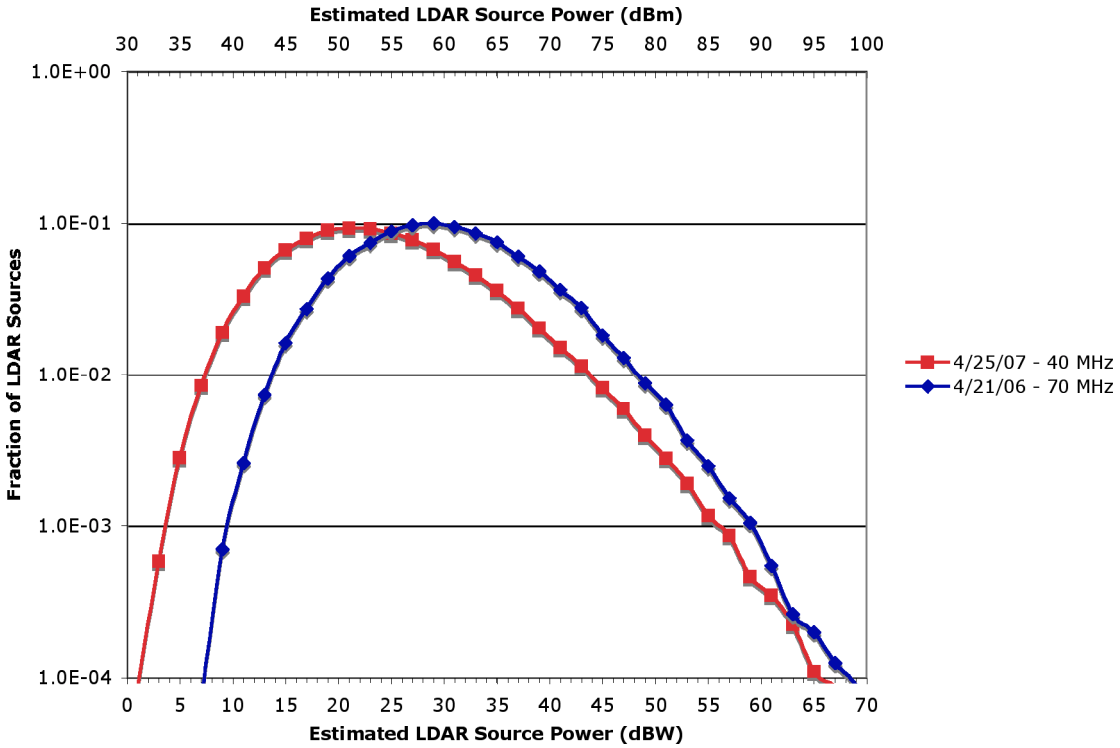

Figure 6.24. VHF source power distributions for all sources over the inner region of the network (0 – 35km diameter) for MCSs that occurred when the LDAR network was operating at 70 MHz and 40 MHz.

well with the real world change, the absolute values of the real world results are lower by 5 – 6 dB. This difference is most likely explained by the assumption in the model that the antenna is isotropic, meaning it has a uniform gain of 1. The calculations used by the Houston LDAR network take in to consideration the antenna gain pattern when estimating VHF lightning source powers [Carey et al., 2005].

6.2.2. Relative Detection Efficiency

Plots of the VHF source power distributions can be utilized to estimate the relative change in detection efficiency radially outward from the center of the LDAR network. The VHF source power distributions were plotted for three MCSs on 31 October 2005 (Figure 6.25), 21 April 2006 (Figure 6.26), and 25 April 2007 (Figure 6.27). All three cases show source power distributions for the first seven range rings are almost identical. The first seven range rings are all located inside the network perimeter, which means the detection efficiency in this region is nearly uniform. Therefore, the first seven range rings are lumped together to create a composite distribution.

All remaining range rings are show a 2 dB loss in the minimum detectable source power as expected, since the range rings were chosen to be 2 dB apart. In addition, each the mode of the distribution for each range ring shifts slightly to higher values, similar, but not as pronounced as the shift observed for the DFW LDAR network Carey et al. [2005]. For each range ring beyond the 31.6 km range ring, the composite curve is integrated from the mode of the distant distribution and up to higher source powers (ex. see Figure 5.9). The results from the integrations give relative detection efficiency

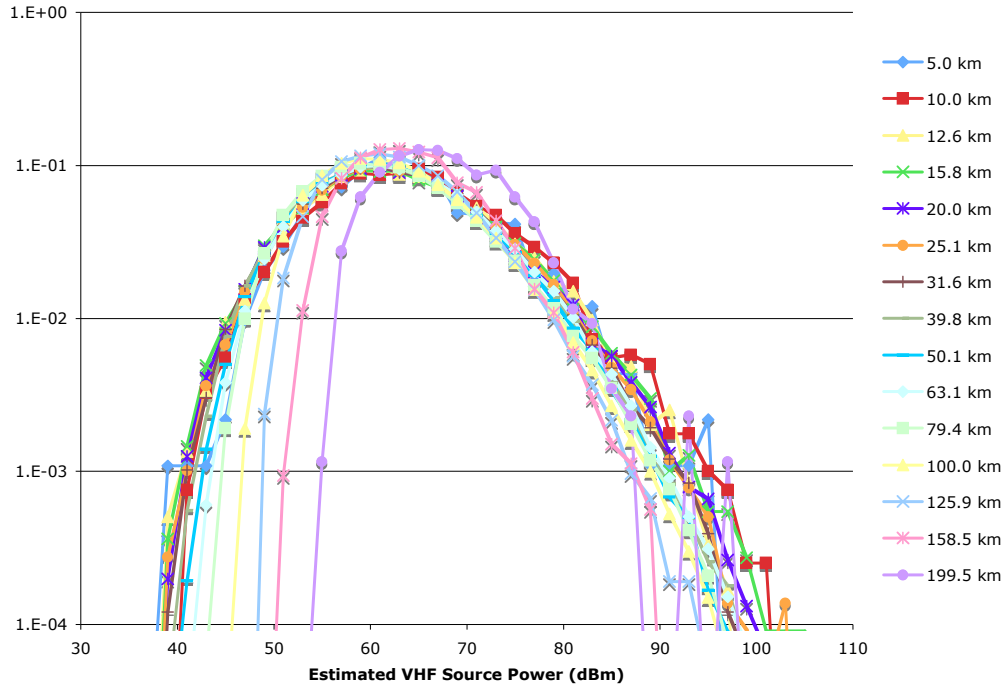

Figure 6.25. Estimated VHF source power distributions of 15 range rings for 31 October 2005. Range rings are spaced 2 dB apart and ~0.75 dB in width.

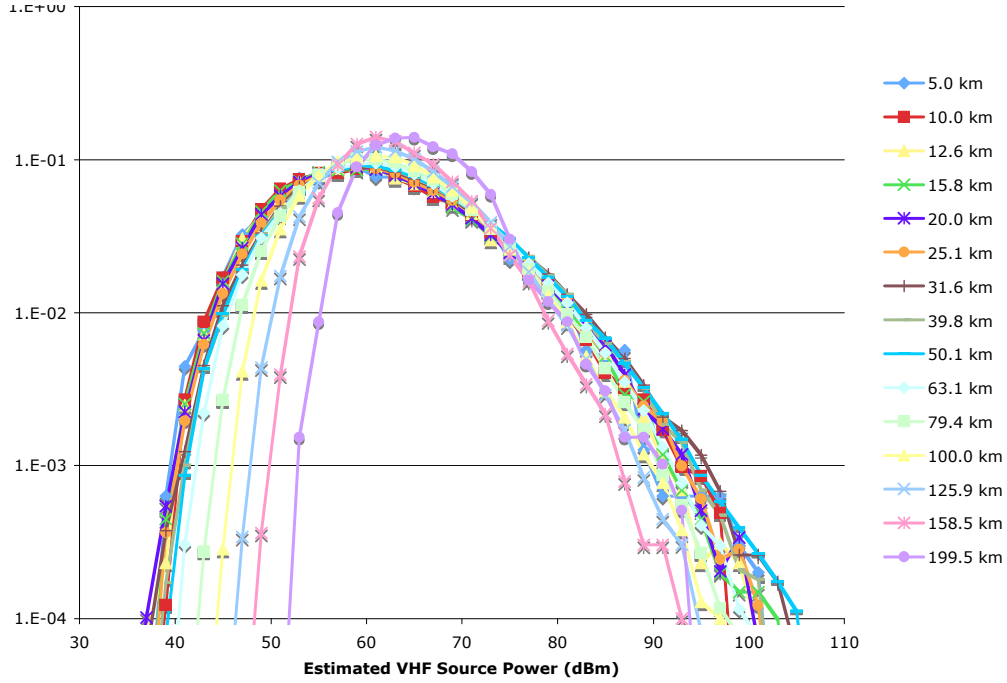

Figure 6.26. Estimated VHF source power distributions of 15 range rings for 21 April 2006. Range rings are spaced 2 dB apart and ~0.75 dB in width.

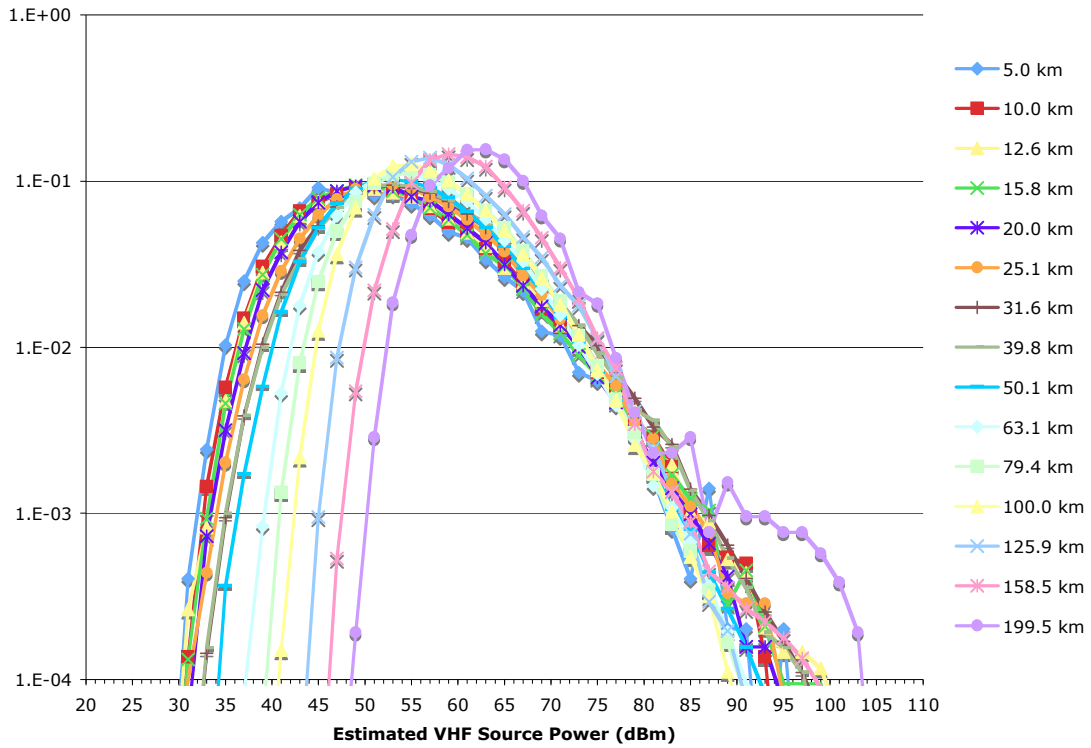

Figure 6.27. Estimated VHF source power distributions of 15 range rings for 25 April 2007. Range rings are spaced 2 dB apart and ~0.75 dB in width.

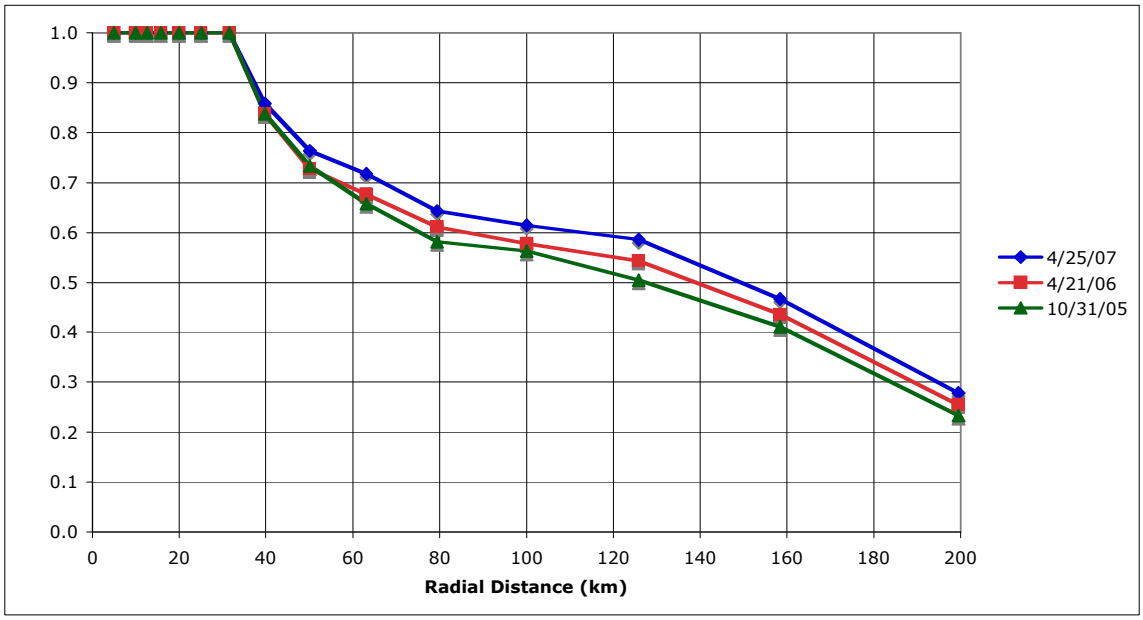

Figure 6.28. Relative detection efficiency curves based on the changes in the VHF source power distributions for the MCSs analyzed.

curves for the three storm days analyzed (Figure 6.28). In all three cases, the fall of with respect to range of relative detection efficiency is very similar. Due to the method of compositing the first seven range rings, the relative detection efficiency out to 31.6 km is set to 1. Beyond that range ring, the relative detection efficiency decreases to ~0.6 at 100 km and 0.25 at 200 km.

6.2.3. VHF Source Power CFADs

In the analysis presented in Section 6.2.2, only the change in VHF source power distribution as a function of horizontal range from the center of the network was examined. Each plot was composed of the VHF sources for the entire vertical column in each range ring. It is also beneficial to examine the VHF source power distributions as a function of altitude. As before, these vertical distributions can be produced for specific horizontal range rings in order to examine any effects due to horizontal distance from the network center. Analyses of these distributions may also reveal additional insight into different aspects change in network performance, operation, and design.

The vertical structures of the LDAR VHF source powers were analyzed using contoured frequency by altitude diagrams (CFADs) for 31 October 2005, 21 April 2006 , and 25 April 2007 storm systems. For these two days, CFADs were created for each of the range rings specified in Section 6.2.2. In these diagrams, VHF source power values are along the x-axis and altitude is along the y-axis. For each plane of constant altitude, the CFAD analysis determines the frequency distribution of VHF source power values across all x, y locations within the range ring being considered. The analysis then contours the VHF source power values of various percentiles (0.1%, 1%, mean, 99%,

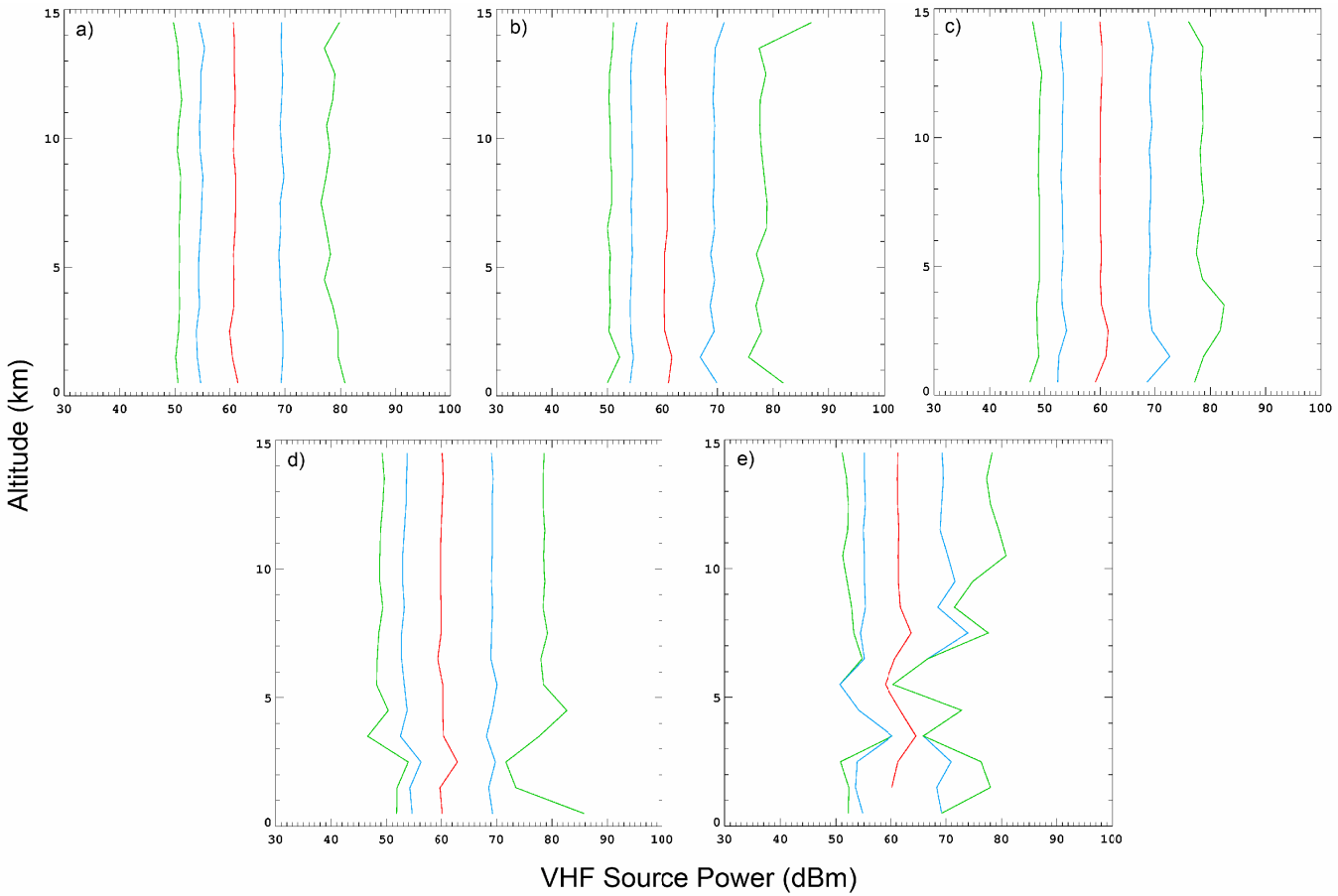

Fig. 6.29. Contoured Frequency by Altitude Diagrams of VHF LDAR source powers for a) 5km, b) 25km, c) 50km, d)100km, and e) 158km range rings. The green lines denote the 1st (99th), blue lines denote 10th (90th), and the red line denotes the 50th percentile.

99.9% in our case) as a function of altitude. These diagrams make it easy to examine how the distribution of reflectivity values changes between different altitudes and times. For additional information on CFAD construction and interpretation, please refer to Yuter and Houze [1995].

Plots for all three storm systems yielded similar results. For the sake of brevity, selected CFADs from 21 April 2006 are shown (Fig. 6.29). The main observation from all five plots is that the distributions of VHF source powers are very similar at all altitudes. It should be stressed that these plots do not give any indications as to number of VHF sources occurring at each level. The CFADs also shows the same skewed power distribution observed in Figures 6.25 – 6.27. In the 100 km range ring CFAD (Fig. 6.29d), the lower altitude distributions begin pinching on both the low and high power sides. By the 158km range ring (Fig. 6.29e), roughly the lowest 8km of altitude have widely varying distributions. The final interesting observation from these CFADs is the approximately 2-3 dB shift towards lower values in the 1^{st} and 10^{th} percentiles between the 25 km (Fig. 6.29c) and 50 km (Fig. 6.29d) range rings. The distribution shift remains until roughly the 100 km range ring.

6.3. Network Range

As stated in Section 5.4, the usable network range for scientific research is based off of two limits. The first is the maximum allowable location uncertainty, which for most research studies is a 1 km maximum uncertainty. The distance limit based on this criterion can be obtained from the results in Section 6.1. The distance does change, as expected, based on size of the measurement errors made by the network. Although, in

practice, as long as the sensor locations remain fixed and the GPS clocks function appropriately, the timing error (location error) should remain at a minimum value.

The other limit to usable network range is obtained by analyzing the VHF source count per range ring. The range rings are the same ones used in the VHF source power distribution analysis and relative detection efficiency section (6.2.1). Figures 6.30, 6.31, 6.32, show the VHF source count for each range ring for 31 October 2005, 21 April 2006, and 25 April 2007, respectively. In all three cases, the VHF source count increases steadily until a distance of ~100 km. The rate of increase is nearly the same as the area of each range ring, suggesting the MCS was a constant VHF source emitter and the network for the 0 – 100 km range has a nearly constant detection efficiency. In all cases, the VHF source count drops off rapidly after 100 km. These results bring credence to the idea that the VHF source power distribution curves are affected by other unknown variables.

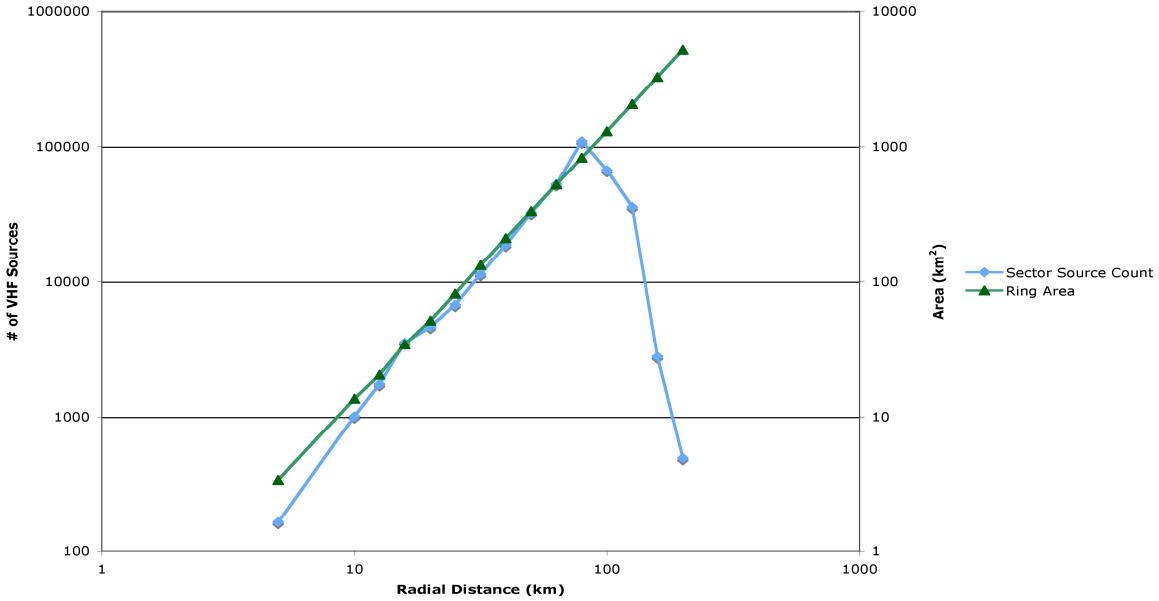

Figure 6.30. Graph showing the trend in VHF source counts for each range ring and compared to the increase in area of each range ring for the 31 October 2005 MCS.

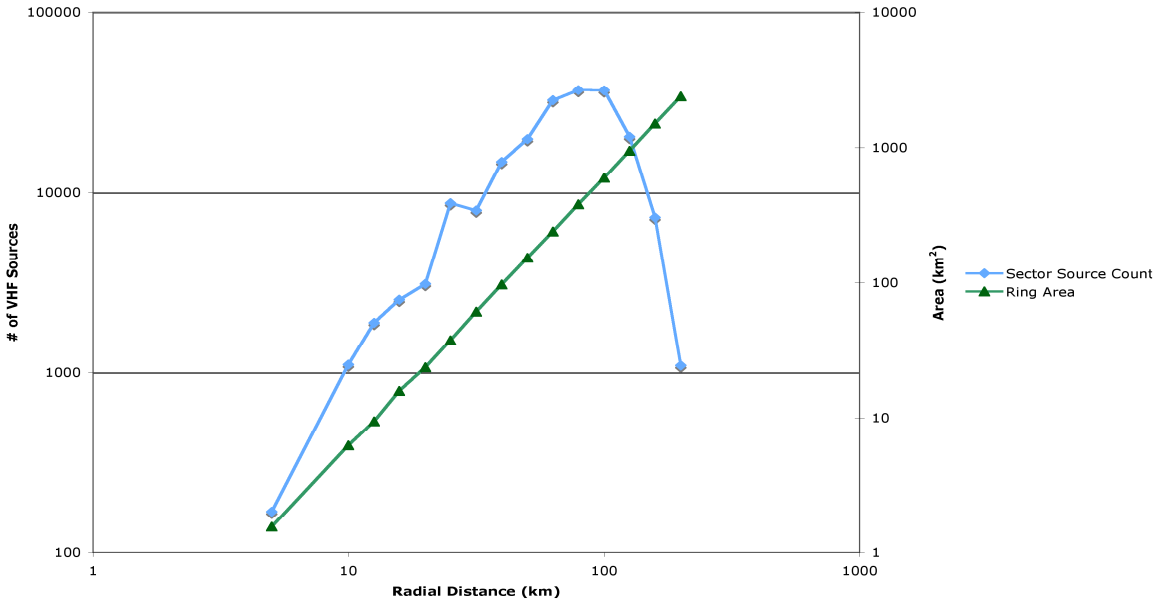

Figure 6.31. Graph showing the trend in VHF source counts for each range ring and compared to the increase in area of each range ring for the 21 April 2006 MCS.

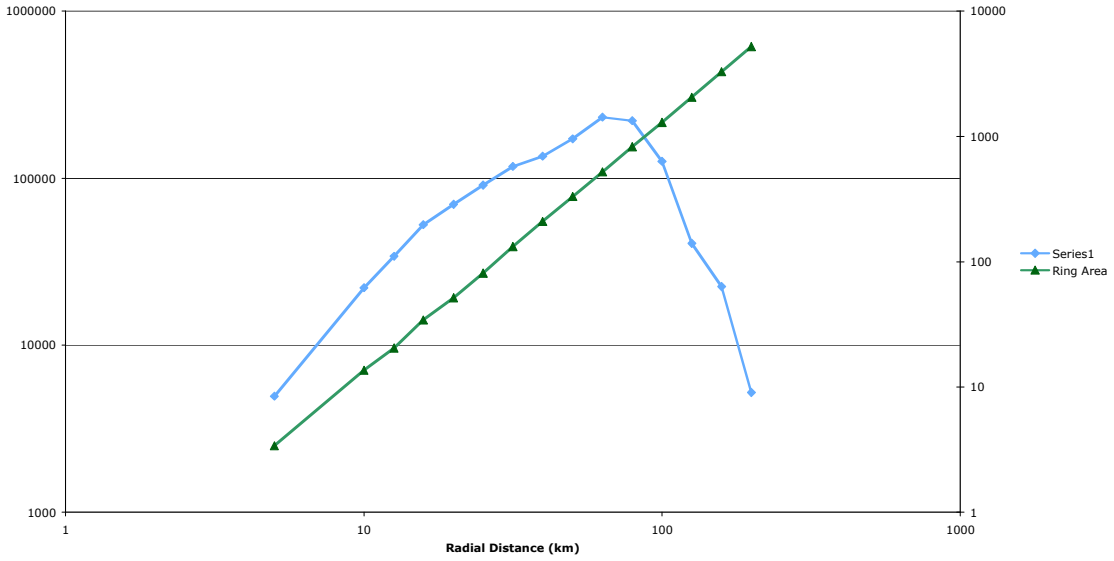

Figure 6.32. Graph showing the trend in VHF source counts for each range ring and compared to the increase in area of each range ring for the 25 April 2007 MCS.

7. NETWORK PERFORMANCE DISCUSSION & CONCLUSIONS

7.1. Location Accuracy

Initial results from the 31 October 2005 MCS timing error analysis reveals a RMS timing error for the Houston LDAR network of 90 ns for 6 sensor solutions (Figure 6.1). This gives a three-dimensional location accuracy of 1 km at a distance of 150 km and 100 m over the center of the network (Figure 6.6). For the DFW LDAR network, Carey et al. [2005] found a network RMS timing error of 75 ns. The New Mexico Tech Lightning Mapping Array (LMA), the system that the LDAR network design is based on, has an RMS timing error of 40 ns [Thomas et al., 2001]. Due to the similarity between the Houston and DFW networks, it is expected they would have similar RMS timing errors.

From the simple equation for measurement errors, $\Delta d = \nu \, \Delta t$, it is possible to lump all errors associated with distance and time into the timing error. Using GPS based timing measurements that are adjusted every second, any error in time measurements should already be minimized. This suggests that the increased timing error of the Houston network compared to the DFW LDAR II network is most likely due to distance measurement errors (ie. sensor location measurement error). Taking the average GPS positional measurements every 5 minutes for 2½ days for each sensor (~700 samples), minimizes the position uncertainty to values below the 3.2 ns timing error due to positional errors in Table 6.1.

Reanalyzing the 31 October 2005 MCS with the updated sensor positions decreased the RMS timing error to 75 ns, similar to the DFW network [Carey et al.,

2005]. This decrease in RMS timing error has the effect of increasing the median three-dimensional location accuracy of the network by ~250 m at a 200 km range (Figure 6.16). Recall from Equation 5.15 that the vertical location accuracy is inversely proportional to the height, z, which means that the vertical location uncertainty will be higher at lower altitudes. Therefore, any decrease in the RMS timing error will have a larger effect on lower altitude VHF source location accuracy (Figures 6.14 and 6.15).

Continued spot checks of the Houston LDAR network timing error, yielded a surprising result for the 25 April 2007 MCS. Analysis of the distributions of goodness-of-fit for 6 sensor solutions gave an estimated network RMS timing error of 90 ns (Figure 6.18). The recent change in network operating frequency from 70 MHz to 40 MHz was not expected to affect the RMS timing error based on equation 5. With the error in sensor locations already minimized, the only other possible cause of the increased error is from a problem in the GPS timing measurements.

Extracting 40 seconds worth of GPS timing correction data from the 25 April 2007 data for the Cypress Fairbanks gave an average timing correct of 5,753 ns, but with a standard deviation of 37.8 ns. Similarly large standard deviations were found in two other sensors for on that day. Remotely accessing the Cypress Fairbanks sensor revealed that even weeks after 25 April 2007, the timing corrections were still drifting wildly. A simple command to reset the GPS system brought the timing corrections back to a constant value of 5650 ns and a standard deviation of 0. Inspection of the timing corrections several weeks after the GPS reset revealed a small increase in the standard deviation to 2.3 ns. This indicates that the GPS antenna over time loses synch with the

GPS satellite system and / or does not maintain connection with the most optimal satellites.

Unfortunately, there is no way of improving the timing error for storm days when the GPS system was not functioning properly. However, an automated script will be implemented to monitor the timing corrections at each sensor. If, during a 60 second sample, the standard deviation is greater than 10 ns and there is no lightning activity detected, the script will issue the GPS reset command. This should keep GPS timing problems to a minimum and bring the network RMS timing error back down to 75 ns for 6 sensor solutions. After the script is implemented, continuous timing error checks should be conducted to verify that the problem has been resolved.

7.2. Detection Efficiency

Previous LDAR networks have found the region between TV station carrier frequencies to have the lowest noise floor. This has yielded decent sensitivities in major urban areas such as Dallas – Ft. Worth. For the first 1½ years, the Houston LDAR network followed the same method of operation by using the 70 MHz frequency. In an attempt to increase network sensitivity, frequencies outside the standard TV channels were examined. Noise survey results (Figs. 5.2, 5.3, and 5.4) indicated that operating in the aviation frequency band would be problematic with an increased noise floor. In addition, testing of sensors at 114 MHz revealed intermittent aviation communications detected at a couple of the sites, which made this frequency range even less appealing. The noise results also revealed that operating at a frequency of 40 MHz should significantly increase network sensitivity despite the number of devices and

communications equipment that operates in this frequency range. Model results suggest that the new operating frequency yields an increase of 9 – 10 dB in network sensitivity (Figure 6.23). Based on the shift in the mode of the power distributions, the 40 MHz LDAR network detects ~3.3 times more VHF sources than the 70 MHz network setting. Analysis of estimated VHF source power distributions of storms detected at 70 MHz and 40 MHz show an improvement in sensitivity of 8 – 9 dB, which is in close agreement with model results.

Although the network shows an increase in sensitivity of 8 – 9 dB, there is definitely still room for improvement. The New Mexico Tech Lightning Mapping Array (LMA), that the Houston LDAR network design is based on, has a much higher VHF source sensitivity [Thomas et al., 2001]. Comparing the mode of the VHF source power distributions for the 70 MHz and 40 MHz in Figure 6.24 to the mode of the LMA VHF source distribution in Figure 7.1, the LMA network is 20 dB more sensitive. There are a couple of possible explanations for the differences in sensitivity. The first is due to the overall noisy nature of a large metropolitan area such as Houston. However, preliminary results from the test LMA in Washington, DC show that the DC system has a network sensitivity near that of the original LMA. The other explanation is related to sensor and antenna design. The LDAR sensor antenna was designed to produce an antenna gain pattern with maximum gain projecting horizontally outward slightly above the Earth's surface. The intention was to detect VHF noise sources from farther storms, but may

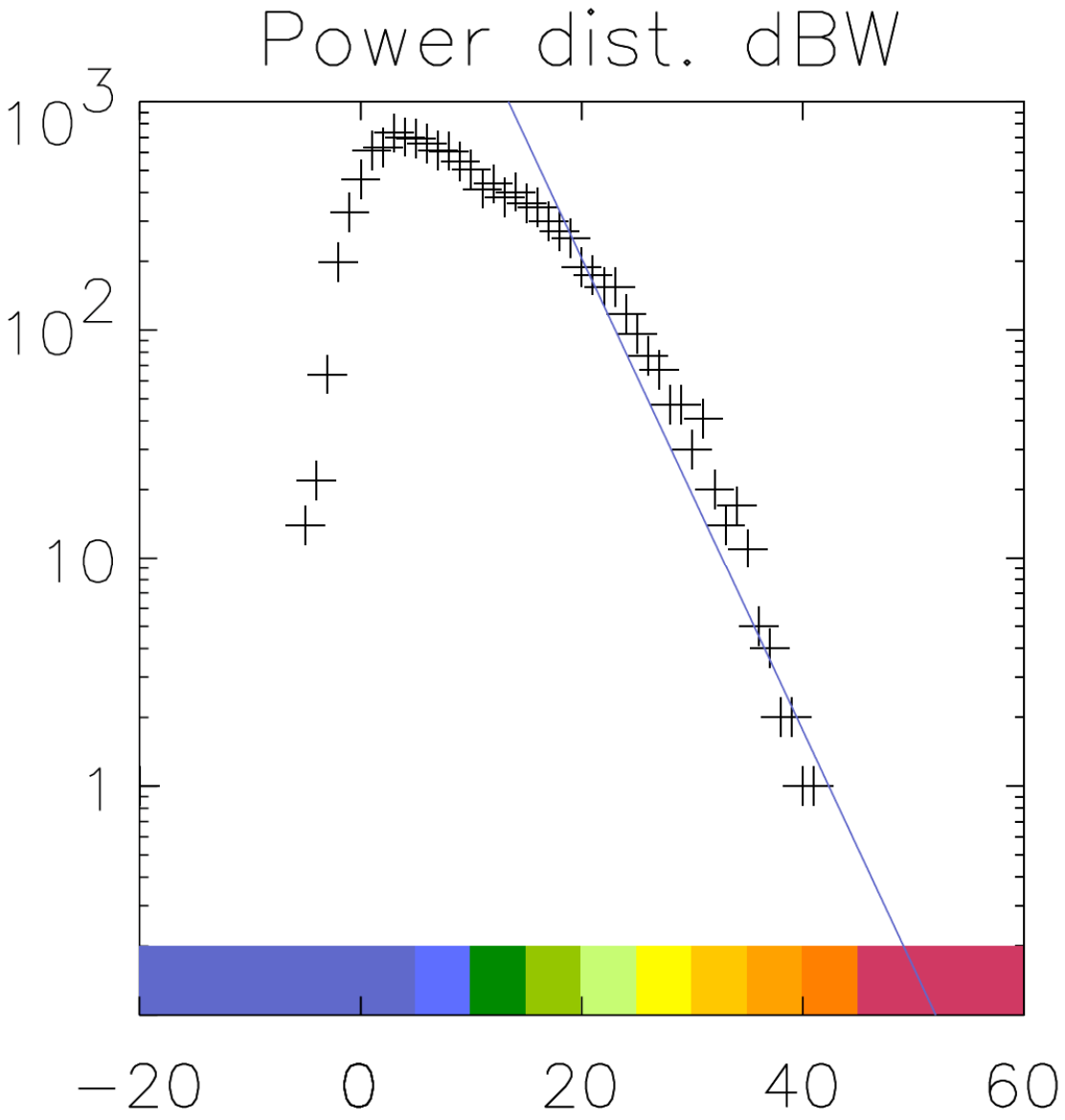

Figure 7.1. Estimated VHF source power distribution from a storm system detected by the New Mexico Tech LMA system. (Adapted from Thomas et al 2001.)

increase the noise floor (decrease sensitivity) from the increased detection of man-made noise produced near ground level. One method of determining whether it is the noise characteristics of the Houston or sensor design would be to operate a set of LMA sensors collocated with the Houston LDAR sensors and operating at the same frequencies.

Examining the change in the VHF source power distribution by range shows a pronounced change in the lower VHF source power detection limit. The range rings used in the analysis were chosen to be 2 dB apart and roughly 0.8 dB in width. All three storm cases analyzed (Figs. 6.25, 6.26, and 6.27) show a relatively constant VHF source power distribution out to the 31.6 km range ring, which indicates relatively uniform detection efficiency out to 31.6 km. This suggests that the detection efficiency within the boundaries of the sensors is nearly uniform, which is similar to results found by Boccippio et al. [2001] for the KSC LDAR system and Carey et al. [2005] for the DFW LDAR network. Beyond the 31.6 km range ring, the relative detection efficiency begins decreasing. The plots clearly show, as expected, the lower limit of VHF source power detection changes by roughly 2 dB, similar to the results of Carey et al. [2005].

Values of the relative detection efficiency at each range ring were obtained by integrating the composite distribution from the mode of the distant range ring towards higher powers. In all three storm cases, the relative detection efficiency followed extremely similar curves (Figure 6.28). Recall that earlier results showed that from the 31 October 2005 storm to the 25 April 2007, the overall sensitivity increased by 8 – 9 dB. Thus the network is currently able to detect many more VHF sources than with the previous 70 MHz configuration. In the cases of the relative detection efficiency by

range, any increase in network sensitivity does not change the rate of decrease in detection efficiency by range.

Examining the CFADs of VHF source power revealed that the distribution is nearly independent of altitude (Fig. 6.29). This indicates that the drop off in detection of lower altitude VHF sources with range does not have an appreciable effect on the change in overall VHF source power with range. However, at larger horizontal ranges greater than 100 km (Figs. 6.29d & e), the drop off in VHF source detection at lower altitudes is clearly observable as a highly variable in the vertical and compressed source power distributions. As previously stated, these observations occurred for each of the three storm days.

The other interesting observation in the CFADs is the leftward shift in the 1st and 10th percentile at all altitudes between the 25 km and 50 km range rings (Figs. 6.29b & c). At the 100 km range ring, the 1st and 10th percentiles begin shifting rightward towards higher VHF source powers. The most likely explanation for this shift would be related to the antenna design. The antennas have been assumed to be isotropic, which is definitely not realistic. As of now, an in-depth analysis of the antenna gain pattern has not been performed in order to take this effect into account.

However, it is known that the antenna gain pattern is more or less doughnut shaped with a maximum gain extending horizontally outward from the antenna and a minimum directly overhead. If this were taken into account in the theoretical minimum detectable signal plots, we would expect to see the following differences. Directly over the network, the minimum detectable signal would actually be a higher value than

currently predicted. As the distance from network center increases, it is expected that the minimum detectable source power value would decrease until a certain distance near the outside edge of the network. After this point, the minimum detectable source power value would again begin to rise as expected. Taking into account the antenna gain pattern may also explain the slight discrepancy between the theoretical and observed minimum source powers detected over the center of the network.

7.3. Network Range

The analysis of the usable network range for research purposes requires an upper limit of 1 km for the median three-dimensional location accuracy. Using the best case scenario of a 75 ns RMS timing error, the 1 km limit is at a range of roughly 175 km and the worst case scenario of a 90 ns RMS timing error, the 1 km limit is at a range of 150 km. Therefore, setting the limit on the conservative side, analysis of storms within 150 km of the center of the network will have a median location accuracy better than 1 km.

The other analysis used to determine the network range is the plot of the number of sources per range ring. The graphs for the 31 October 2005 (Figure 6.29), 21 April 2006 (Figure 6.30), and the 25 April 2007 (Figure 6.31) show the number of VHF sources follow the same increasing trend as the range ring area until roughly 100 km in range. This says that the MCS was an almost constant VHF source generator as it approached the LDAR network. However, beyond 100 km the number of VHF sources drops off significantly. These graphs indicate that the detection efficiency of the network falls off very little for the first 100 km and decreases significantly out to 200

km. From these results the recommendation of using 100 km as the maximum analysis range is made.

This sharp decrease in VHF source counts at the 100 km range is in contrast to the more gentle decrease in detection efficiency determined from the VHF source power distributions. This difference casts doubt on the accuracy of the VHF source power method of determining detection efficiency. This also makes the similar suggestion made by Boccippio et al. [2001] that the increase in the lowest detectable VHF source power by range is not the only constraint on the network's detection efficiency. This constraint may be caused by unknown signal attenuation or due to constraints in the location algorithm that determines what is or is not a valid VHF source. From this uncertainty, an analysis of the network detection efficiency from the distribution of VHF source densities could be conducted once a sufficiently large enough data set has been accumulated. Until then, the results from the VHF source power distributions can be used as a reasonable guide.

REFERENCES

Bevington, P. R., and K. D. Robinson, (2002), *Data Reduction and Error Analysis for the Physical Sciences,* 336 pp., McGraw-Hill, New York.

Boccippio, D. J., S. J. Heckman, and S. J. Goodman (2001), A diagnostic analysis of the Kennedy Space Center LDAR network: 1. Data characteristics*, J. Geophys. Res., 106*, 4769– 4786.

Brown, R. A., V. T. Wood, and D. Sirmans, (2000), Improved WSR-88D scanning strategies for convective storms, *Wea. Forecasting*, *15*, 208-220.

Carey, L. D., M. J. Murphy, T. L. McCormick, and N. W. S. Demetriades, (2005), Lightning location relative to storm structure in a leading-line, trailing-stratiform mesoscale convective system, *J. Geophys. Res., 110*, doi:10.1029/2003JD004371.

Cressman, G.P., (1959), An Operational objective analysis system, *Mon. Wea. Rev*., 87, 367-364.

Crum T. D., R. L. Alberty, and D. W. Burgess, (1993), Recording, archiving, and using WSR-88D data, *Bull. Amer. Meteor. Soc.*, *74*, 645–653.

Koshak, W. J., and R. J. Solakiewicz (1996), On the retrieval of lightning radio sources from the time-of-arrival data, *J. Geophys. Res., 101*, 26,631– 26,639.

Koshak, W. J., R. J. Solakiewicz, R. J. Blakeslee, S. J. Goodman, H. J. Christian, et al., (2004), North Alabama Lightning Mapping Array (LMA): VHF source retrieval algorithm and error analyses, *J. Atmos. Oceanic Technol., 21*, 543– 558.

Krehbiel, P. R., R. J. Thomas, W. Rison, T. Hamlin, J. Harlin, and M. Davis, (2000), GPS-based mapping system reveals lightning inside storms, *EOS Trans., 81*, 21-25.

Lennon, C. L., (1975), LDAR: New lightning detection and ranging system, *EOS Trans. AGU, 56*(12), 991.

Lennon, C. L., and L. Maier, (1991), Lightning mapping system, *NASA Conf. Publ*., *3106*(2), 89.1–89.10.

Lhermitte, R., and P. R. Krehbiel (1979), Doppler radar and radio observations of thunderstorms, *IEEE Trans. Geosci. Electron., GE-17*, 162– 171.

MacGorman, D. R., and W. D. Rust, (1998), *The Electrical Nature of Storms*, 422 pp., Oxford Univ. Press, New York.

Maier, L., C. Lennon, and T. Britt, (1995) Lightning detection and ranging (LDAR) system performance analysis, *Proceedings of 6th Conference on Aviation Weather Systems, P8.9*.

Mazur, V., E. Williams, R. Boldi, L. Maier, and D. E. Proctor, (1997), Initial comparison of lightning mapping with operational time-of-arrival and interferometric systems, *J. Geophys. Res., 102*, 11,071– 11,085.

Miller, J., C. G. Mohr, and A. J. Weinheimer, (1986), The simple rectification to Cartesian space of folded radial velocities from Doppler radar sampling. *J. Atmos. Oceanic Technol., 3*, 162–174.

Orville, R. E., G. Huffines, J. Nielsen-Gammon, R. Zhang, B. Ely, S. Steiger, S. Phillips, S. Allen, W. Read, (2001), Enhancement of cloud-to-ground lightning over Houston, Texas. *Geophys. Res. Lett*., *28*, 2597-2600, doi:10.1029/2001GL012990.

Oye D., and M. Case, (1995), REORDER: A program for gridding radar data. Research Data program, Atmospheric Technology Division, National Center for Atmospheric Research, Boulder, CO.

Poehler, H., and C. Lennon, (1979) Lightning detection and ranging system (LDAR): System description and performance objectives, *NASA Tech. Rep., TM-74105,* 1 – 86 .

Proctor, D. E., (1971), A hyperbolic system for obtaining VHF radio pictures of lightning, *J. Geophys. Res., 76*, 1478-1489.

Proctor, D. E., (1981), VHF radio pictures of cloud flashes, *J. Geophys. Res., 86*, 4041–4071.

Proctor, D. E., R. Uytenbogaardt, and B. M. Meredith, (1988), VHF radio pictures of lightning flashes to ground, *J. Geophys. Res., 93*, 12,683–12,727.

Rison, W., R. J. Thomas, P. R. Krehbiel, T. Hamlin, and J. Harlin, (1999), A GPS-based three-dimensional lightning mapping system: Initial observations in central New Mexico, *Geophys. Res. Lett., 26*, 3573–3576.

Steiger S. M., R. E. Orville, and G. Huffines, (2002), Cloud-to-ground lightning characteristics over Houston, Texas: 1989–2000, *J. Geophys. Res., 107*, doi:10.1029/2001JD001142.

Thomas, R. J., P. R. Krehbiel, W. Rison, T. Hamlin, J. Harlin, and D. Shown, (2001), Observations of VHF source powers radiated by lightning, *Geophys. Res. Lett., 28*, 143– 146.

Thomas, R. J., P. R. Krehbiel, W. Rison, S. J. Hunyady, W. P. Winn, T. Hamlin, and J. Harlin, (2004), Accuracy of the lightning mapping array, *J. Geophys. Res., 109*, doi: 10.1029/2004JD004549.

Uman, M. A., W. H. Beasley, J. A. Tiller, Y. Lin, E. P. Krider, (1978), An unusual lightning flash at Kennedy Space Center, *Science, 201*, 9 – 16.

Yuter, S. E., and R. A. Houze Jr., (1995), Three-dimensional kinematic and microphysical evolution of Florida Cumulonimbus. Part II: Frequency distributions of vertical velocity, reflectivity, and differential reflectivity, *Mon. Wea. Rev., 123*, 1941–1963.

VITA

Brandon Lee Ely was born in March of 1976 to Mr. and Mrs. Robert F. Ely of Baldwinsville, NY. He graduated from Charles W. Baker High School in May of 1994.

On the 15th day of May 1999, Brandon Ely graduated from the State University of New York at Oswego with a B.S. in meteorology. After taking two semesters off to work in computers, he enrolled at Texas A&M University as a master's degree candidate. He received his M.S. in atmospheric science in December of 2002. He continued his education at Texas A&M University, receiving his Ph.D. in atmospheric sciences in August 2008.

He is currently a software engineer in the Silicon Valley. He can be reached at the following address:

OSIsoft Inc.

777 Davis St.

Suite 250

San Leandro, CA 94577

He can also be reached by e-mail at:

bely300@gmail.com